

I

THE INVESTIGATION OF THE ALLOY SYSTEM LEAD-THALLIUM

II

THE INVESTIGATION OF THE CRYSTAL STRUCTURE OF
THE COMPLEX OF HEXAMETHYLENETETRAMINE WITH MANGANOUS CHLORIDE

Thesis by

You-Chi Tang

In Partial Fulfillment of the Requirements

For the Degree of

Doctor of Philosophy

California Institute of Technology

Pasadena, California

1950

ACKNOWLEDGEMENTS

It is a great pleasure to express my gratitude to Professors Linus Pauling and J. H. Sturdivant for their constant guidance and encouragement.

I owe Professor Pauling a debt of deep gratitude for many helpful discussions regarding the structures, bond types and bond distances.

I am deeply indebted to Professor Sturdivant for my introduction to X-ray crystallography either through his lectures in the course or our private conversations, and his valuable suggestions. I wish to express my thanks also for his generous assistance in the preparation of this thesis.

ABSTRACT

I. The Investigation of the Alloy System Lead-Thallium.

The lattice spacings for alloys in the lead phase of the system lead-thallium were accurately determined. The lattice-spacing—composition curve disagrees with that previously constructed by Olander on the basis of his fewer determinations. The new curve indicated that ordered phases $PbTl_3$ and $PbTlTl_6$ probably occur.

II. The Investigation of the Crystal Structure of the Complex of Hexamethylenetetramine with Manganous Chloride.

Suitable crystals of the complex of hexamethylenetetramine with manganous chloride were grown in a 1:1 mixture of alcohol and acetone. By chemical analysis the composition was shown to correspond to the formula, $2(CH_2)_6N_4 \cdot MnCl_2 \cdot 2H_2O$. The crystal has a pseudo unit cell with $a_1 = 11.80 \text{ \AA}$., $a_2 = 22.00 \text{ \AA}$., $a_3 = 7.21 \text{ \AA}$., and $Z = 4$. The pseudo space group is $C_{2v}^9 - P2_1nb$. A few weak reflections indicate that the a_1 axis should be doubled, but no account was taken of this in the present determination.

A trial structure derived from steric considerations and the intensities of reflections $h00$ led to a satisfactory interpretation of the Patterson distribution function. The approximate structure based on the Patterson syntheses was confirmed by the Fourier projections $\rho(x)$ and $\rho(y, z)$, and by calculation of structure factors for reflections $h00$ and $0k\Omega$.

ABSTRACT (Continued)

The structure has the following important features. A manganese atom lies on the common three-fold axis of two hexamethylenetetramine molecules at the center of symmetry of a complex molecule, and the Mn-Cl bonds are approximately perpendicular to the Mn-N bonds. Both the Patterson syntheses and the Fourier projections indicate that two molecules of water are present in each complex molecule, and the Mn-O bonds are approximately normal to the plane of the Mn-Cl and Mn-N bonds.

TABLE OF CONTENTS

<u>PART</u>	<u>TITLE</u>	<u>PAGE</u>
I.	The Investigation of the Alloy System Lead-Thallium	1
	1. Introduction	1
	2. Preparation of the Alloys.	2
	3. Powder Photography and Diffraction Patterns.	6
	4. Theoretical Possibilities of Superstructures in the Lead Phase.	8
	5. Accurate Determination of d_{100} for Alloys in the Lead Phase	12
	(1) Discussion of errors.	12
	(2) Procedure for evaluating d_{100} from powder photograph	14
	(3) Results	15
	6. Critical Review of Previous Work on the Alloy System	28
	7. The Probable Structure of the Alloys in the Lead Phase	32
	8. Conclusions.	36
	9. References	37
II.	The Investigation of the Crystal Structure of the Complex of Hexamethylenetetramine with Manganous Chloride	38
	1. Introduction	38
	2. Previous Work on the Compound.	40
	3. The Preparation of the Crystals.	41
	4. Morphological and Physical Properties of the Crystal.	43
	5. X-ray Crystallography.	46
	6. The Symmetry, Unit Cell, and Space Group of the Crystal.	47

TABLE OF CONTENTS (Continued)

<u>PART</u>	<u>TITLE</u>	<u>PAGE</u>
7.	The Collection of Intensity Data	57
8.	The Search for a Trial Structure	61
	(1) The number of complex molecules in the unit cell	62
	(2) The orientation of the hexamethylene- tetramine molecules in the crystal.	63
	(3) The symmetry of the complex molecule.	65
	(4) The coordination of the two hexa- methylenetetramine molecules in a single complex molecule along a ₁ . .	66
	(5) The location of the manganese atom and the centers of the hexamethyl- enetetramine molecules, with ref- erence to the y, z coordinates only.	67
	(6) The x coordinates of the two chlorine atoms in the complex molecule . . .	68
9.	The Determination of the Approximate Structure.	69
	Summary.	69
	(1) The application of the Patterson synthesis	70
	(a) Determination of the coordinates of the heavy atoms in the crystal by the Patterson synthesis.	72
	(b) Determination of the position of hexamethylenetetramine molecules in the crystal by the Patterson synthesis.	78
	(2) Projections of the distribution function for electron density; the calculation of structure factors. .	81
	(a) The Fourier projection $\rho(x)$ and the calculation of structure factors for reflections $h00$. .	82
	(b) The Fourier projection $\rho(y, z)$ and the calculation of structure factors for reflec- tions $0k\ell$	83
	(3) The probable positions of the oxygen atoms in the crystal.	85

TABLE OF CONTENTS (Continued)

<u>PART</u>	<u>TITLE</u>	<u>PAGE</u>
9.	Continued	
	(4) The description of the approximate structure	89
10.	Conclusions.	91
11.	References	93

I

THE INVESTIGATION OF THE ALLOY SYSTEM LEAD-THALLIUM

1. INTRODUCTION

The system lead-thallium, on investigation by the methods of thermal analysis, gives an unusual type of phase diagram (Figure 12). The freezing-point curve in the wide solid solution region has a maximum point between 62.5 and 64.3 atomic percent of thallium. The nature of this maximum point has not previously been made clear. The experimental evidence from investigations by the methods of electric conductivity and X-ray diffraction indicates that a compound, such as PbTl_2 or Pb_2Tl_3 , does not exist.

In 1934 A. Olander⁽¹⁾ published his interesting determination of lattice spacings of eleven alloys in the lead phase. For the lattice-spacing--composition curve (Figure 15) he drew two straight lines intersecting at 54.6 atomic percent of thallium. He postulated that below 54.6 atomic percent of thallium the alloys are in a random-solid-solution phase α , and that above this point the alloys are in a partially ordered phase β (Figure 16). According to him, the perfectly ordered arrangement would conform to the formula PbTl_7 .

It was a very good point to bring forward that the alloys in the lead phase might have superstructures. However, in view of the small number and poor distribution of his samples and the low maximum Bragg angles which he observed, it seemed highly desirable to redetermine the lattice-spacing--composition curve for the alloys in the lead phase.

Due to the fact that lead and thallium have almost the same atomic scattering factors, we knew that even a failure to observe the superlattice lines in our case would not necessarily mean that the superstructures do not occur.

This investigation was undertaken, therefore, to test Olander's lattice-spacing determination and to seek new information regarding the probable structures of the lead-phase alloys by the X-ray powder method.

This work was suggested by Professor Linus Pauling and carried out under the supervision of Professors J. H. Sturdivant and Linus Pauling.

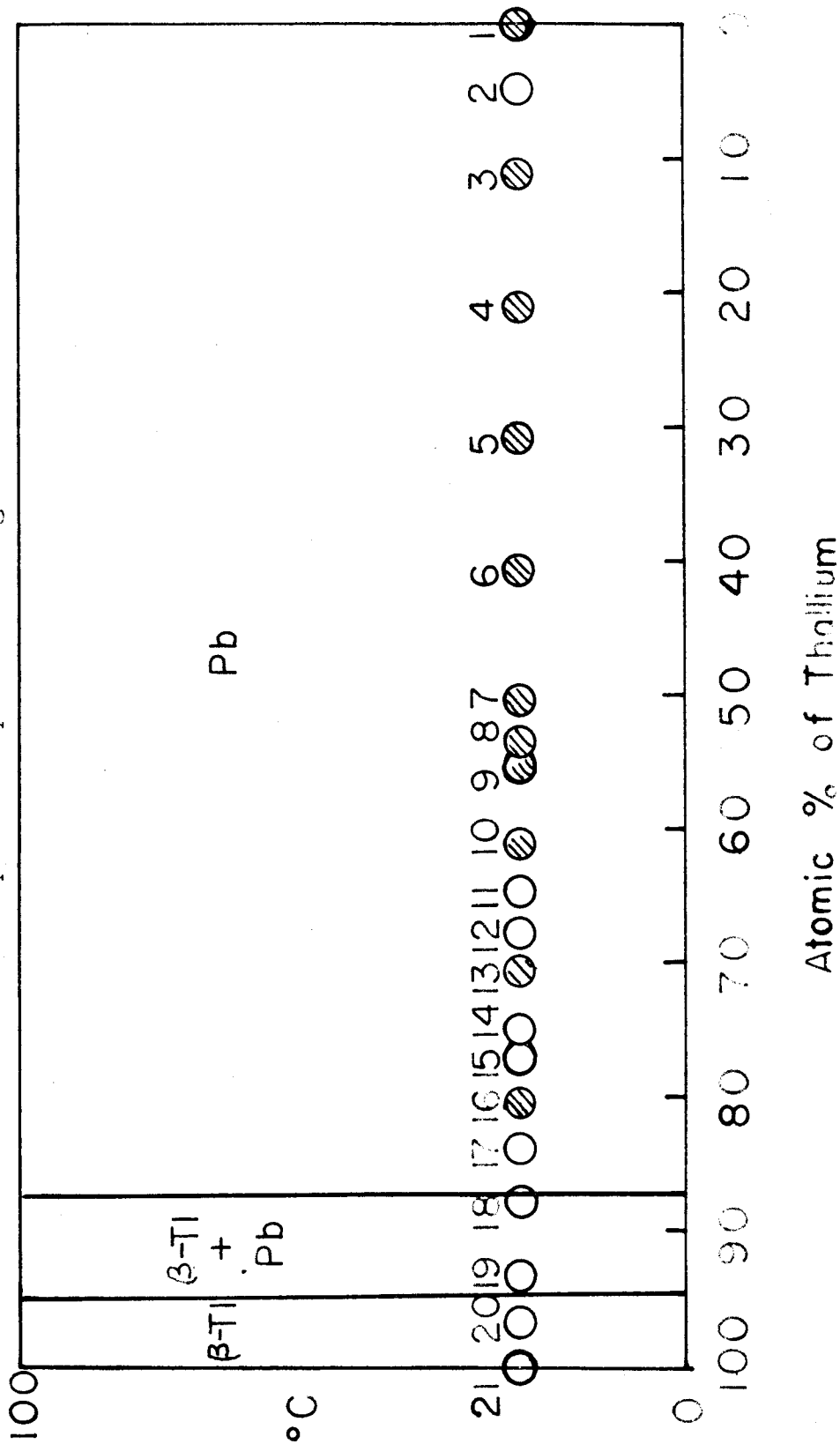
2. THE PREPARATION OF ALLOYS

Figure 1 shows the distribution over the complete composition range of the alloy samples prepared for this investigation. The shaded circles stand for large 100-gram samples made on Professor Pauling's suggestion.* The smaller samples represented by the unshaded circles were made subsequently. Reasons for choosing this distribution will become obvious.

Due to the fact that lead and thallium are readily oxidized on exposure to air I prepared the alloys by melting weighed amounts of the pure metals together in Pyrex tubes under a vacuum of about 10^{-5} mm. Hg. The uniformity of the reguli with respect to their composition was achieved by the following

* Memorandum dated January 21, 1947, from Professor Pauling.

Figure 1. The distribution of the alloy samples over the complete composition range.



two measures. First, the alloys were kept in a molten state at temperatures about 100°C above their respective melting points for more than two hours. Second, effective agitation was provided by a magnetically driven stirring device.

The pure lead used in the preparations was c. p. granular test lead (silver, gold, and bismuth free) supplied by the Fisher Scientific Company. The thallium metal was supplied by the Varlacoid Chemical Company. The result of qualitative spectrographic examination** on these two pure metals is presented in Table I.

Table I.

(From Smith-Emery report 290340-61, April 15, 1948)

Lead	Major Constituents	Lead	
	Minor Constituents	Iron	Approximately 0.005%
		Thallium	Approximately .001%
Copper		Approximately .001%	
Thallium	Major Constituents	Thallium	
	Minor Constituents	Lead	Approximately 0.01 %
		Iron	Approximately .005%
Copper		Approximately .001%	

The compositions of samples 2, 17, and 18 were calculated from the proportions of the pure metals mixed for melting. The other samples were analyzed. Two small 2-gram samples A and B

** All spectrographic and chemical analyses reported in this work were made by Smith-Emery Laboratory, Los Angeles, California.

for chemical determination were taken from each sample of a particular composition. The result of the chemical determinations is presented in Table II. The deviation of the total from 100 percent in each determination probably gives a rough idea of the accuracy of the chemical determination. Within the limits of error of the chemical analysis each alloy sample is homogeneous. I give an ample allowance for the uncertainty in the atomic percentage of thallium in the last column of Table II.

Table II.

Sample	Result of Determination**			Average Atomic Percent of Thallium	
	Lead Wt. Percent	Thallium Wt. Percent	Total Wt. Percent		
1	99.95	Trace	99.95	0	
2				4.9 \pm 1.0	*
3	A 88.85	11.06	99.91	11.2 \pm 0.5	
	B 88.90	10.98	99.88		
4	A 79.00	20.88	99.88	21.1 \pm 0.5	
	B 79.20	20.72	99.92		
5	A 69.40	30.48	99.88	30.8 \pm 1.0	
	B 69.70	30.22	99.92		
6	A 59.80	40.10	99.90	40.6 \pm 1.0	
	B 59.55	40.34	99.89		
7	A 50.00	49.85	99.85	50.4 \pm 0.5	
	B 49.90	50.01	99.91		
8	A 46.95	52.94	99.89	53.5 \pm 1.0	
	B 46.40	53.48	99.88		
9	A 44.85	55.06	99.91	55.4 \pm 1.0	
	B 45.20	54.70	99.90		
10	A 39.30	60.59	99.89	61.1 \pm 1.0	
	B 38.80	61.10	99.90		
11	A 35.26	64.49	99.75	64.7 \pm 1.0	
	B 35.35	64.40	99.75		
12	A 32.25	67.29	99.54	67.6 \pm 1.0	
	B 32.52	67.12	99.64		
13	A 29.35	70.55	99.90	70.6 \pm 1.0	
	B 29.80	70.10	99.90		
14	A 25.15	74.62	99.77	75.0 \pm 1.0	
	B 24.87	74.78	99.65		
15	A 22.68	76.96	99.64	77.1 \pm 1.0	
	B 22.95	76.65	99.60		
16	A 19.50	80.39	99.89	80.5 \pm 1.0	
	B 19.75	80.13	99.88		
17				83.9 \pm 1.0	*
18				87.8 \pm 1.0	*
19	A 6.57	93.16	99.73	93.4 \pm 1.0	
	B 6.57	93.40	99.97		
20	A 2.73	97.22	99.95	96.9 \pm 1.0	
	B 3.12	96.51	99.63		
21	0.01	99.95	99.96	100.0	

* Atomic percent of thallium calculated from the proportion of pure thallium mixed for melting.

** From Smith-Emery Reports 290340-61, April 15, 1948, and 298009-20, October 9, 1948.

3. POWDER PHOTOGRAPHY AND DIFFRACTION PATTERNS

Each specimen for powder photography was prepared by filing the regulus, passing the filings through a 200-mesh sieve, and putting them into thin-walled glass capillaries about 1/2 to 3/4 mm. in diameter. All these operations were performed in an atmosphere of carbon dioxide. The capillaries were then sealed under vacuum. The specimens were annealed at 280°C for at least 40 hours and allowed to cool at a fairly constant rate of about 0.001°C per second.

A first complete series of powder photographs was taken in a 5-centimeter-radius cylindrical camera. The gap in the film was placed in the back-reflection region. The construction of the camera permits a maximum Bragg angle of 79°. Copper K α radiation filtered through 0.001-inch nickel foil was used.

A second complete series of powder photographs was taken in a Norelco camera with circumference 360 mm. The construction of the camera is based on Straumanis' scheme, and permits a maximum Bragg angle of 87.5°. Copper K α radiation was used.

Eastman No-Screen X-ray film was used throughout. All photographs were taken at room temperature, 26° \pm 2°C.

The diffraction patterns for the alloy samples 1 through 18 inclusive show the same set of well-defined, face-centered cubic lines in the same positions and relative intensities as the diffraction pattern of pure lead.

The powder photographs in the first series for the lead-

phase alloys contain lines (111), (200), (220), (311), (222), (400), (331), (420), (422) $\alpha_{1,2}$, (333) $\alpha_{1,2}$, (440) $\alpha_{1,2}$, (531) $\alpha_{1,2}$, (600) $\alpha_{1,2}$, (442) $\alpha_{1,2}$. The maximum Bragg angle in the whole series is about 72.5°. For the last four lines the α_1 and α_2 doublets separate nicely. A print of a representative photograph is shown in Figure 2.

The powder photographs in the second series for the lead-phase alloys containing thallium less than 70 percent give an extra line, (620) $\alpha_{1,2}$, in addition to those mentioned above. The maximum Bragg angle now varies from 80.7° for sample 1 to 85.5° for sample 13. As we shall see later, this significantly improves the determination of lattice spacings of these lead-phase alloys.

Up to sample 18, the alloys give only the diffraction pattern of pure lead. Sample 19 gives a two-phase pattern. Pure thallium has an A3 structure at room temperature. Figure 3 shows diffraction patterns for the lead-thallium alloys at room temperature.

Unannealed specimens give diffuse lines due to the fact that the lattice is distorted by the filing. Annealing always removes such distortion effectively. No other effects of annealing were noticed. The annealing temperature and cooling rate given in Section 2 are considered to be adequate for the alloys under investigation.

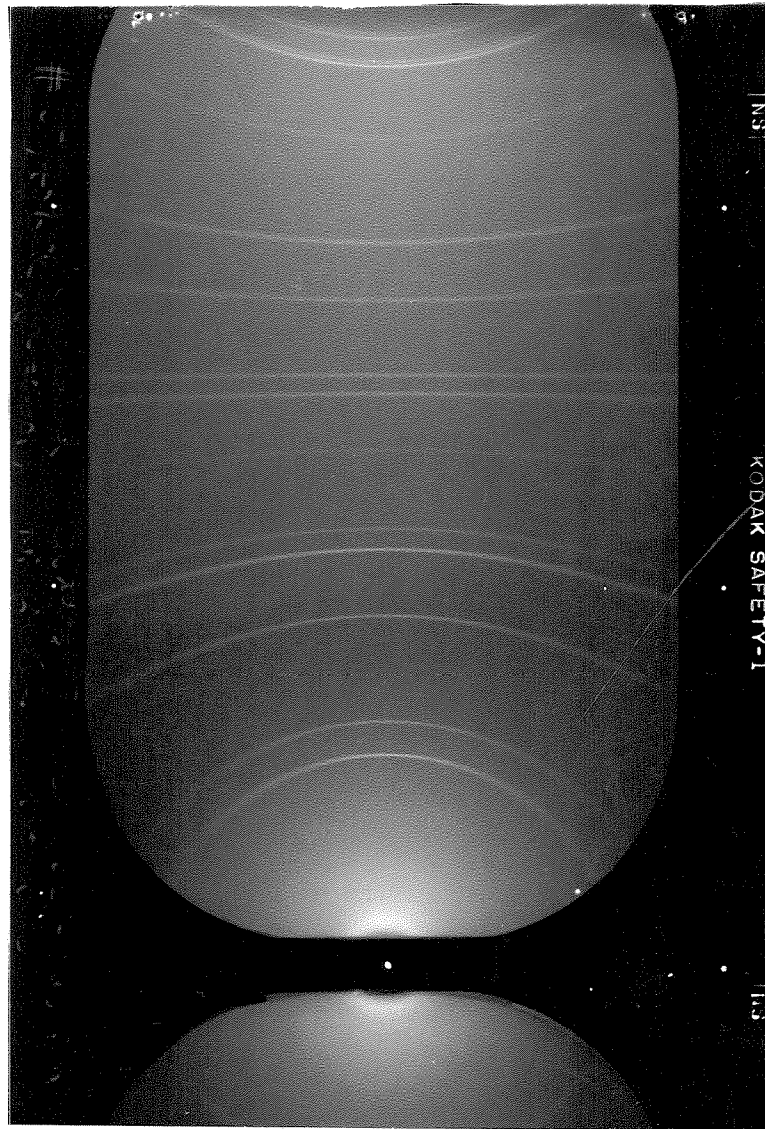


Figure 2. Powder photograph of a lead-thallium alloy (sample 6) taken in a five-centimeter-radius camera.

Figure 3. Diffraction patterns of the lead-thallium alloys. Photographs were taken in the 360 mm.-circumference camera.

Atomic %
of
Thallium

0

55.4

-70-

75.0

93.4

100

Phases
Present

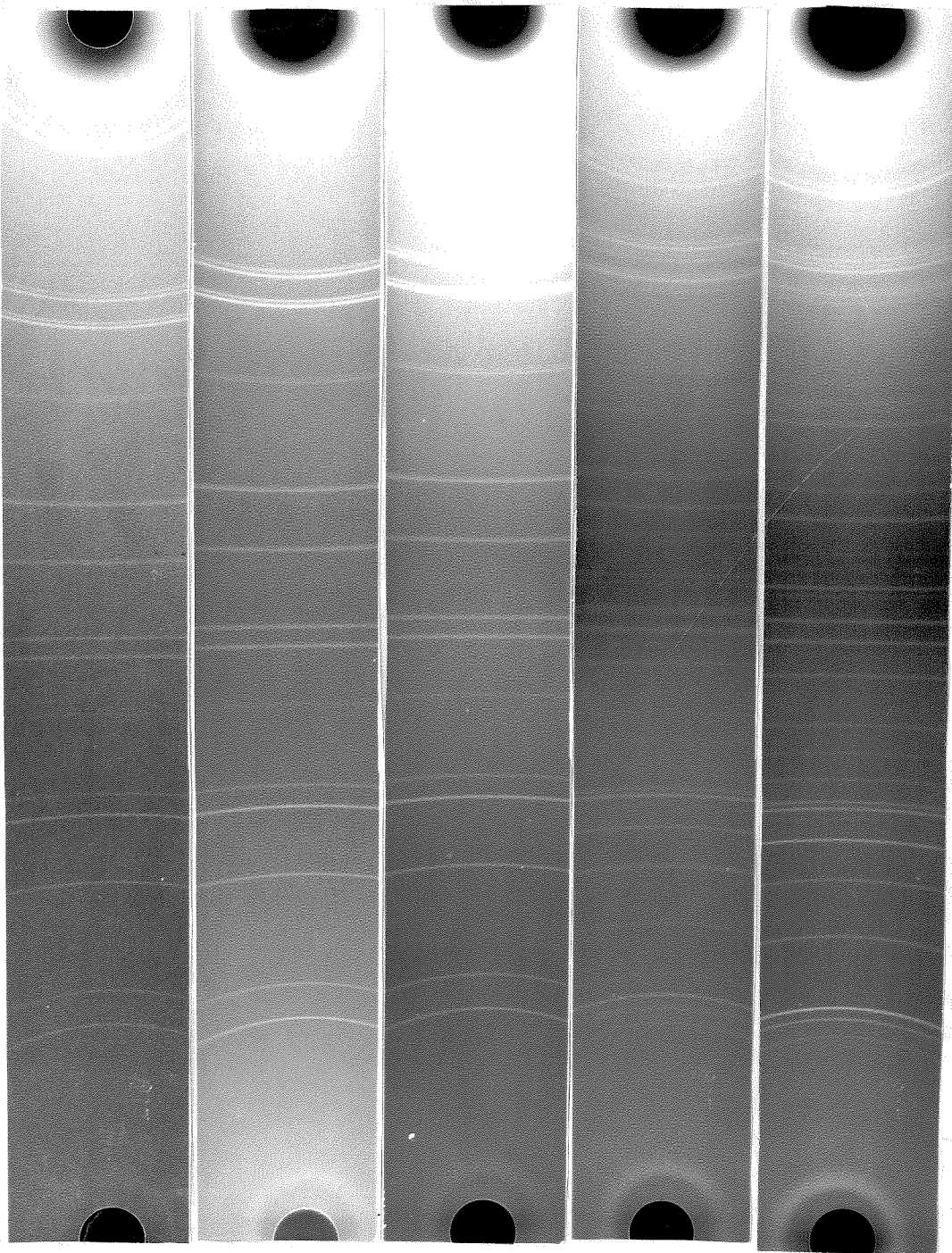
Pb

Pb

Pb

Pb+ β -Tl

β -Tl



4. THEORETICAL POSSIBILITIES OF SUPERSTRUCTURE IN THE LEAD PHASE

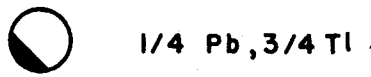
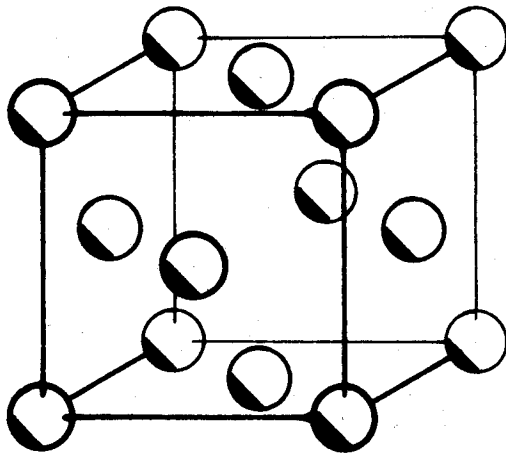
At this stage I want to discuss theoretically whether there can be any superstructure in the lead phase alloys and which are the types of superstructures permitted by the observed diffraction patterns.

Despite the fact that no superlattice lines have ever been observed on the powder photographs of the lead phase alloys, superstructures, of the type PbTl_3 , for instance, are not excluded. Figure 4 (1) shows the random solid solution containing 25 percent lead and 75 percent thallium, while Figure 4 (2) illustrates the superstructure PbTl_3 . The two structures would give X-ray diffraction patterns indistinguishable from each other. Due to the fact that lead and thallium have very much the same atomic scattering factor for X-rays, superlattice lines, namely lines with mixed hkl , would be much too weak to be observed on the photograph. Therefore it is necessary to have other experimental evidence*, before one can tell if the superstructure in 4 (2) does occur or not.

However, superstructures which give rise to split diffraction lines are eliminated here. For illustration, Figure 5 (2) gives a superstructure PbPbTlTl which does not have the

* Evidence from experiments like neutron diffraction or anomalous scattering of X-rays or measurement of conductivities or determination of the lattice-spacing-composition curve may help.

-8a- (1)



(2)

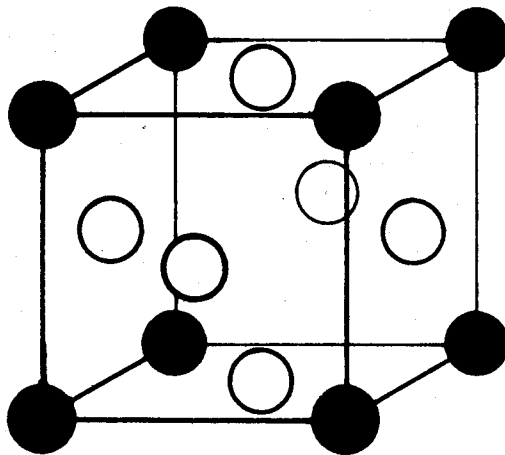
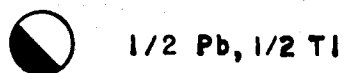
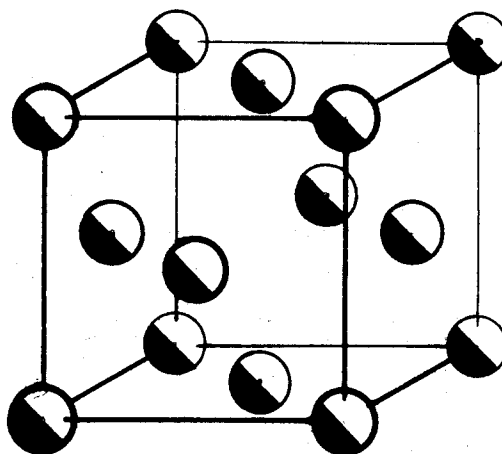


Figure 4. (1) The random solid solution containing 25 atomic percent lead and 75 atomic percent thallium.
(2) The superstructure PbTl_3 .

(1)



(2)

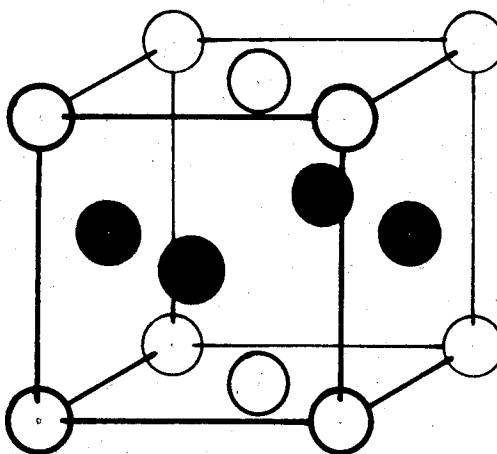


Figure 5. (1) The random solid solution containing 50 atomic percent lead and 50 atomic percent thallium.

(2) The superstructure PbPbTlTl.

symmetry of the cubic system, and hence would give rise to splitting of the cubic powder lines.* The observed well-defined face-centered cubic diffraction pattern makes the tetragonal superstructure in Figure 5 (2) very improbable.

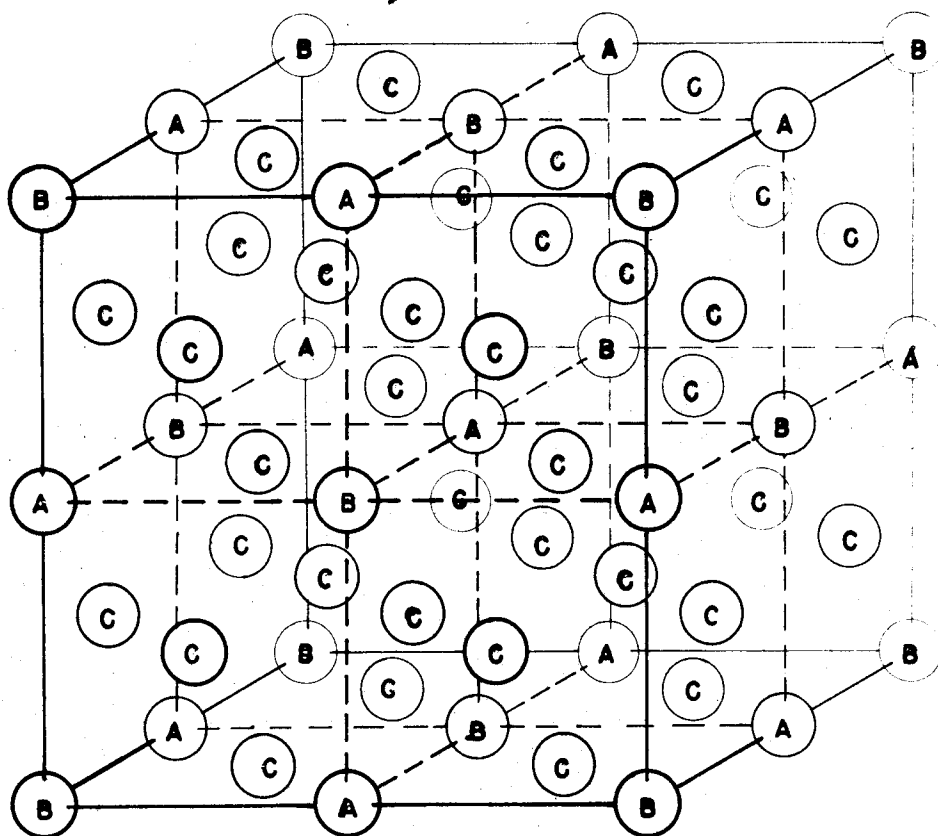
We can prove with one reasonable assumption that the superstructure of the general type ABC_6 as shown in Figure 6 contains all theoretical possibilities compatible with the observed diffraction patterns.

The fact that we observe well-defined and single lines indicates that the lattice from which they arise must have cubic symmetry.** The diffraction pattern shows that the edge of the real or pseudo unit cell of this cubic lattice is about 5 Å long. The density proves that each 5-Å cube contains four atoms. Now we assume that any non-cubic arrangement of these four atoms within the 5-Å cell would distort it perceptibly from a cube. Then such a non-cubic arrangement is eliminated.***

* I estimate by comparison with the alloy in the system copper-gold that if the superstructure $PbPbTlTl$ does exist, the powder line (600) would split into two components separated by a distance of 5 mm.

** I estimate here that a deviation from unity greater than 0.0002 in the axial ratio could be readily detected. The corresponding splitting of the powder line, say (600) or (442), would be about 0.1 mm. The powder lines are about 0.2 mm. in half width.

*** We may estimate the maximum deviation from the ideal pseudo unit of Figure 7(1) in terms of the fraction of the sites which may be taken by an atom of the wrong kind. In the system lead-thallium the cube edge varies between 4.842 Å. for $(TlTl_3)$ and 4.947 Å. for $PbPb_3$ (Figure 20). If about one percent of the sites are taken by atoms of the wrong kind, a deviation from unity of one in 5000 can be predicted in the axial ratio. This is about the limit which is detectable. Hence, I must leave open the possibility of imperfections or defects in the type of structure of Figure 6 to the extent that one percent of A or B or C sites may be taken by atoms of a wrong kind.



ABC_6

$z = 4$

Figure 6. The superstructure of the general type ABC_6 .

However the only way of arranging the four atoms of lead and thallium to produce cubic symmetry and also to give very low structure factors for lines which are observed to be absent is to place them at $000, 1/2, 1/2, 0, \bar{0}$, with the atoms at 000 either all equivalent or in two tetrahedral sets A and B, and with those at $1/2, 1/2, 0, \bar{0}$ in an octahedral set C.

Then the $5\text{-}\overset{\circ}{\text{A}}$ cell contains $1/2 \text{ABC}_6$ (see Figure 7).

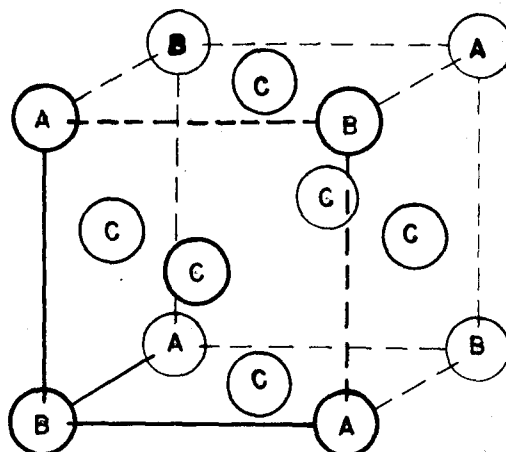
However, in the special case that A's and B's are identical, the $5\text{-}\overset{\circ}{\text{A}}$ cube contains AC_3 as shown in Figure 7 (2). The superlattice unit will be built up by juxtaposition of $5\text{-}\overset{\circ}{\text{A}}$ cubes. In view of the fact that the cubes in Figure 7 (1) and (2) cannot share a face with each other, they can never occur together. Therefore the general type ABC_6 containing AC_3 as a special case is the only theoretically possible type.

In the general case eight and only eight $5\text{-}\overset{\circ}{\text{A}}$ cubes as shown in Figure 7 (1) are needed to give a complete true unit cell in Figure 6. The combination of the $5\text{-}\overset{\circ}{\text{A}}$ cubes containing $1/2 \text{ABC}_6$ into a larger unit or into any coherent structure is a unique one. If A and B are identical, the cube AC_3 itself is a true unit cell.

In the general structure type ABC_6 , the A sites (or B or C sites) may be occupied by Pb or by Tl or by (Pb,Tl).* I list all theoretically possible ordered arrangements with the range

* I say that a set of equivalent sites A (or B, or C) is occupied by (Pb,Tl) if random sites making up a fraction x of the total in the set are occupied by Tl and the remaining fraction (1-x) are occupied by Pb. The fraction x may vary from 0 to 1. In Figure 4 and elsewhere I write for the statistical atom (1-x)Pb, xTl.

(1)



(2)

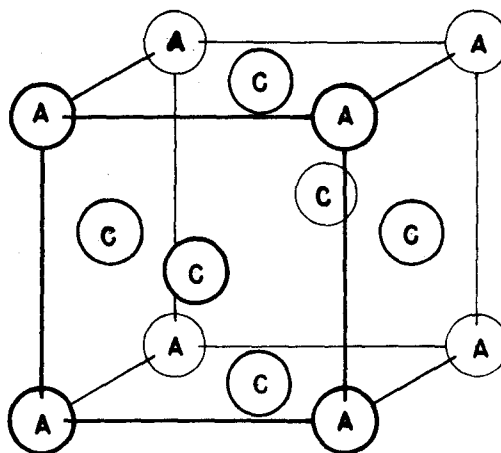


Figure 7. (1) An asymmetric octant of a unit cell for ABC_6 , $Z=4$.
(2) A unit cell for AC_3 .

of composition in Table III. The cases with $A = B = C$ are trivial. I shall present experimental evidence which indicates strongly that the arrangements followed by an asterisk in Table III may occur.

Table III



A = B, A ≠ C AC_3			A ≠ B ABC_6			
A	C	Atomic Per- cent of Thallium	A	B	C	Atomic Per- cent of Thallium
Pb	(Pb,Tl)	0-75 *	(Pb,Tl)	Pb	Tl	75-87.5 *
Pb	Tl	75 *	Pb	Tl	Tl	87.5 *
Tl	Pb	25	Tl	(Pb,Tl)	Pb	87.5-100
Tl	(Pb,Tl)	25-100	(Pb,Tl)	Pb	Pb	0-12.5
(Pb,Tl)	Pb	0-25	Pb	Tl	Pb	12.5
(Pb,Tl)	Tl	75-100	Tl	(Pb,Tl)	Pb	12.5-25
			(Pb,Tl)	Pb	(Pb,Tl)	0-87.5
			Pb	Tl	(Pb,Tl)	12.5-87.5
			Tl	(Pb,Tl)	(Pb,Tl)	12.5-100

5. ACCURATE DETERMINATION OF d_{100} FOR
ALLOYS IN THE LEAD PHASE

The final values of d_{100} were obtained from the second series of powder photographs. With the help of the line (620), one can attain precision of one part in five thousand. This matches the accuracy of the chemical determination in most cases. When the line (620) is not present we can expect the precision to be only two parts in five thousand.

(1) Discussion of errors.--Under this title I shall discuss accuracy of the determination and reproducibility of the result separately.

The Straumanis scheme takes care of the radius and shrinkage errors automatically. One may hope that the manufacturer of the camera has set the crystal spindle concentric with the camera axis within 0.04 mm. If he has achieved this reasonable accuracy, then the eccentricity error is small in comparison with the random error. The success of the extrapolations to be described later indicates that eccentricity is indeed negligible, and that the random error fixes the limit of error for the entire determination.

Absorption error is important in our case. However, the Nelson and Riley⁽²⁾ function will take care of it, and it falls off rapidly with the Bragg angle.

By considering the manner in which I measured the photographs, the sharpness of the powder lines, the film material,

the camera construction and other factors I estimate an overall random error limit of 0.1 mm. in measuring the arc on the film determined by the angle 2θ , which corresponds to $\Delta\theta = 0.00087$. Figure 8 gives a plot of the function $\Delta d_{100} = d_{100} \cot \theta \cdot \Delta\theta$ against Bragg angle and the Nelson and Riley function. In Figure 8 I use two values for $\Delta\theta$, namely 0.00087 and 0.00174. The latter must be very safe limit for the random error. Figure 8 is very useful in fixing a straight line for the extrapolation of d_{100} against the Nelson and Riley function. In most cases the lower curve alone is sufficient.

With a given specimen or capillary I always found it easy to reproduce d_{100} well within the limits of error I claimed, by taking a new photograph, measuring it, and carrying out the calculation.

However, it is also important to test if one can reproduce the result by changing the experimental conditions previous to the capillary stage.

I put the same filings into two capillaries of diameter 0.25 mm. and 0.5 mm. respectively (Specimen 3-1, 3-2). The result is given in Figure 9. The diameter of the capillary fixes the slope of the straight line, but does not affect the intercept.

The second experiment is to test the reproducibility of the result by changing the conditions before the stage of filing. I filed different pieces of an alloy (Sample 11), passed

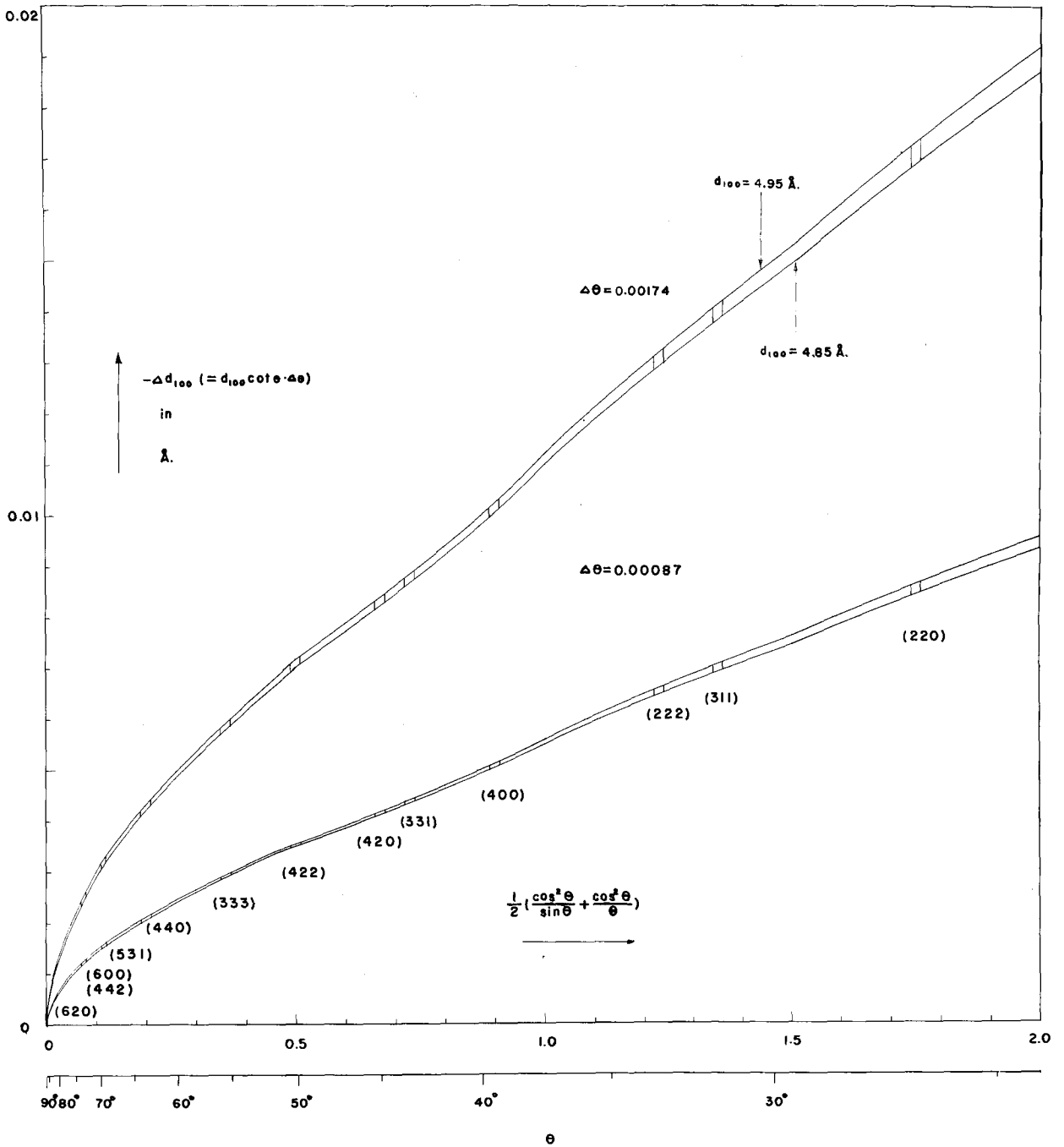


Figure 8. A plot of $\Delta d_{100} = -d_{100} \cot \theta \cdot \Delta \theta$ against Bragg angle and the Nelson and Riley function for $\Delta \theta = 0.00087$ and 0.00174 and $d_{100} = 4.85$ to 4.95 \AA . Indices of the order lines are given at respective Bragg-angular ranges.

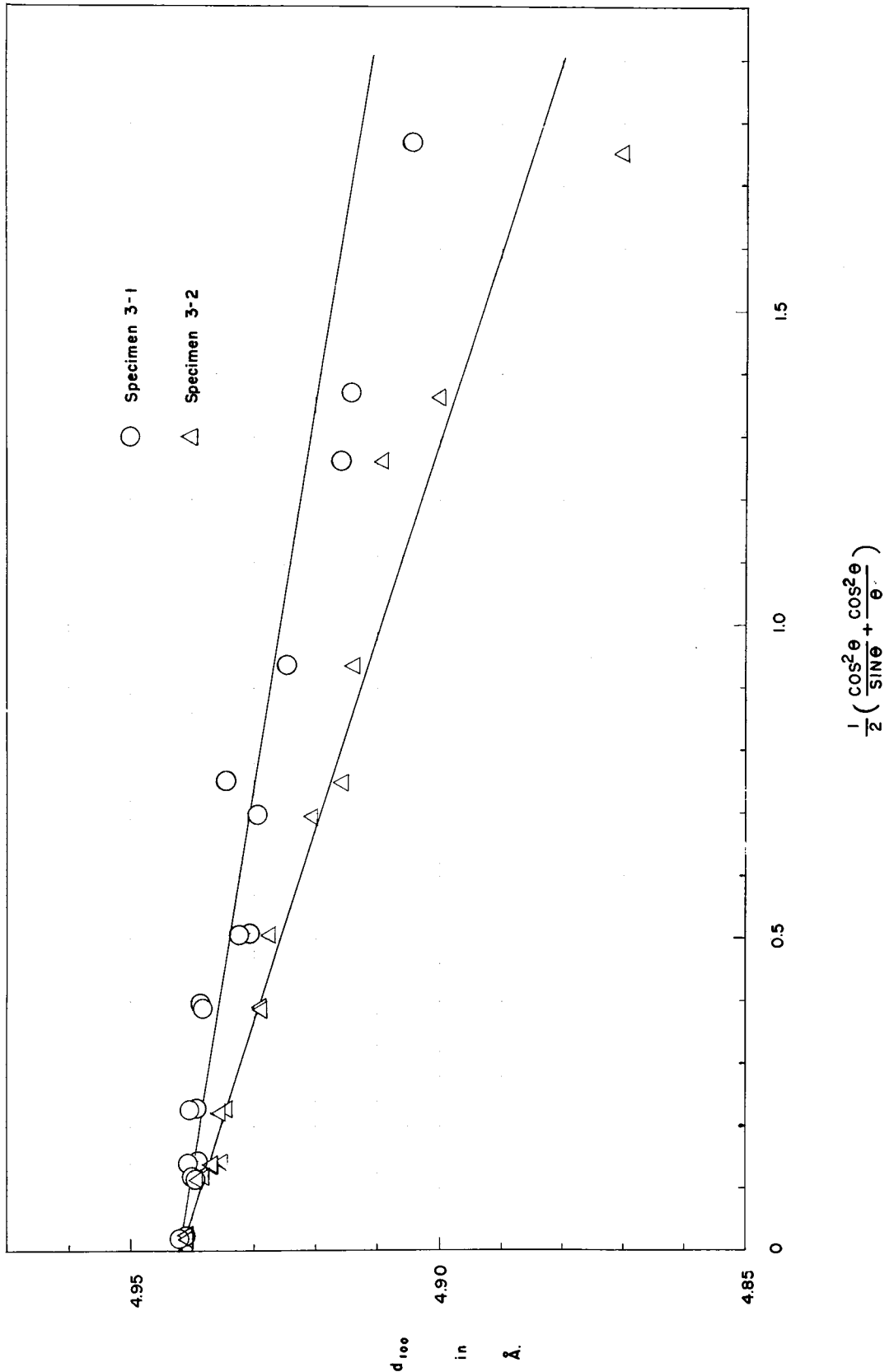


Figure 9. A plot of d_{100} for the specimens 3-1 and 3-2 against the Nelson and Riley function. The specimens 3-1 and 3-2 are 0.25 and 0.50 mm. in diameter respectively.

the filings through 200 mesh separately, and put them into separate capillaries (Specimens 11-1, 11-2). The value is also reproducible within the limits of error (Table 4).

(2) Procedure of evaluating d_{100} from the powder

photograph.--The measurement of the photographs was carried out in a rather usual manner. A brass scale with a vernier has been used most of the time. It seems to me that the brass scale is fairly uniform. However, it is not long enough for Norelco-camera powder photographs. I had to measure twice for each photograph. A steel rule has been also used.

In translating the film distances to lattice spacings I used the following wave lengths:

$$\text{Copper } K\alpha_1 = 1.5405 \text{ \AA.}$$

$$\text{Copper } K\alpha_2 = 1.5443 \text{ \AA.}$$

$$\text{Copper } K\alpha = 1.5418 \text{ \AA. (weighted average)}$$

I calculated the value for d_{100} by use of the formula

$$d_{100} = \frac{\sqrt{\sum h^2} \cdot \lambda / 2}{\sin \theta} .$$

The numerator is calculated once for all.

Absorption error is taken care of by means of the Nelson and Riley function. A straight line is fitted with the help of random error limits given in Figure 8. I always drew the straight line passing through the point representing the line occurring at maximum Bragg angle. I estimated the limits of error of the entire determination to be equal to the random

error limit given in Figure 8 for the powder line occurring at maximum Bragg angle on the photograph.

(3) Results.--I present the numerical values of all determinations in Table IV. Figures 10 (1), (2) give the extrapolations for all of the determinations. Figure 11 shows the lattice-spacing--composition curve based on these values. The edge lengths of the squares and rectangles give the magnitude of the uncertainties along each direction.

It is very remarkable that two different specimens (14-1, 2) from alloy sample 14 give quite different values. A change of composition as small as 0.5 percent of thallium can be responsible for a change of $0.004 \text{ \AA}.$ in d_{100} in the neighborhood of 75 percent of thallium. Such a small change of composition is possible from an experimental point of view. On the other hand this interesting discrepancy gives further support for the shape of the lattice-spacing--composition curve in Figure 11. The two rectangles at 75 percent of thallium stand for the specimens 14-1,2 in Figure 11.

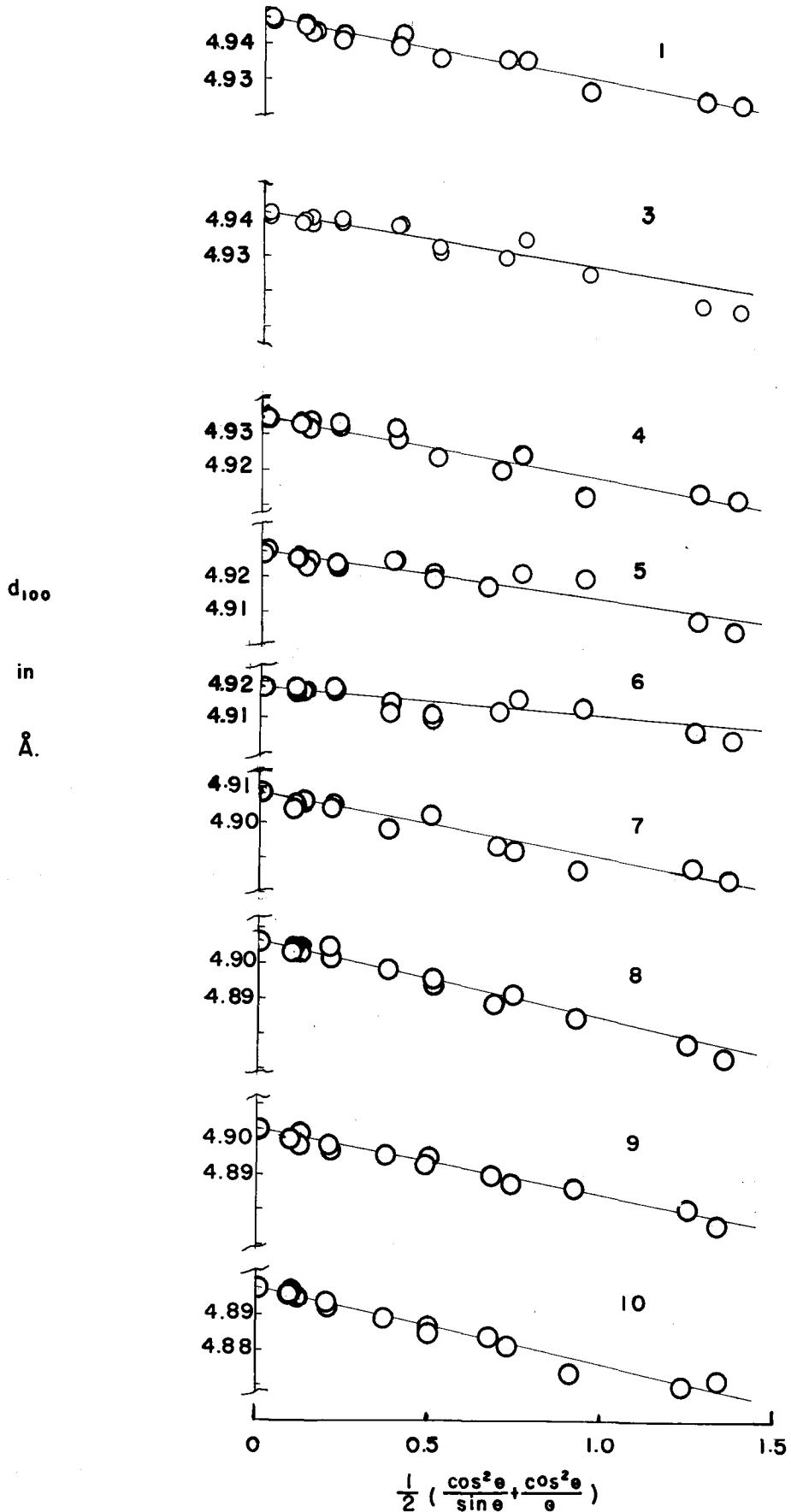


Figure 10 (1). The extrapolation of the calculated values of d_{100} for all specimens against the Nelson and Riley function.

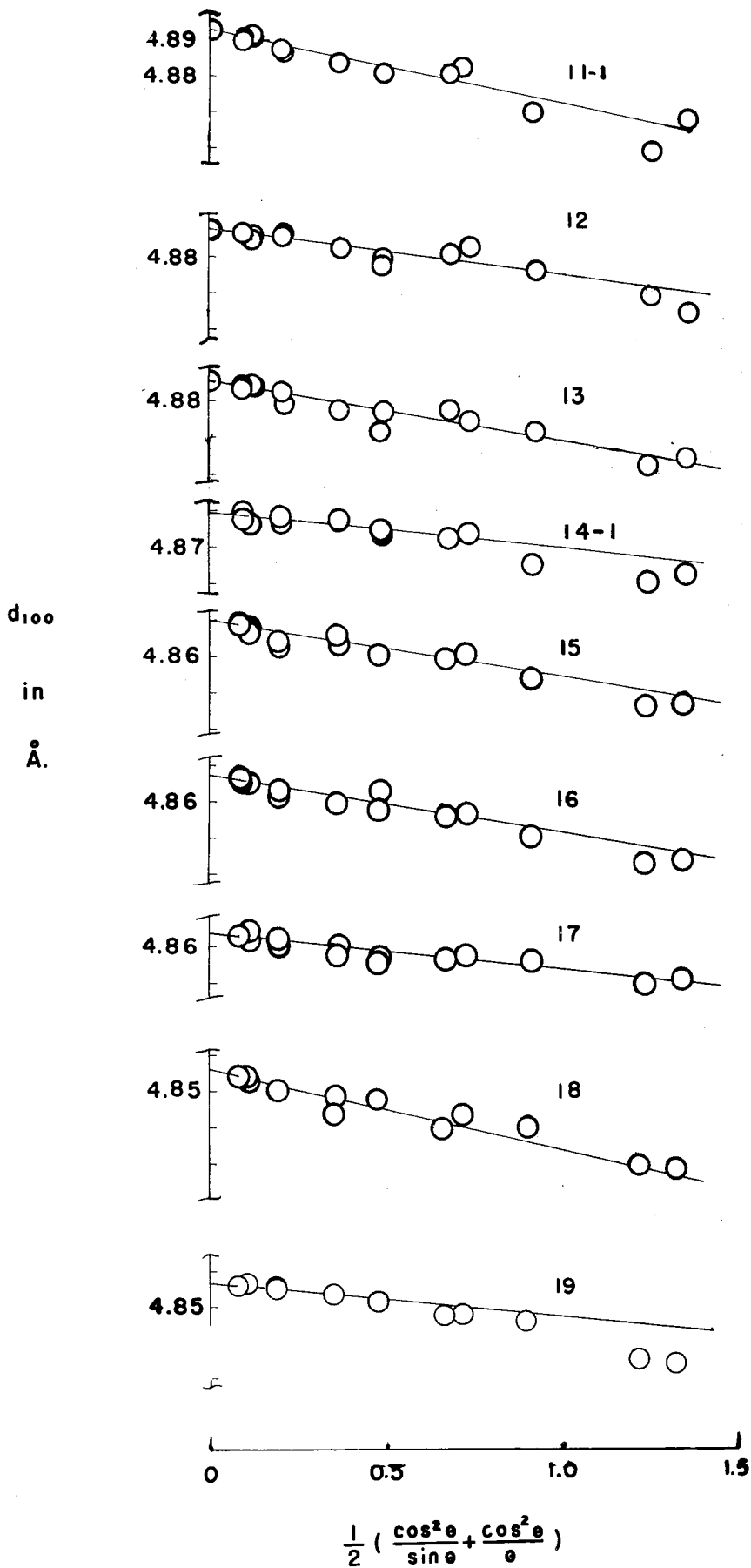


Figure 10 (2). The extrapolation of the calculated values of d_{100} for all specimens against the Nelson and Riley function.

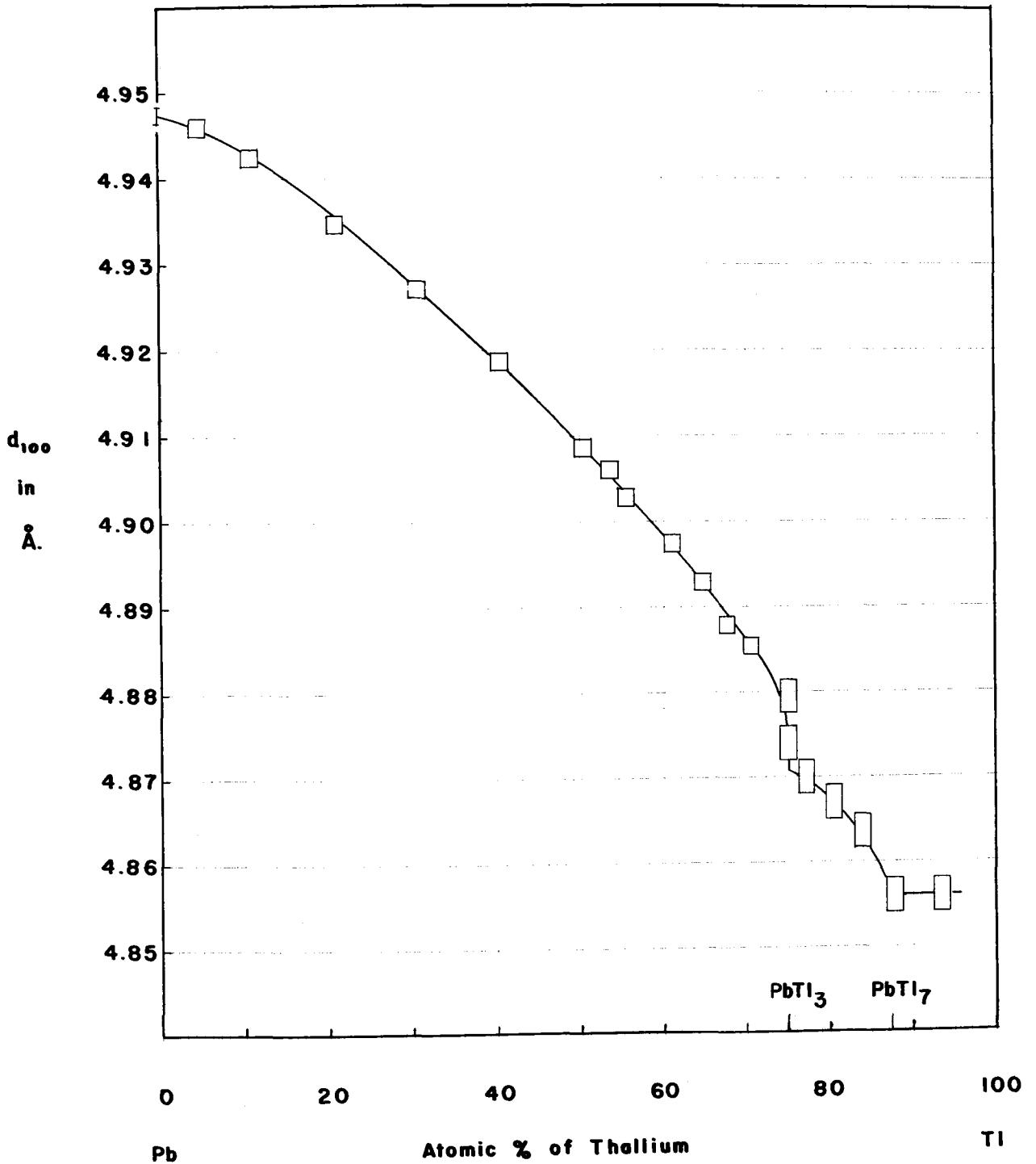


Figure 11. The lattice-spacing-composition curve based on the values given in Table 4. The edge lengths of squares and rectangles give the magnitude of uncertainties in d_{100} and composition.

Table IV

Specimen 1	Thallium Content			O Atomic %
d_{100}	$4.9474 \pm 0.001 \text{ \AA}$			
(hkl)	Σh^2	θ	$\sin \theta$	d_{100}
(111)	3	0.2771	0.27357	4.8810
(200)	4	0.3208	0.31533	4.8895
(220)	8	0.4606	0.44449	4.9054
(311)	11	0.5462	0.51944	4.9222
(222)	12	0.5733	0.54241	4.9234
(400)	16	0.6764	0.62599	4.9260
(331)	19	0.7490	0.68091	4.9350
(420)	20	0.7734	0.69857	4.9351
(422)	24	0.8713	0.76517	4.9356
(333) α 1	27	0.9438	0.80980	4.9425
(333) α 2	27	0.9482	0.81237	4.9390
(440) α 1	32	1.0793	0.88163	4.9422
(440) α 2	32	1.0845	0.88407	4.9409
(531) α 1	35	1.1728	0.92184	4.9433
(531) α 2	35	1.1789	0.92419	4.9429
(600), (442) α 1	36	1.2068	0.93448	4.9455
(600), (442) α 2	36	1.2138	0.93695	4.9448
(620) α 1	40	1.3965	0.98485	4.9464
(620) α 2	40	1.4104	0.98716	4.9472

Specimen 2-(1) (0.25 mm. ϕ)	Thallium Content			
d_{100}	$4.9460 \pm 0.0001 \text{ \AA}$	$4.9 \pm 1.0 \text{ Atomic \%}$		
(hkl)	Σh^2	θ	$\sin \theta$	d_{100}
(111)	3	0.2773	0.27376	4.8776
(200)	4	0.3210	0.31552	4.8865
(220)	8	0.4598	0.44377	4.9134
(311)	11	0.5462	0.51944	4.9222
(222)	12	0.5732	0.54232	4.9242
(400)	16	0.6754	0.62521	4.9321
(331)	19	0.7496	0.68135	4.9318
(420)	20	0.7731	0.69836	4.9366
(422)	24	0.8709	0.76491	4.9373
(333) α 1	27	0.9442	0.81003	4.9411
(333) α 2	27	0.9477	0.81208	4.9408
(440) α 1	32	1.0795	0.88172	4.9417
(440) α 2	32	1.0847	0.88416	4.9404
(531) α 1	35	1.1720	0.92153	4.9449

Table IV (Continued)

Specimen 2-(1)

(hkl)	Σh^2	θ	$\sin \theta$	d_{100}
(531) α 2	35	1.1781	0.92388	4.9446
(600), (442) α 1	36	1.2070	0.93455	4.9452
(600), (442) α 2	36	1.2148	0.93730	4.9429
(620) α 1	40	1.3972	0.98497	4.9458
(620) α 2	40	1.4121	0.98743	4.9459

Specimen 2-(2) (0.5 mm. ϕ) Thallium Content

(hkl)	Σh^2	θ	$\sin \theta$	d_{100}
$d_{100} \quad 4.9460 \pm 0.001 \text{ \AA.} \quad 4.9 \pm 1 \text{ Atomic \%}$				
(111)	3	0.2794	0.27578	4.8419
(200)	4	0.3222	0.31665	4.8691
(220)	8	0.4610	0.44484	4.9015
(311)	11	0.5483	0.52124	4.9052
(222)	11	0.5745	0.54342	4.9142
(400)	16	0.6776	0.62693	4.9186
(331)	19	0.7509	0.68230	4.9250
(420)	20	0.7745	0.69936	4.9295
(422)	24	0.8714	0.76523	4.9352
(333) α 1	27	0.9456	0.81085	4.9361
(333) α 2	27	0.9482	0.81237	4.9390
(440) α 1	32	1.0792	0.88158	4.9425
(440) α 2	32	1.0836	0.88365	4.9432
(531) α 1	35	1.1735	0.92211	4.9418
(531) α 2	35	1.1787	0.92411	4.9434
(600), (442) α 1	36	1.2076	0.93477	4.9440
(600), (442) α 2	36	1.2145	0.93720	4.9434
(620) α 1	40	1.3988	0.98525	4.9444
(620) α 2	40	1.4127	0.98753	4.9454

Table IV (Continued)

Specimen 3-(1) (0.25 mm. ϕ) Thallium Content

d_{100}	$4.942_4 \pm 0.001 \text{ \AA.}$	11.2 ± 0.5	Atomic %	
(hkl)	Σh^2	θ	$\sin \theta$	d_{100}
(111)	3	0.2772	0.27366	4.8973
(200)	4	0.3209	0.31542	4.8881
(220)	8	0.4607	0.44458	4.9044
(311)	11	0.5472	0.52030	4.9141
(222)	12	0.5743	0.54325	4.9158
(400)	16	0.6766	0.62615	4.9247
(331)	19	0.7491	0.68098	4.9345
(420)	20	0.7745	0.69936	4.9295
(422) α 1	24	0.8715	0.76530	4.9307
(422) α 2	24	0.8741	0.76697	4.9323
(333) α 1	27	0.9449	0.81044	4.9386
(333) α 2	27	0.9484	0.81248	4.9383
(440) α 1	32	1.0804	0.88215	4.9393
(440) α 2	32	1.0847	0.88416	4.9404
(531) α 1	35	1.1740	0.92261	4.9391
(531) α 2	35	1.1800	0.92461	4.9407
(600), (442) α 1	36	1.2097	0.93551	4.9401
(600), (442) α 2	36	1.2167	0.93796	4.9394
(620) α 1	40	1.4029	0.98594	4.9410
(620) α 2	40	1.4169	0.98818	4.9421

Specimen 3-(2) (0.50 mm. ϕ) Thallium Content

d_{100}	$4.942_4 \pm 0.001 \text{ \AA.}$	11.2 ± 0.5	Atomic %	
(hkl)	Σh^2	θ	$\sin \theta$	d_{100}
(220)	8	0.4642	0.44771	4.8701
(311)	11	0.5490	0.52183	4.8997
(222)	12	0.5752	0.54400	4.9090
(400)	16	0.6784	0.62755	4.9137
(331)	19	0.7527	0.68361	4.9155
(420)	20	0.7763	0.70064	4.9205
(422)	24	0.8733	0.76645	4.9274
(333) α 1	27	0.9476	0.81202	4.9289
(333) α 2	27	0.9511	0.81405	4.9288
(440) α 1	32	1.0823	0.88304	4.9343
(440) α 2	32	1.0866	0.88505	4.9354
(531) α 1	35	1.1767	0.92334	4.9352
(531) α 2	35	1.1819	0.92533	4.9368
(600), (442) α 1	36	1.2108	0.93590	4.9380
(600), (442) α 2	36	1.2169	0.93803	4.9391
(620) α 1	40	1.4031	0.98597	4.9408
(620) α 2	40	1.4188	0.98847	4.9407

Table IV (Continued)

Specimen 4 Thallium Content 21.1 \pm 0.5 Atomic %

d_{100} 4.934₇ \pm 0.001 Å.

(hkl)	Σh^2	θ	$\sin \theta$	d_{100}
(111)	3	0.2783	0.27472	4.8606
(200)	4	0.3220	0.31646	4.8720
(220)	8	0.4610	0.44484	4.9015
(311)	11	0.5475	0.52055	4.9117
(222)	12	0.5746	0.54350	4.9135
(400)	16	0.6786	0.62770	4.9125
(331)	19	0.7511	0.68244	4.9239
(420)	20	0.7764	0.70072	4.9199
(422) α 1	24	0.8743	0.76709	4.9233
(333) α 1	27	0.9477	0.81208	4.9286
(333) α 2	27	0.9503	0.81359	4.9316
(440) α 1	32	1.0832	0.88346	4.9320
(440) α 2	32	1.0875	0.88547	4.9331
(531) α 1	35	1.1775	0.92365	4.9336
(531) α 2	35	1.1845	0.92631	4.9316
(600), (442) α 1	36	1.2134	0.9368	4.9332
(600), (442) α 2	36	1.2204	0.93924	4.9327
(620) α 1	40	1.4109	0.98724	4.9345
(620) α 2	40	1.4275	0.98975	4.9343

Specimen 5 Thallium Content 30.8 \pm 1.0 Atomic %

d_{100} 4.927₁ \pm 0.001 Å.

(hkl)	Σh^2	θ	$\sin \theta$	d_{100}
(111)	3	0.2779	0.27434	4.8673
(200)	4	0.3215	0.31599	4.8793
(220)	8	0.4611	0.44493	4.9005
(311)	11	0.5484	0.52132	4.9045
(222)	12	0.5754	0.54417	4.9075
(400)	16	0.6775	0.62685	4.9192
(331)	19	0.7517	0.68288	4.9208
(420)	20	0.7770	0.70114	4.9170
(422) α 1	24	0.8739	0.76684	4.9208
(422) α 2	24	0.8774	0.76908	4.9187
(333) α 1	27	0.9489	0.81278	4.9243
(333) α 2	27	0.9524	0.81481	4.9242
(440) α 1	32	1.0868	0.88514	4.9226
(440) α 2	32	1.0912	0.88718	4.9236
(531) α 1	35	1.1819	0.92533	4.9246
(531) α 2	35	1.1889	0.92796	4.9228
(600), (442) α 1	36	1.2177	0.93831	4.9253
(600), (442) α 2	36	1.2247	0.94070	4.9250
(620) α 1	40	1.4202	0.98868	4.9273
(620) α 2	40	1.4394	0.99138	4.9262

Table IV (Continued)

Specimen 6 Thallium Content 40.6 \pm 1.0 Atomic %

d_{100} 4.918₇ \pm 0.001 Å.

(hkl)	$\sum h^2$	θ	$\sin \theta$	d_{100}
(111)	3	0.2762	0.27270	4.8966
(200)	4	0.3207	0.31523	4.8910
(220)	8	0.4612	0.44502	4.8996
(311)	11	0.5485	0.52141	4.9036
(222)	12	0.5756	0.54434	4.9059
(400)	16	0.6786	0.62770	4.9125
(331)	19	0.7528	0.68368	4.9150
(420)	20	0.7781	0.70193	4.9115
(422)	24	0.8767	0.76863	4.9094
(422)	24	0.8793	0.77029	4.9110
(333) α 1	27	0.9518	0.81446	4.9142
(333) α 2	27	0.9561	0.81695	4.9113
(440) α 1	32	1.0888	0.88607	4.9174
(440) α 2	32	1.0932	0.88810	4.9185
(531) α 1	35	1.1857	0.92676	4.9170
(531) α 2	35	1.1918	0.92904	4.9171
(600), (442) α 1	36	1.2224	0.93992	4.9169
(600), (442) α 2	36	1.2285	0.94199	4.9183
(620) α 1	40	1.4327	0.99048	4.9183
(620) α 2	40	1.4519	0.99294	4.9184

Specimen 7 Thallium Content 50.4 \pm 0.5 Atomic %

d_{100} 4.908₆ \pm 0.001 Å.

(hkl)	$\sum h^2$	θ	$\sin \theta$	d_{100}
(111)	3	0.2801	0.27645	4.8302
(200)	4	0.3229	0.31732	4.8588
(220)	8	0.4636	0.44717	4.8760
(311)	11	0.5510	0.52354	4.8837
(222)	12	0.5781	0.54643	4.8872
(400)	16	0.6829	0.63105	4.8865
(331)	19	0.7572	0.68689	4.8920
(420)	20	0.7817	0.70449	4.8936
(422)	24	0.8795	0.77042	4.9020
(333) α 1	27	0.9564	0.81712	4.8982
(333) α 2	27	0.9599	0.81913	4.8982
(440) α 1	32	1.0936	0.88829	4.9052
(440) α 2	32	1.0989	0.89071	4.9041
(531) α 1	35	1.1915	0.92893	4.9055
(531) α 2	35	1.1976	0.93117	4.9059
(600), (442) α 1	36	1.2291	0.94219	4.9051
(600), (442) α 2	36	1.2370	0.94481	4.9036
(620) α 1	40	1.4484	0.99252	4.9082
(620) α 2	40	1.4703	0.99495	4.9085

Table IV (Continued)

Specimen 8 Thallium Content 53.5 \pm 1.0 Atomic %

d_{100} 4.906₂ \pm 0.001 Å.

(hkl)	Σh^2	θ	$\sin \theta$	d_{100}
(111)	3	0.2801	0.27645	4.8302
(200)	4	0.3237	0.31808	4.8472
(220)	8	0.4651	0.44851	4.8614
(311)	11	0.5523	0.52465	4.8733
(222)	12	0.5794	0.54752	4.8774
(400)	16	0.6832	0.63128	4.8847
(331)	19	0.7574	0.68703	4.8911
(420)	20	0.7827	0.70520	4.8887
(422) α 1	24	0.8805	0.77106	4.8939
(422) α 2	24	0.8831	0.77271	4.9856
(333) α 1	27	0.9564	0.81712	4.8982
(333) α 2	27	0.9599	0.81913	4.8982
(440) α 1	32	1.0952	0.88902	4.9011
(440) α 2	32	1.0987	0.89062	4.9047
(531) α 1	35	1.1920	0.92911	4.9046
(531) α 2	35	1.1990	0.93168	4.9032
(600), (442) α 1	36	1.2296	0.94236	4.9042
(600), (442) α 2	36	1.2374	0.94494	4.9030
(620) α 1	40	1.4521	0.99296	4.9060
(620) α 2	40	1.4757	0.99548	4.9059

Specimen 9 Thallium Content 55.4 \pm 1.0 Atomic %

d_{100} 4.902₈ \pm 0.001 Å.

(hkl)	Σh^2	θ	$\sin \theta$	d_{100}
(111)	3	0.2795	0.27588	4.8401
(200)	4	0.3232	0.31760	4.8545
(220)	8	0.4647	0.44815	4.8653
(311)	11	0.5520	0.52439	4.8758
(222)	12	0.5790	0.54719	4.8804
(400)	16	0.6830	0.63112	4.8859
(331)	19	0.7581	0.68754	4.8874
(420)	20	0.7825	0.70505	4.8897
(422) α 1	24	0.8803	0.77093	4.8947
(422) α 2	24	0.8838	0.77315	4.8928
(333) α 1	27	0.9572	0.81758	4.8954
(333) α 2	27	0.9607	0.81959	4.8955
(440) α 1	32	1.0969	0.88980	4.8968
(440) α 2	32	1.1012	0.89175	4.8983
(531) α 1	35	1.1938	0.92977	4.9011
(531) α 2	35	1.2017	0.93265	4.8981
(600), (422) α 1	36	1.2328	0.94342	4.8987
(600), (422) α 2	36	1.2392	0.94552	4.8999
(620) α 1	40	1.4584	0.99369	4.9024
(620) α 2	40	1.4828	0.99613	4.9027

Table IV (Continued)

Specimen 10 Thallium Content 61.1 \pm 1.0 Atomic %

d_{100} 4.897₄ \pm 0.001 $\overset{\circ}{\text{A}}$.

(hkl)	$\sum h^2$	θ	$\sin \theta$	d_{100}
(111)	3	0.2802	0.27655	4.8284
(200)	4	0.3238	0.31817	4.8458
(200)	8	0.4652	0.44860	4.8605
(311)	11	0.5525	0.52482	4.8718
(222)	12	0.5804	0.54836	4.8700
(400)	16	0.6851	0.63275	4.8733
(331)	19	0.7593	0.68841	4.8812
(420)	20	0.7837	0.70590	4.8838
(422)	24	0.8823	0.77220	4.8867
(422)	24	0.8858	0.77442	4.8848
(333) \times 1	27	0.9591	0.81868	4.8888
(333) \times 2	27	0.9626	0.82068	4.8890
(440) \times 1	32	1.0988	0.89066	4.8921
(440) \times 2	32	1.1031	0.89261	4.8936
(531) \times 1	35	1.1974	0.93109	4.8942
(531) \times 2	35	1.2035	0.93330	4.8947
(600), (442) \times 1	36	1.2340	0.94382	4.8966
(600), (442) \times 2	36	1.2419	0.94640	4.8954
(620) \times 1	40	1.4679	0.99471	4.8974

Specimen 11-(1) Thallium Content 64.7 \pm 1.0 Atomic %

d_{100} 4.892₉ \pm 0.001 $\overset{\circ}{\text{A}}$.

(hkl)	$\sum h^2$	θ	$\sin \theta$	d_{100}
(111)	3	0.2807	0.27703	4.8201
(200)	4	0.3252	0.31950	4.8257
(220)	8	0.4657	0.44905	4.8556
(311)	11	0.5530	0.52524	4.8679
(222)	12	0.5819	0.54961	4.8589
(400)	16	0.6857	0.63321	4.8698
(331)	19	0.7591	0.68827	4.8822
(420)	20	0.7844	0.70640	4.8804
(422)	24	0.8848	0.77379	4.8807
(333) \times 1	27	0.9607	0.81959	4.8834
(333) \times 2	27	0.9642	0.82159	4.8836
(440) \times 1	32	1.1013	0.89180	4.8858
(440) \times 2	32	1.1057	0.89378	4.8872
(531) \times 1	35	1.1991	0.93171	4.8909
(531) \times 2	35	1.2052	0.93391	4.8915
(600), (442) \times 1	36	1.2375	0.94497	4.8906
(600), (442) \times 2	36	1.2453	0.94749	4.8898
(620) \times 1	40	1.4775	0.99565	4.8928

Table IV (Continued)

Specimen 11-(2) Thallium Content 64.7 \pm 1.0 Atomic %

d_{100} 4.892₉ \pm 0.001 $\overset{\circ}{\text{A}}$.

(hkl)	$\sum h^2$	θ	$\sin \theta$	d_{100}
(111)	3	0.2806	0.27693	4.8218
(200)	4	0.3242	0.31855	4.8401
(220)	8	0.4664	0.44967	4.8489
(311)	11	0.5536	0.52575	4.8631
(222)	12	0.5816	0.54936	4.8611
(400)	16	0.6854	0.63298	4.8716
(331)	19	0.7604	0.68921	4.8756
(420)	20	0.7848	0.70668	4.8784
(422) α 1	24	0.8852	0.77404	4.8791
(422) α 2	24			
(333) α 1	27	0.9602	0.81931	4.8851
(333) α 2	27	0.9645	0.82176	4.8826
(440) α 1	32	1.1006	0.89148	4.8876
(440) α 2	32	1.1059	0.89387	4.8867
(531) α 1	35	1.1992	0.93175	4.8907
(531) α 2	35	1.2062	0.93427	4.8896
(600), (442) α 1	36	1.2367	0.94471	4.8920
(600), (442) α 2	36	1.2455	0.94756	4.8894
(620) α 1	40	1.4784	0.99573	4.8924

Specimen 12 Thallium Content 67.6 \pm 1.0 Atomic %

d_{100} 4.887₈ \pm 0.001 $\overset{\circ}{\text{A}}$.

(hkl)	$\sum h^2$	θ	$\sin \theta$	d_{100}
(111)	3	0.2813	0.27760	4.8102
(200)	4	0.3241	0.31846	4.8414
(220)	8	0.4650	0.44842	4.8624
(311)	11	0.5534	0.52558	4.8647
(222)	12	0.5805	0.54844	4.8693
(400)	16	0.6846	0.63236	4.8763
(331)	19	0.7590	0.68820	4.8827
(420)	20	0.7843	0.70633	4.8809
(422) α 1	24	0.8841	0.77334	4.8795
(422) α 2	24	0.8876	0.77556	4.8776
(333) α 1	27	0.9611	0.81982	4.8820
(333) α 2	27	0.9646	0.82182	4.8822
(440) α 1	32	1.1010	0.98166	4.8866
(440) α 2	32	1.1063	0.89405	4.8857
(531) α 1	35	1.2017	0.93265	4.8860
(531) α 2	35	1.2087	0.93516	4.8849
(600), (442) α 1	36	1.2402	0.94585	4.8861
(600), (442) α 2	36	1.2472	0.94810	4.8866
(620) α 1	40	1.4895	0.99670	4.8876

Table IV (Continued)

Specimen 13 Thallium Content 70.6 \pm 1.0 Atomic %

d_{100} 4.885₅ \pm 0.001 Å.

(hkl)	Σh^2	θ	$\sin \theta$	d_{100}
(111)	3	0.2807	0.27703	4.8201
(200)	4	0.3244	0.31874	4.8372
(220)	8	0.4660	0.44932	4.8527
(311)	11	0.5534	0.52558	4.8647
(222)	12	0.5814	0.54919	4.8626
(400)	16	0.6854	0.63298	4.8716
(331)	19	0.7606	0.68936	4.8745
(420)	20	0.7850	0.70683	4.8774
(422) α 1	24	0.8847	0.77372	4.8771
(422) α 2	24	0.8891	0.77650	4.8717
(333) α 1	27	0.9625	0.82062	4.8773
(333) α 2	27	0.9660	0.82262	4.8775
(440) α 1	32	1.1041	0.89306	4.8790
(440) α 2	32	1.1076	0.89463	4.8826
(531) α 1	35	1.2028	0.93305	4.8839
(531) α 2	35	1.2089	0.93523	4.8846
(600), (442) α 1	36	1.2413	0.94621	4.8842
(600), (442) α 2	36	1.2491	0.94870	4.8835
(620) α 1	40	1.4956	0.99717	4.8853

Specimen 14-(1) Thallium Content 75.0 \pm 1.0 Atomic %

d_{100} 4.879₅ \pm 0.002 Å.

(hkl)	Σh^2	θ	$\sin \theta$	d_{100}
(111)	3	0.2811	0.27741	4.8135
(200)	4	0.3248	0.31912	4.8314
(220)	8	0.4663	0.44958	4.8499
(311)	11	0.5537	0.52584	4.8623
(222)	12	0.5817	0.54945	4.8603
(400)	16	0.6865	0.63383	4.8650
(331)	19	0.7608	0.68950	4.8735
(420)	20	0.7861	0.70760	4.8721
(422) α 1	24	0.8857	0.77436	4.8731
(422) α 2	24	0.8884	0.77606	4.8745
(333) α 1	27	0.9626	0.82068	4.8769
(333) α 2	27	0.9661	0.82267	4.8772
(440) α 1	32	1.1051	0.89351	4.8765
(440) α 2	32	1.1094	0.89543	4.8782
(531) α 1	35	1.2064	0.93434	4.8771
(531) α 2	35	1.2134	0.93681	4.8763
(600), (442) α 1	36	1.2440	0.94708	4.8797
(600), (442) α 2	36	1.2527	0.94983	4.8777

Table IV (Continued)

Specimen 14-(2) Thallium Content 75.0 \pm 1.0 Atomic %

d_{100} 4.874₀ \pm 0.002 Å.

(hkl)	Σh^2	θ	$\sin \theta$	d_{100}
(111)	3	0.2811	0.27741	4.8135
(200)	4	0.3257	0.31997	4.8186
(220)	8	0.4673	0.45048	4.8402
(311)	11	0.5555	0.52737	4.8482
(222)	12	0.5835	0.55095	4.8471
(400)	16	0.6892	0.63592	4.8490
(331)	19	0.7644	0.69210	4.8552
(420)	20	0.7880	0.70894	4.8629
(422)	24	0.8885	0.77613	4.8659
(422)	24			
(333) α 1	27	0.9654	0.82228	4.8674
(333) α 2	27	0.9694	0.82455	4.8660
(440) α 1	32	1.1078	0.89472	4.8699
(440) α 2	32	1.1131	0.89707	4.8693
(531) α 1	35	1.2092	0.93533	4.8720
(531) α 2	35	1.2162	0.93779	4.8712
(600), (442) α 1	36	1.2476	0.94823	4.8738
(600), (442) α 2	36	1.2555	0.95070	4.8733

Specimen 15 Thallium Content 77.1 \pm 1.0 Atomic %

d_{100} 4.870₀ \pm 0.002 Å.

(hkl)	Σh^2	θ	$\sin \theta$	d_{100}
(111)	3	0.2815	0.27780	4.8067
(200)	4	0.3269	0.32111	4.8015
(220)	8	0.4675	0.45066	4.8382
(311)	11	0.5557	0.52754	4.8466
(222)	12	0.5836	0.55103	4.8464
(400)	16	0.6884	0.63530	4.8538
(331)	19	0.7634	0.69138	4.8603
(420)	20	0.7888	0.70951	4.8590
(422)	24	0.8900	0.77707	4.8601
(333) α 1	27	0.9668	0.82307	4.8628
(333) α 2	27	0.9695	0.82460	4.8658
(440) α 1	32	1.1109	0.89610	4.8624
(440) α 2	32	1.1153	0.89804	4.8640
(531) α 1	35	1.2113	0.93607	4.8681
(531) α 2	35	1.2191	0.93879	4.8661
(600), (442) α 1	36	1.2506	0.94917	4.8690
(600), (442) α 2	36	1.2584	0.95160	4.8686

Table IV (Continued)

Specimen 16 Thallium Content 80.5 \pm 1.0 Atomic %

d_{100} 4.867₁ \pm 0.002 $\overset{\circ}{\text{A}}$.

(hkl)	Σh^2	θ	$\sin \theta$	d_{100}
(111)	3	0.2815	0.27780	4.8067
(200)	4	0.3253	0.31959	4.8243
(220)	8	0.4678	0.45092	4.8354
(311)	11	0.5561	0.52788	4.8435
(222)	12	0.5841	0.55145	4.8427
(400)	16	0.6890	0.63577	4.8502
(331)	19	0.7642	0.69196	4.8564
(420)	20	0.7895	0.71000	4.8556
(422) α 1	24	0.8883	0.77600	4.8628
(422) α 2	24	0.8927	0.77877	4.8575
(333) α 1	27	0.9679	0.82370	4.8591
(333) α 2	27	0.9714	0.82568	4.8594
(440) α 1	32	1.1113	0.89628	4.8614
(440) α 2	32	1.1157	0.89822	4.8631
(531) α 1	35	1.2127	0.93657	4.8655
(531) α 2	35	1.2197	0.93900	4.8650
(600), (442) α 1	36	1.2530	0.94993	4.8651
(600), (442) α 2	36	1.2599	0.95206	4.8663

Specimen 17 Thallium Content 83.9 \pm 1.0 Atomic %

d_{100} 4.863₆ \pm 0.002 $\overset{\circ}{\text{A}}$.

(hkl)	Σh^2	θ	$\sin \theta$	d_{100}
(111)	3	0.2800	0.27636	4.8317
(200)	4	0.3246	0.31893	4.8343
(220)	8	0.4679	0.45101	4.8345
(311)	11	0.5552	0.52711	4.8506
(222)	12	0.5832	0.55070	4.8493
(400)	16	0.6880	0.63499	4.8561
(331)	19	0.7640	0.69182	4.8572
(420)	20	0.7894	0.70993	4.8561
(422) α 1	24	0.8898	0.77695	4.8568
(422) α 2	24	0.8933	0.77914	4.8552
(333) α 1	27	0.9676	0.82353	4.8601
(333) α 2	27	0.9720	0.82601	4.8574
(440) α 1	32	1.1118	0.89650	4.8602
(440) α 2	32	1.1161	0.89839	4.8621
(531) α 1	35	1.2148	0.93730	4.8617
(531) α 2	35	1.2201	0.93913	4.8643
(600), (442) α 1	36	1.2542	0.95030	4.8632
(600), (442) α 2	36	1.2620	0.95270	4.8630

Table IV (Continued)

Specimen 18 Thallium Content 87.8 \pm 1.0 Atomic %

$d_{100} = 4.856_0 \pm 0.002 \overset{0}{\text{Å}}$

(hkl)	Σh^2	θ	$\sin \theta$	d_{100}
(111)	3	0.2822	0.27847	4.7951
(200)	4	0.3268	0.32101	4.8030
(220)	8	0.4699	0.45280	4.8154
(311)	11	0.5581	0.52958	4.8280
(222)	12	0.5860	0.55303	4.8289
(400)	16	0.6908	0.63715	4.8397
(331)	19	0.7668	0.69383	4.8431
(420)	20	0.7929	0.71239	4.8393
(422)	24	0.8933	0.77914	4.8471
(422)	24			
(333) α 1	27	0.9710	0.82545	4.8487
(333) α 2	27	0.9763	0.82843	4.8433
(440) α 1	32	1.1160	0.89835	4.8502
(440) α 2	32	1.1203	0.90023	4.8522
(531) α 1	35	1.2198	0.93903	4.8528
(531) α 2	35	1.2259	0.94111	4.8541
(600), (442) α 1	36	1.2600	0.95209	4.8541
(600), (442) α 2	36	1.2679	0.95448	4.8540

Specimen 19 Thallium Content 93.4 \pm 1.0 Atomic %

$d_{100} = 4.856_4 \pm 0.002 \overset{0}{\text{Å}}$

(hkl)	Σh^2	θ	$\sin \theta$	d_{100}
(111)	3	0.2827	0.27895	4.7771
(200)	4	0.3270	0.32120	4.7915
(220)	8	0.4688	0.45182	4.8162
(311)	11	0.5574	0.52898	4.8237
(222)	12	0.5852	0.55237	4.8249
(400)	16	0.6898	0.63638	4.8358
(331)	19	0.7659	0.69319	4.8378
(420)	20	0.7913	0.71127	4.8373
(422)	24	0.8923	0.77852	4.8413
(333)	27	0.9709	0.82539	4.8433
(440) α 1	32	1.1138	0.89738	4.8457
(440) α 2	32	1.1192	0.89975	4.8450
(531) α 1	35	1.2178	0.93834	4.8465
(531) α 2	35	1.2247	0.94070	4.8464
(600), (442) α 1	36	1.2591	0.95182	4.8457
(600), (442) α 1	36	1.2670	0.95421	4.8456

6. CRITICAL REVIEW OF PREVIOUS WORK ON THE ALLOY SYSTEM

The result of Kurnakow and Pushin's work⁽³⁾ on the phase diagram is given in Figure 12(1), Lewkonja⁽⁴⁾ obtained almost the same result except that she found the maximum point at 33.5 atomic percent of lead, which corresponds to the formula $PbTl_2$. Hence, she suggested the compound $PbTl_2$ as shown in Figure 12(2). However, Kurnakow⁽⁵⁾ disproved the existence of this compound by the following three arguments:

1) The position of the maximum point after careful determination on a great number of samples lies between 35.7 and 37.5 atomic percent of lead, which does not correspond to any simple rational formula.

2) Microscopic study shows that pure lead and the entire series of lead-phase alloys up to 75.7 atomic percent of thallium crystallize in the form of regular octahedrons, while thallium and the solid solutions containing up to 6 percent of lead give hexagonal stars and plates. If the compound $PbTl_2$ should exist, it probably would give a break in the crystal form at 33.5 percent of lead.

3) On introducing a third component to the system, the maximum point is strongly shifted. Therefore the composition of the maximum point is variable and cannot correspond to any compound of constant ratio.

Furthermore, Kurnakow and Schemtschushny⁽⁶⁾ measured the electrical conductivities of a series of lead-thallium alloys at room temperature, and found no evidence for the existence

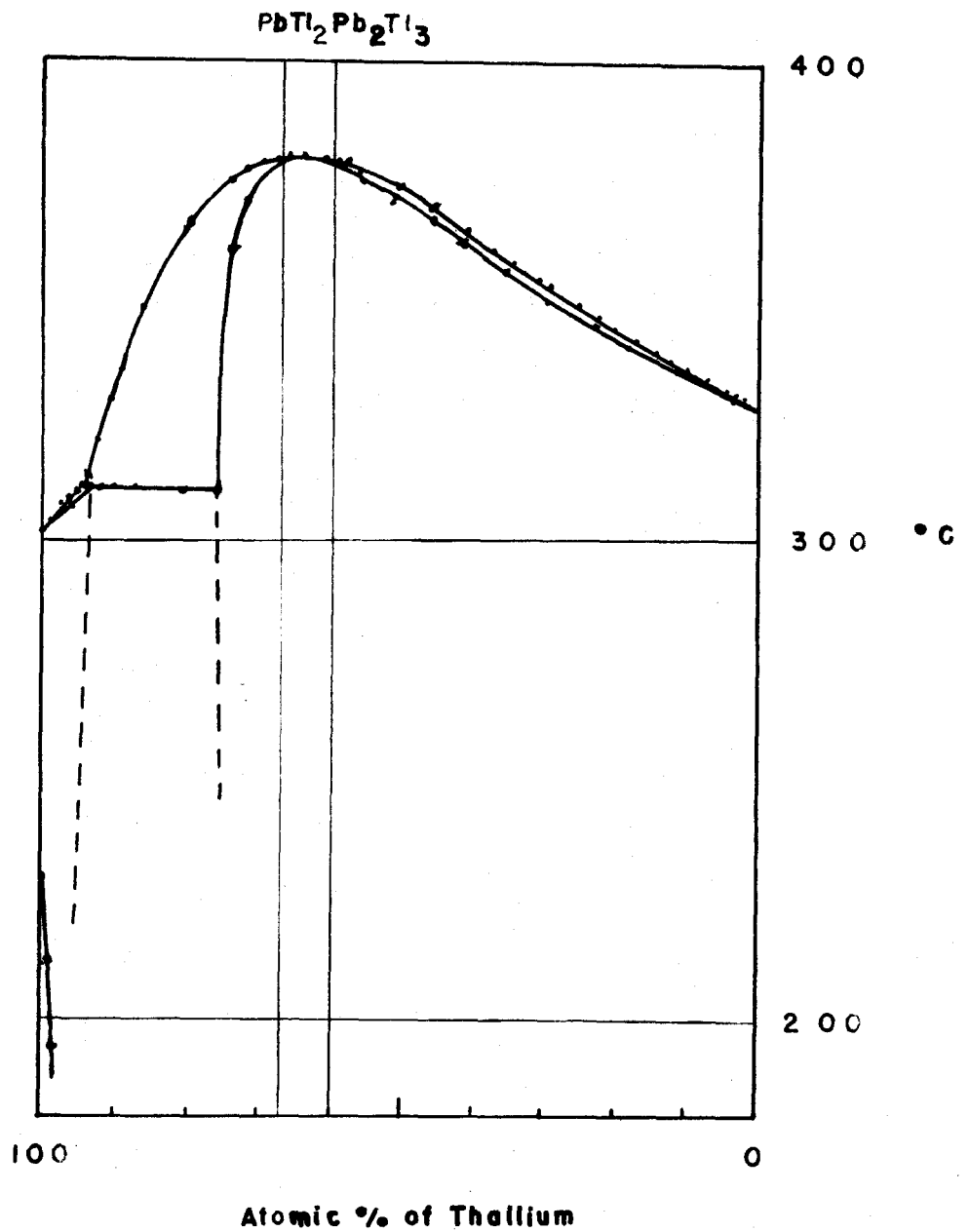


Figure 12 (1). The curves in the upper part of the phase diagram of the alloy system lead-thallium as determined by Kurnakow and Pushin.

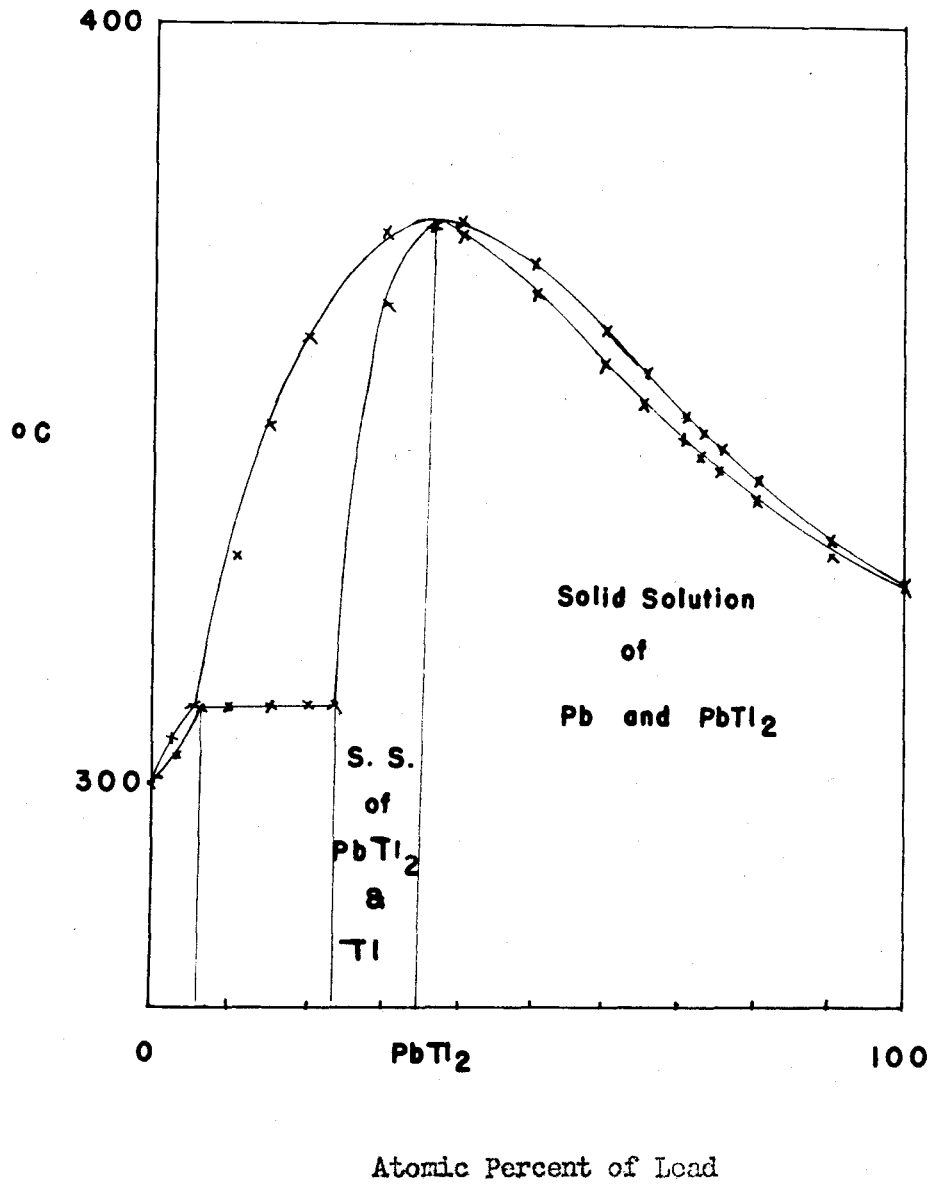


Figure 12 (2). The curves in the upper part of the phase diagram as determined and interpreted by Lewkonja.

of a compound (Figure 16-(a)). Guertler and Schulze⁽⁷⁾ investigated the electrical conductivities over a temperature range of 0° to 250°C and obtained the curves in the lower part of the phase diagram as shown in Figure 14. The result of their determination is reproduced in Figure 13.

McMillan and Pauling⁽⁸⁾ investigated this alloy system by the X-ray powder method. Table V is taken from their work.

Table V.

Alloy No.	1	2	3	4	5	6	7	8	9	10
Atomic % of Pb	0	4	7	10	20	25	33.3	45	75	100
Pattern shown	Tl	Tl 4	Tl lines	3 Tl	Pb	Pb	Pb	Pb	Pb	Pb
		4 Pb lines	5 Pb lines	Pb						
d_{100} for Pb phase kX. U.						4.864	4.892	4.948		
						4.858	4.879	4.920		

This result confirms the conclusion that the lead phase is homogeneous, and is against the existence of the compound $PbTl_2$. The lattice spacings with a probable error of 0.1 percent are given in Table V and in Figure 15.

F. Halla and R. Stauffer⁽⁹⁾ prepared a single crystal out of an alloy containing 35 atomic percent of lead. They suspected that the alloy No. 7 of McMillan and Pauling might not be in the most stable state. However, their single crystal gave within the limits of error the same result as the powders of the alloy No. 7 of McMillan and Pauling.

A. Olander⁽¹⁾ investigated this alloy system by the method of electrode potential and by the X-ray powder method. The result by the latter method has actually induced this work.

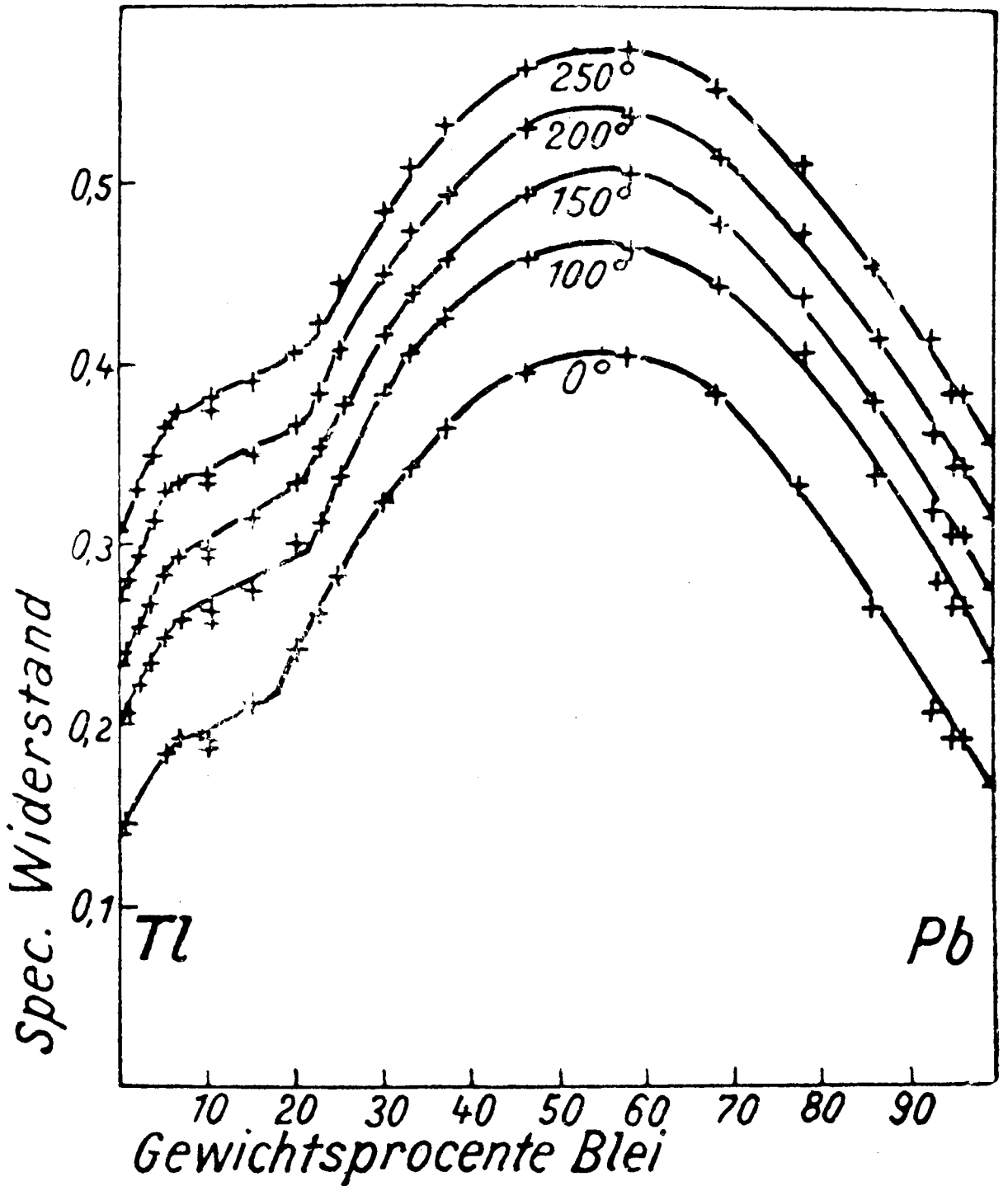


Figure 13. The resistivities of the lead-thallium alloys over a temperature range of 0 to 250°C as determined by Guertler and Schulze.

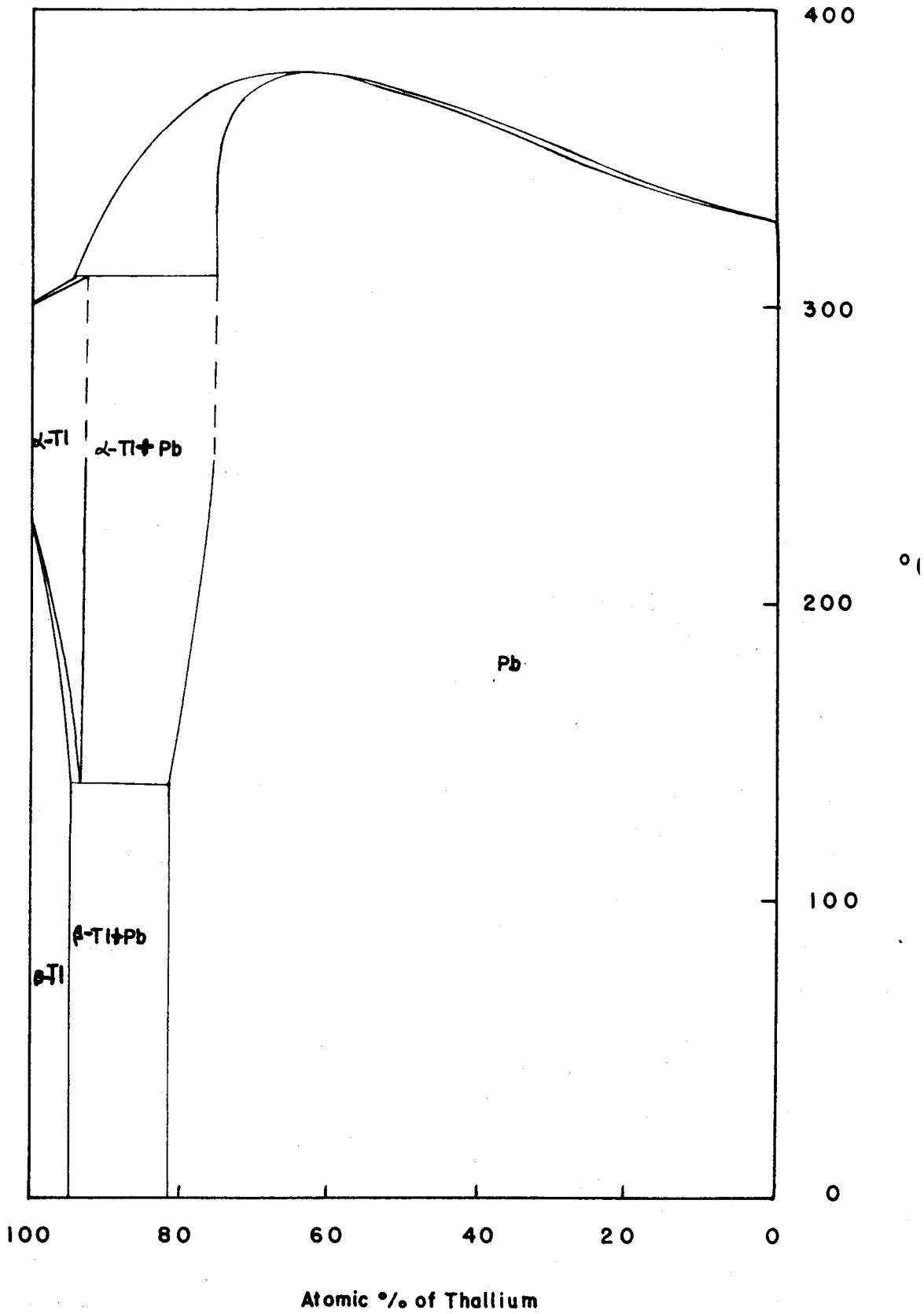
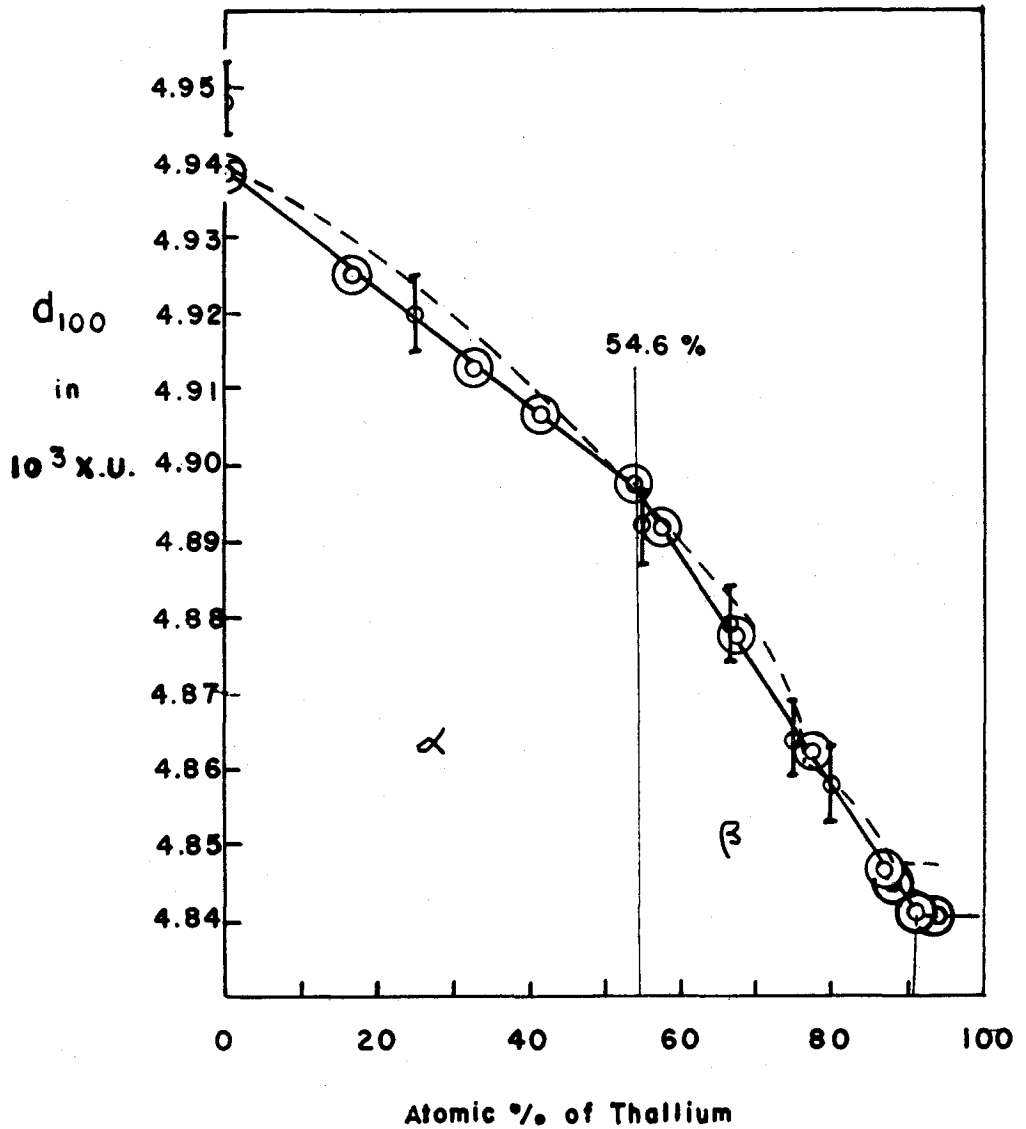


Figure 14. The phase diagram constructed on the basis of the result of Kurnakow's work and their own work by Guertler and Schulze.







-  Ölander
-  McMillan and Pauling
-  Ölander
-  Tang

Figure 15. The two-straight-line result as reported by Ölander. McMillan and Pauling's values are given for comparison. The new lattice-spacing-composition curve is also included.

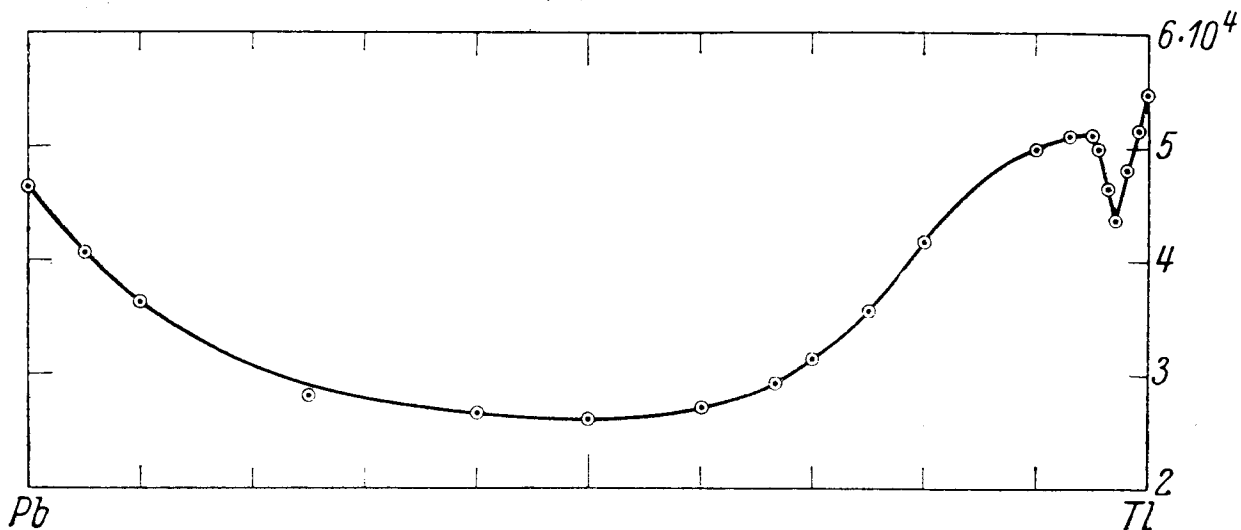
"
Olander made twelve alloy samples by melting the metals together at 270°C in evacuated quartz tubes for 4 days, filed the samples, and annealed the filings in evacuated glass tubes at 250°C for 20 minutes. The filings were photographed with Chromium K radiation. The following ten lines were observed and measured: $K\alpha_1$ and $K\alpha_2$ of the orders 311, 222 and 400 and $K\beta_1$ of the orders 222, 400, 331 and 420. The result is given in Table VI.

Table VI.

Atomic % of Tl	0	16.7	32.8	41.4	53.9	57.5
d_{100} in KX. U.	4.9382	4.9251	4.9129	4.9068	4.8974	4.8919
Atomic % of Tl	67.6	77.7	87.2	88.5	91.4	94.0
d_{100} in KX. U.	4.8775	4.8622	4.8468	4.8450	4.8411	4.8407

He claimed that the precision of his determination was better than one part in five thousand. I shall show that this estimate of error cannot be correct. His lattice spacing-composition plot is reproduced in Figure 15 with solid lines. It consists of two straight lines intersecting at 54.6 percent of thallium. Besides he found that the boundary between the lead-phase and the two-phase region lies at 91 atomic percent of thallium. Figure 16-(B) gives the phase diagram revised by Olander. He formulated a new phase β to take care of the transition point at 54.6 percent of thallium. He also moved the boundary between the lead phase and the two-phase region from 75 percent to 91 percent of thallium.

(a)



(b)

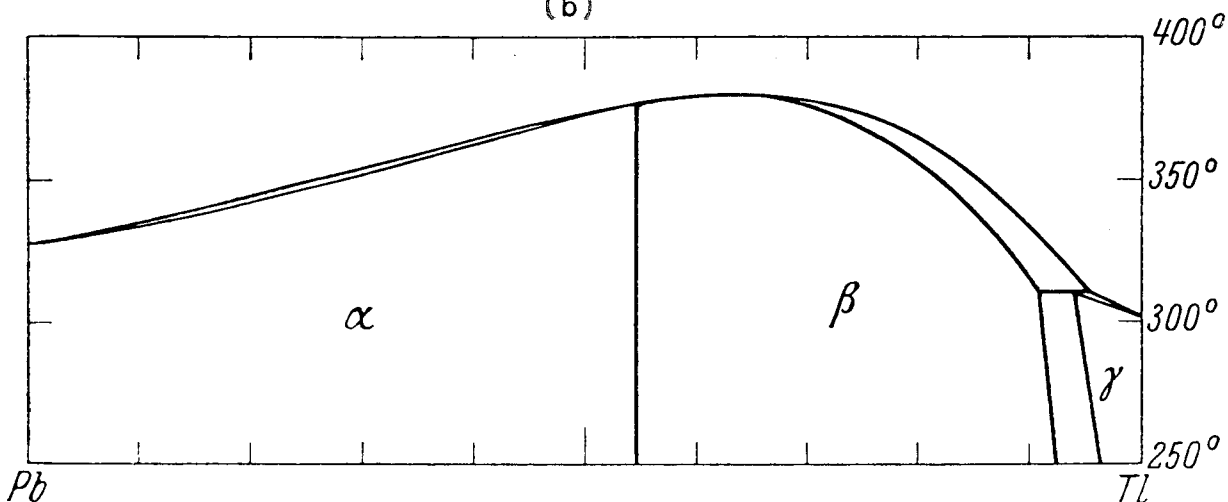


Figure 16. (a) Conductivities of the lead-thallium alloys at 18°C as taken from Kurnakow and Schemtschushny's work.

(b) The phase diagram as revised and interpreted by Olander largely on the basis of his X-ray investigation at room temperature.

First, on the basis of the fact that one cannot draw any straight line passing through all the squares between 0 to 55 percent of thallium in Figure 11, one may conclude that within safe limits of experimental error such a two-straight-line result as reported by Olander does not exist. The formulation of the phase β is ad hoc.

Second, his revised phase diagram is incompatible with the results of thermal analysis. He did not explain why or on the basis of what evidence he had to move the boundary to 91 percent of thallium even for elevated temperatures. The discrepancy of 16 percent (91-75) is well beyond the limits of experimental error of thermal analysis.

The maximum Bragg angle he observed for the $K\alpha_2$ line of the order 400 on his photographs with chromium radiation varied from 68 to 71 degrees over the complete composition range of the lead phase. The random error limits for d_{100} at such a Bragg angle can be two or three parts in five thousand. Besides, it is rather doubtful that he had taken adequate care of the absorption error. Absorption error is extremely important for the lead-thallium alloys, especially when one observes a low maximum Bragg angle.

He figured out that the two-phase region starts at 91 percent thallium (Figure 15 and 16(b)). However, McMillan and Pauling observed 3 thallium lines on the photograph for their alloy sample No. 4, which contained 90 percent thallium. I found that within the limits of experimental error my alloy

samples 18 and 19 have almost the same d_{100} . Should this be correct, the two-phase region would start at 87.5 percent of thallium (Figure 11). It is certain that at room temperature the lower limit of the two-phase region lies in the neighborhood of 87.5 percent instead of 75 percent of thallium.

However, the fact remains unexplained that even at room temperature a break in crystal habit as observed with the microscope occurs at 75 percent thallium.

The conductivity data determined by the two groups^{(6),(7)} made it quite clear that a compound such as $PbTl_2$ or Pb_2Tl_3 corresponding to the maximum point on the freezing point curve does not exist. I shall show in the next section that the data can be interpreted satisfactorily in the light of the probable structure I shall propose, despite the fact that they are rather incomplete.

7. THE PROBABLE STRUCTURE OF THE ALLOYS IN THE LEAD PHASE

In Section 4 I have limited the theoretical possibilities of the superstructures. Due to the fact that lead and thallium are almost equally good scatterers for X-rays, the diffraction pattern alone does not help us to pick the superstructures out of the theoretically possible varieties. However, the experimental evidence in Figure 11 indicates that the superstructures $PbTl_3$ and $PbTl_7$ probably occur.

The resistivity data reveal that the alloys containing thallium up to 75 percent may have a structure based on the

formula $Pb (Pb,Tl)_3$ or a structure for the random solid solution of the two components $Pb Pb_3$ and $Pb Tl_3$. I plot the resistivity data against the mole-percentage of $PbTl_3$ in Figure 17. The maximum point is only a little shifted from the center line at 50 percent to the side of $PbTl_3$, which is a poorer conductor than lead. The slope on each side of the maximum point is approximately same. These features are characteristic of a complete series of disordered alloys⁽¹⁰⁾, for example, the system indium-lead.

I believe that from 75 percent of thallium on the phase $(Pb,Tl) Pb Tl_6$ begins to occur. This is strongly indicated by the lattice-spacing--composition curve in Figure 11. The microscopic study shows that from 75 percent up the alloys cease to appear in the form of octahedra. If $(Pb,Tl) Pb Tl_6$ occurs, such a break in the habit of crystallization at 75 percent is expected. $(Pb,Tl) Pb Tl_6$ is based upon a cubic face-centered lattice with a unit cell eight times larger than the $5\text{-}\overset{\circ}{A}$ cube (Figures 6 and 7). The asymmetric octant in Figure 7-(1) does not have the symmetry of a cube or octahedron as the unit cell for $PbTl_3$ in Figure 7-(2), but has only the symmetry of a tetrahedron.

The conductivity data taken from Kurnakow and Schemtshushny's⁽⁶⁾ work is presented in Figure 18. I drew a proper curve for the phases $Pb Pb_3$, $Pb (Pb,Tl)_3$ and $PbTl_3$ and a straight line for the two-phase alloys. I believe, if we had enough data between 75 and 87.5 percent, we probably would

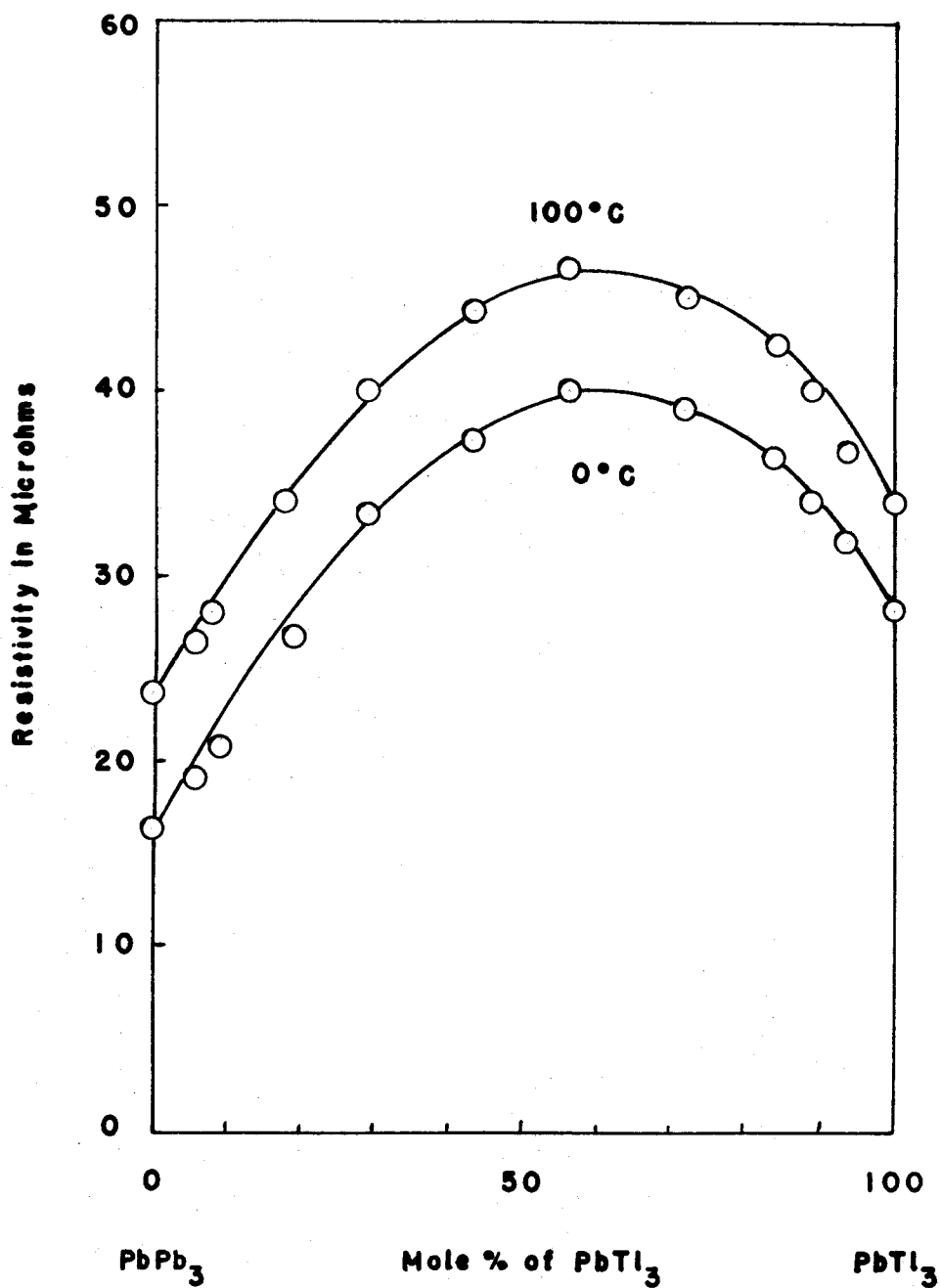


Figure 17. The resistivity of the lead-thallium alloys in the phase $Pb(Pb,Tl)_3$ at 0 to 100°C as plotted against the mole percentage of $PbTl_3$.

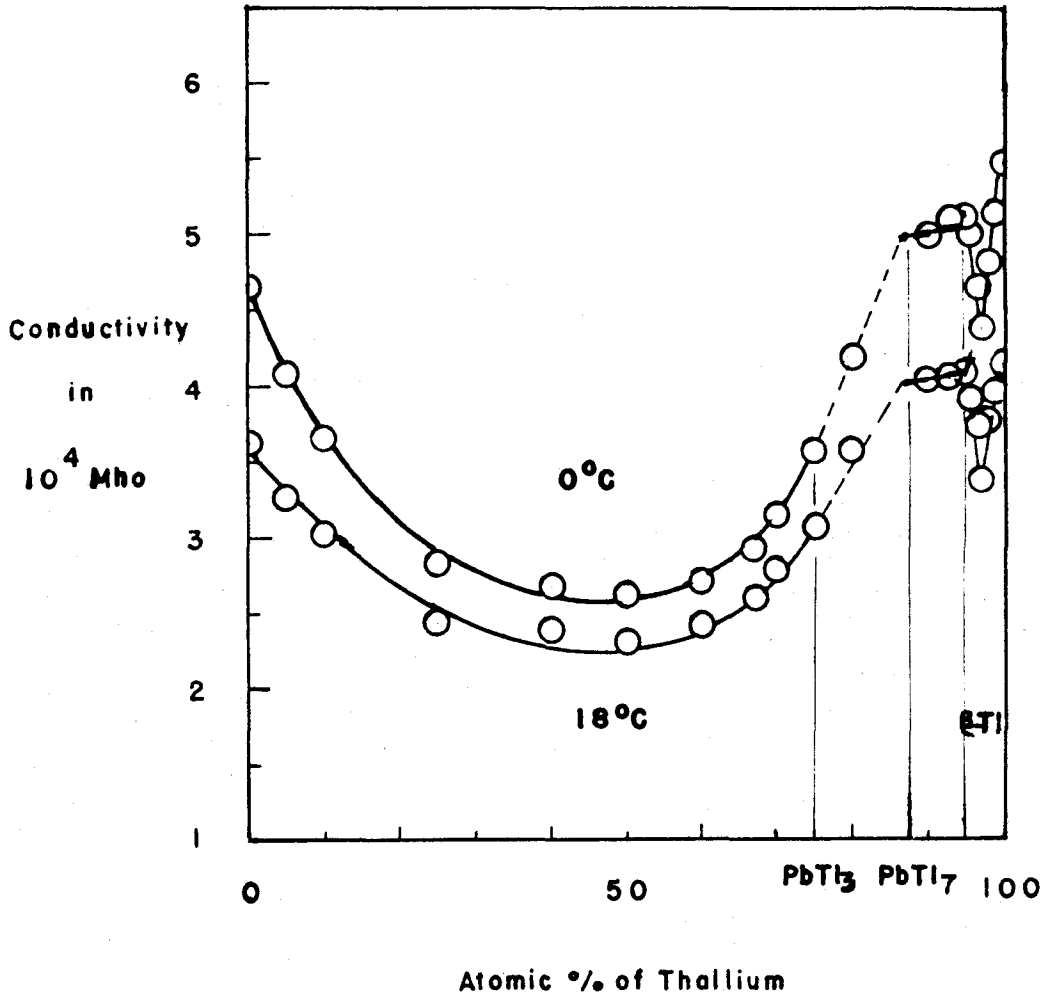


Figure 18. Conductivities of the lead-thallium alloys at $0^\circ C$ and $18^\circ C$ as interpreted in the light of the proposed structures.

find further evidence for the existence of the phase (Pb,Tl) Pb Tl₆. It seems to me that the interpretation of the conductivity data in the light of the model I proposed here is much more satisfactory than any other available in the literature.

I present in Figure 19 the phase diagram of the system lead-thallium constructed on the basis of the evidence provided by the thermal analysis, microscopic study, conductivity data over the temperature range 0 to 250°C and the X-ray investigations, particularly my own work. The structures of Pb(A) and Pb(B) can be expressed in terms of the formulas Pb (Pb,Tl)₃ and (Pb,Tl) Pb Tl₆ respectively. The structure of β-Tl has an A₃ structure. The structure of α-Tl was redetermined by Lipson and Stokes⁽¹¹⁾. On the basis of their powder photograph taken in a high-temperature camera α-Tl has an A₂ structure instead of an A₁ as reported by Sekito⁽¹²⁾, who carried out the experiments on specimens quenched from near the melting point.

Experimental evidence indicates that the mixture corresponding to the maximum point on the freezing-point curve in the system lead-thallium is probably analogous to the azeotropic mixture in the system hydrochloric acid-water.

By means of the equation chosen by Professor Pauling in his work on atomic radii and interatomic distances in metals⁽¹³⁾,

$$R(1) - R(n) = 0.300 \log n,$$

one can calculate the radius R(CN12) for β-thallium which has a structure A₃ with $a = 3.450 \text{ \AA}$., $c = 5.514 \text{ \AA}$ at 18°C. Each

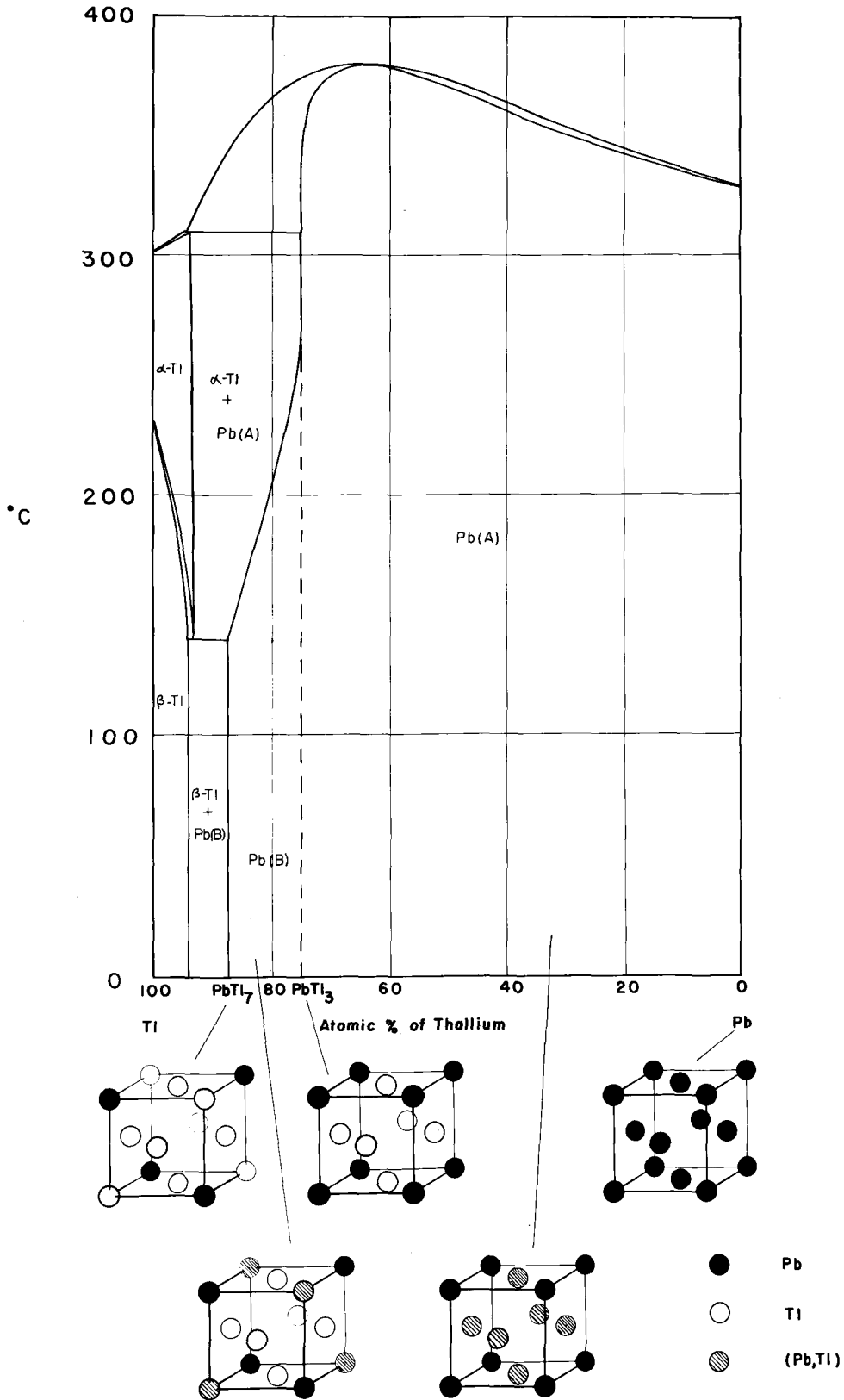


Figure 19. The phase diagram of the alloy system lead-thallium as revised on the basis of the new evidence from this X-ray investigation. The lead phases are illustrated with their probable structures.

thallium atom is surrounded by two sets of six neighbors at 3.401 and 3.450 Å. respectively. Application of the above equation leads to $v/10.14$ for the bond number of the shorter bonds, and hence to 0.0218 Å. for the correction to CN12. The value thus calculated for $R(\text{CN12})$ is 1.712 Å.⁽¹³⁾ The hypothetical A1 structure for β-thallium would have a cube edge $2\sqrt{2} \times 1.712$ or 4.842 Å. in length.

It is very remarkable that in Figure 20 the dotted straight line connecting 4.947 Å. for PbPb_3 and 4.842 Å. for the hypothetical structure (TlTl_3) passes also through the points at PbTl_3 , PbTlTl_6 on the lattice-spacing—composition curve. The solid curve deviates from the dotted straight line because of the effect of disorder on the interatomic distances.

The new notation $[(1-x) \text{Pb}, x \text{Tl}]$ which I introduce here stands for a hypothetical atom which resembles a thallium atom in every respect except that its $R(\text{CN12})$ is $[(1-x)R_{\text{Pb}}(\text{CN12}) + xR_{\text{Tl}}(\text{CN12})]$ instead of $R_{\text{Tl}}(\text{CN12})$. The general notation $[\text{Pb}, \text{Tl}]$ stands for $[(1-x)\text{Pb}, x \text{Tl}]$ with $x = 0$ to 1.

In Figure 20 the hypothetical phases $(\text{Pb} [\text{Pb}, \text{Tl}]_3)$, $(\text{Pb} [\text{Pb}, \text{Tl}] \text{Tl}_6)$, $([\text{Pb}, \text{Tl}] \text{TlTl}_6)$ and (TlTl_3) are always included within parenthetical marks in distinction from those which actually occur.

This discussion of interatomic distances observed in the system lead-thallium based on Pauling's value for $R(\text{CN12})$ of thallium leads to additional evidence in favor of the structure proposed for the lead-phase alloys.

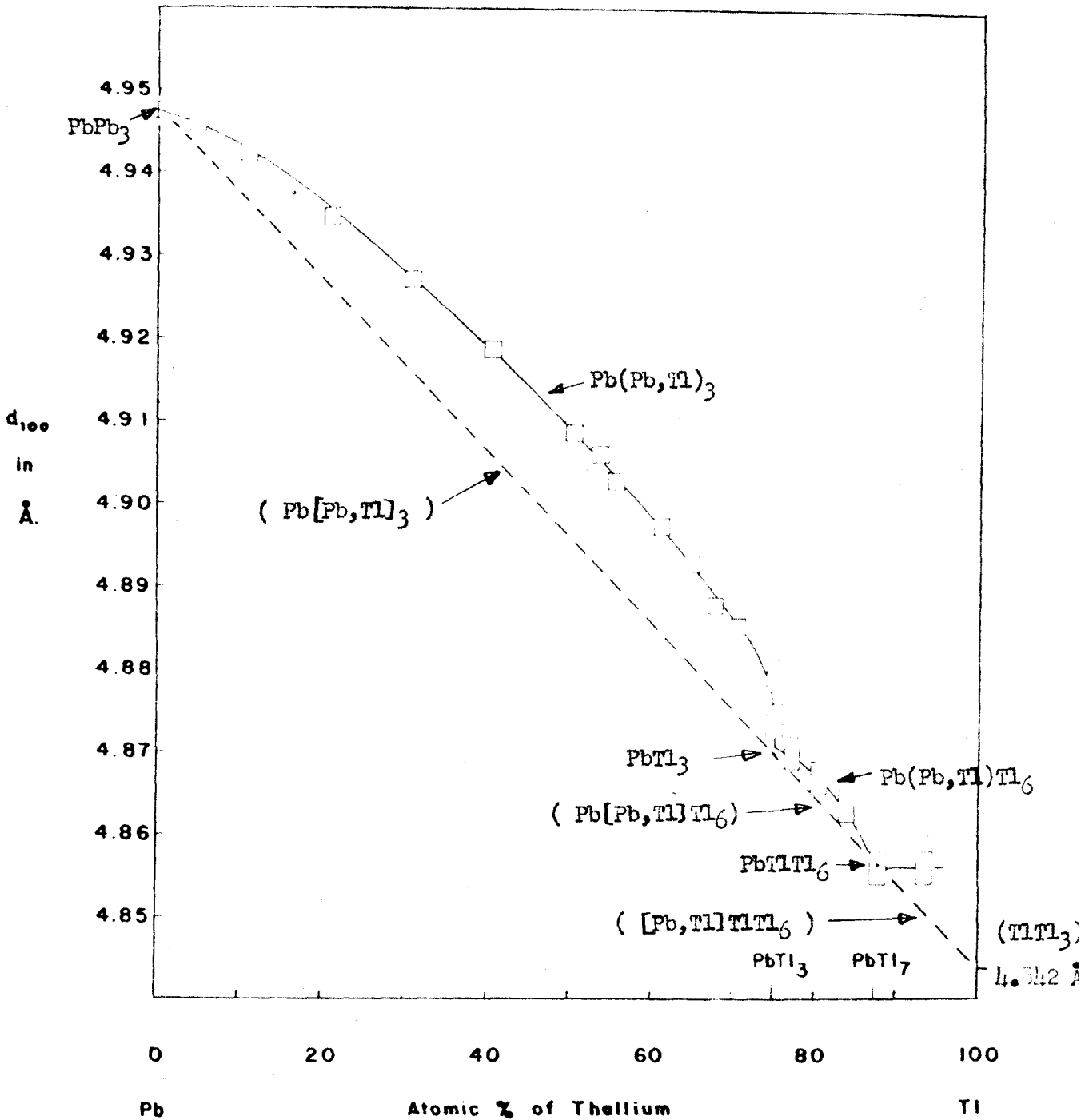


Figure 20. The observed lattice-spacing—composition curve for the lead-thallium alloys as compared with one predicted for the hypothetical phases.

8. CONCLUSIONS

In view of the experimental procedure and reasonably great number of samples distributed properly over the complete range of composition the lattice-spacing--composition curve obtained in the current research is highly probably a correct one. The two-straight-line result reported by A. Ölander["] is incorrect. The transition at 54.6 percent of thallium does not seem to exist.

The evidence provided by the lattice-spacing--composition curve, thermal analysis, microscopic study, and conductivity data provides strong support for the proposed structure for the lead-phase alloys as presented in Figure 19.

9. REFERENCES

- (1) A. Olander, Z. physikal. Chem., (1934), (A) 168, 274.
- (2) Nelson and Riley, Proc. Phys. Soc., (1945), 57, 160.
- (3) Kurnakow and Pushin, Z. Anorg. Chem., (1907), 52, 430.
- (4) K. Lewkonja, Z. Anorg. Chem., (1907), 52, 452.
- (5) N. S. Kurnakow, Zhur. Russ. Fiziko-Khimich. Obsch., (1907), 39, 657.
- (6) N. S. Kurnakow and Schemtschushny, Z. anorg. Chem., (1909), 64, 149.
- (7) W. Guertler and A. Schulze, Z. physikal, Chem., (1923), 104, 269.
- (8) E. McMillan and L. Pauling, J.A.C.S., (1927), 49, 666.
- (9) F. Halla and R. Staufer, Z. Krist., (1928), 67, 440.
- (10) Mott and Jones, The Theory of the Properties of Metals and Alloys, (1939), pp. 297-9, Oxford Press.
- (11) H. Lipson and A. R. Stokes, Nature, (1941), 148, 437.
- (12) S. Sekito, Z. Krist., (1930), 74, 189.
- (13) L. Pauling, J.A.C.S., (1947), 69, 542.

II

THE INVESTIGATION OF THE CRYSTAL STRUCTURE OF THE
COMPLEX OF HEXAMETHYLENETETRAMINE WITH MANGANOUS CHLORIDE

1. INTRODUCTION

Hexamethylenetetramine precipitates from water or organic solvents in crystalline complexes with a surprisingly great number of inorganic compounds. In fact, hexamethylenetetramine serves as a precipitant for microchemical detection of metals. In the earlier literature attempts to explain the formation and stability of the complex compounds have been recorded. The crystal structure of hexamethylenetetramine was determined by X-ray diffraction by R. G. Dickinson and others⁽¹⁾. The hexamethylenetetramine molecules are arranged in such a way that the unshared pair of electrons of each nitrogen atom in a hexamethylenetetramine molecule interacts with the three nearest hydrogen atoms in an adjacent molecule. The twelve interactions of this sort per molecule adequately explain the stability of the crystal. In view of the fact that hexamethylenetetramine sublimes with partial decomposition when those interactions are disturbed by thermal agitation, the van der Waals interaction in the crystal does not contribute much to its stability. From this one may expect that the unshared pair of electrons of the nitrogen atom in hexamethylenetetramine can play an important role in complex formation. To a certain extent an analogy exists between the ammonia complexes and the hexamethylenetetramine compounds. The analogy seems to be much limited due to the difference in size of the respective molecules and to other factors.

It was considered of interest to investigate by X-ray diffraction the structure of one of those hexamethylenetetramine complex compounds, which may be representative of a great many others. F. D. Ordway⁽²⁾ investigated the hexamethylenetetramine complex with stannic chloride by X-ray diffraction, and found a structure for the compound which gave good agreement with X-ray intensities. According to his investigation the compound $\text{SnCl}_4 \cdot 4(\text{CH}_2)_6\text{N}_4$ has the following crystal structure. The space group is C_{3v}^5 -R3m. There is three-quarters of a molecule in the hexagonal unit with $a = b = 8.95 \text{ \AA}$., $c = 8.95 \text{ \AA}$. The hexamethylenetetramine molecules are in general arrangement and orientation like those in the hexamethylenetetramine crystal, except that the lattice along c has been so much elongated that a chlorine atom can be accommodated between two successive hexamethylenetetramine molecules along that axis. The rhombohedral angle 109.5° and the axial ratio $c/a = 0.61$ corresponding to the body-centered cubic lattice have been modified to 97.2° and 1.00 respectively. The one-quarter of a tin atom is lost in the different holes in the structure. The halogen atom alone is the determining factor for the structure.

While the proposed structure is consistent with X-ray evidence, the information does not explain adequately the stability of this crystal, nor does it add to our general understanding of the nature of the bonds operating in most of the complex compounds of this particular type.

The current research was undertaken to seek an explanation for the stability of the complex compound $\text{MnCl}_2 \cdot 2(\text{CH}_2)_6\text{N}_4$, and to learn any possible change in bond type and interatomic distances of the manganous chloride molecule, and the coordination of hexamethylenetetramine molecules with the manganese atom.

This work has been carried out under the supervision of Professors J. H. Sturdivant and Linus Pauling.

2. PREVIOUS WORK ON THE COMPOUND

L. Vanino and A. Schinner⁽³⁾ reported the compound $\text{MnCl}_2 \cdot (\text{CH}_2)_6\text{N}_4 \cdot 8\text{H}_2\text{O}$. Anhydrous complex compounds from alcoholic solutions were reported by Scaglirini and G. Tartarini⁽⁴⁾. F. D. Ordway prepared the manganese complex from acetone solution. An organic solvent was preferred because water of hydration would have been likely further to complicate the work. After recrystallizing the voluminous precipitates in an apparatus he described in his Thesis⁽²⁾ he obtained tiny but usable needles. The needles were presumed to be anhydrous and to have the formula $\text{MnCl}_2 \cdot 2(\text{CH}_2)_6\text{N}_4$. These two points, however, were not settled. The needles were not suitable for goniometric measurement at all, but Laue photographs along two axes normal to the needle were taken, and the Laue symmetry was found to be D_{2h} -mmm. He also took a set of four 24° oscillation photographs about the needle axis with Cu $K\alpha$ radiation, and indexed the zero layer line or reflections $hk0$ on the basis that $a_1 = 11.86 \text{ \AA}$.

$a_2 = 21.92 \text{ \AA}$, and $a_3 = 7.23 \text{ \AA}$. The density of the crystal was determined to be 1.55 g./cm^3 . He also tabulated the extinctions he observed among 133 reflections $hk0$. He was fairly sure about the a_2 glide plane normal to a_3 , the needle axis, but much less confident about the n glide plane normal to a_2 .

3. THE PREPARATION OF CRYSTALS

Before beginning to grow crystals for X-ray work, I was anxious to find out two things. First, would we always get the same precipitate, if we mixed manganous chloride and hexamethylenetetramine in an organic solvent, say acetone, according to different ratios? Second, would different organic solvents give different crystal forms of the compound, so that crystals would be available for X-ray work in forms other than needles?

Solutions of manganous chloride and hexamethylenetetramine in acetone were mixed according to five widely different molal ratios of manganous chloride to hexamethylenetetramine; namely, 1:10, 1:4, 1:1, 15:1, and 50:1. The preparations were kept in five stoppered test tubes for a week. The precipitates were washed with benzene and air-dried. From their powder patterns I found that they were the same substance, except that the precipitate from the solution 50:1 may have been hydrated due to the residual water present in the manganous chloride. The powder pattern for the first four is also identical with one obtained by F. D. Ordway.

I also prepared the compound from absolute alcohol solution, and observed that the precipitate very often occurred in poor thin plates, and that after standing for a few days it occasionally recrystallized into thicker plates. The needles, the only form obtainable from acetone solution, were not satisfactory for X-ray work, nor were the plates from alcohol. It was very clear that the growth of the crystal is favored along the needle axis by acetone, and along the other by alcohol. It was soon realized that an optimum mixture of acetone and alcohol would give good crystals which grew equally along all directions. Of the twelve preparations the 1:1 mixture gave the best result. After a few days the voluminous precipitate first formed in this mixture changed into surprisingly nice crystals which are suitable for morphological study as well as X-ray work along all axes.

The crystals used in this work were all prepared according to the following procedure. Anhydrous manganous chloride was prepared from c.p. manganous chloride tetrahydrate. The water of hydration was removed quantitatively by heating repeatedly to 150 or 200°C, as was checked by following the loss of weight. About 2 g. of anhydrous manganous chloride and a stoichiometric quantity of c.p. hexamethylenetetramine were dissolved separately in 100 ml. of absolute alcohol respectively. The two solutions were then mixed, and distributed into stoppered flasks. An equal volume of c.p. acetone was added to each flask to make up

a 1:1 mixture. After standing for ten days the solvent was decanted, and the wet crystals were dried either on an unglazed porcelain plate or by centrifuging. Air-dried crystals were kept in a silica-gel desiccator until they reached constant weight.

The crystals dissolve in water readily. The air-dried crystals still lose a considerable amount of weight after being in a silica-gel desiccator for a few days. However, the completely dried crystals which have reached constant weight in a desiccator retain their form and transparency well, and do not further lose weight after their surface exposed to silica gel has been increased more than tenfold by pulverization. This suggests that the substances lost during the drying process occurred on the surface rather than in the interior of the crystals.

4. MORPHOLOGICAL AND PHYSICAL PROPERTIES OF THE CRYSTAL

Morphological Study.---The microscopic and goniometric examinations indicated that the crystals are orthorhombic. Figure 1 shows the habit of the crystals from a 1:1 mixture of alcohol and acetone. Figure 2 is a drawing of the crystal habit from a mixture of slightly different composition (1.4:1). From goniometric measurement and the assignment of indices to faces shown in Figure 1 and Figure 2, I obtained the axial ratios $a_1:a_2:a_3 = 0.530:1:0.325$, with which I shall compare the ratios obtained from X-ray measurement in Section 6. It will

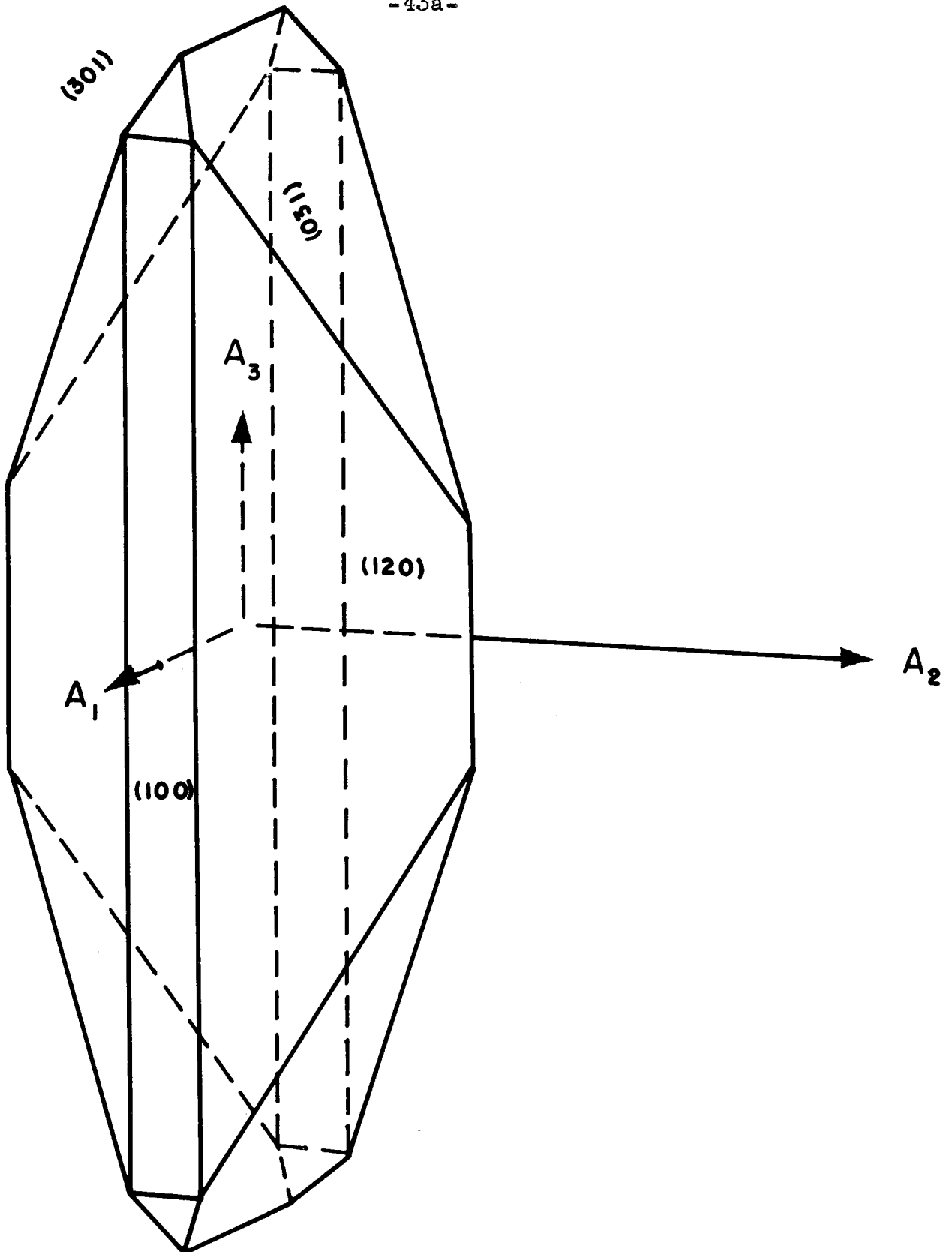


Figure 1. Crystals prepared from a 1 : 1 mixture of alcohol and acetone.

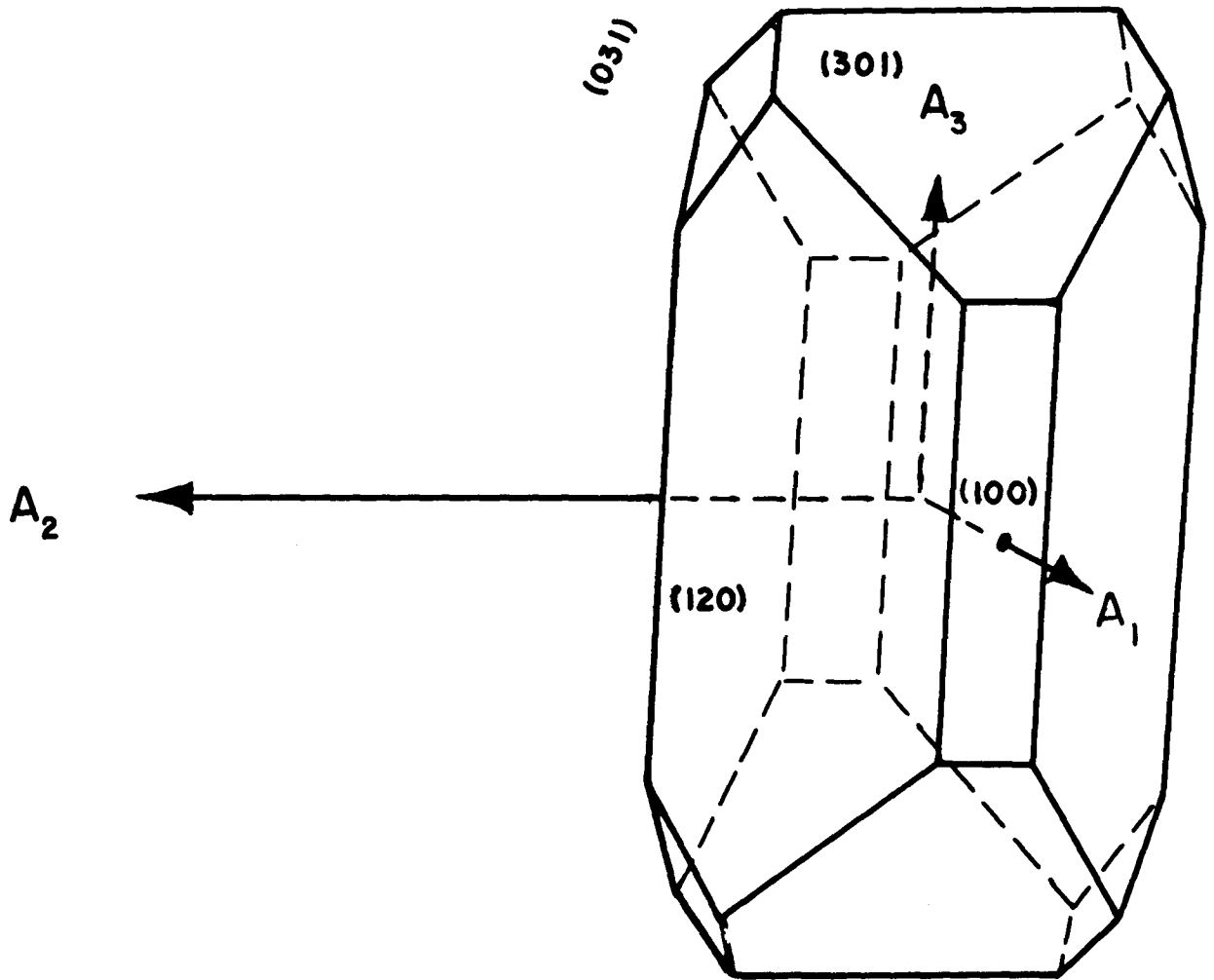


Figure 2. Crystals prepared from a 1.4 : 1 mixture of alcohol and acetone.

be also mentioned that morphological evidence was sought as to the presence or absence of a center of symmetry, and the result was in line with the piezo-electric measurement.

Piezo-electricity.---The piezo-electric test of this crystal was made by Dr. William N. Lipscomb with his "electronic corn-popper". The sample consisted of numerous tiny crystals. He stated that he found a fairly strong positive test, and that there can be no doubt about the space group being non-centro-symmetric. As I shall show in Section 6, this fairly strong piezo-electricity is in line with morphological evidence, and is supported by considerations regarding the structure.

Magnetic Susceptibility.---In the determination of a structure which contains manganese atoms, as this one does, one has good reason to expect that the magnetic criterion will be useful. Using a sample of about 10 g. of powdered crystals we* made a determination of the magnetic susceptibility of the compound at room temperature with a Gouy magnetic balance. Two different packings agreed in the result of the magnetic determination within one percent. A run made at elevated temperature (40.5°C) indicated that within the limits of experimental error Curie's law holds, and the temperature-dependent part of the magnetic moment is negligible. If we assume that the compound

* I am indebted to Mr. David L. Douglas for assistance in the magnetic determination.

contains as much manganese as the formula $\text{MnCl}_2 \cdot 2(\text{CH}_2)_6\text{N}_4$ indicates, namely 13.52 percent, we have 4.96 unpaired electrons for each manganese atom. If we use 12.25 percent for manganese content as we found from microchemical analysis, we get 5.17 unpaired electrons. Due to the lack of a satisfactory way of packing the crystals in the tube, the error could amount to a few percent. Thus within the limits of experimental error each manganese atom contains five unpaired electrons. I shall discuss the meaning of this result later.

Density.---For attaining high precision the displacement method with a sample of 1.5 g. of powdered crystals was employed. The displacement medium was high grade paraffin oil which was previously degased by evacuation, and kept over sodium threads. Unusual care was exercised in following the procedure for displacement method. Adequate means were provided to eliminate various sources of error. The pycnometer was always kept in the thermostat long enough to justify the calculation which was based upon the temperature of the thermostat. The air bubbles were practically completely removed by adequate evacuation by a mechanical pump. The data are given in Table I.

Table I.

Pycnometer	31.3896 g.
Pycnometer + Water at 25.00°C	42.9037 g.
Pycnometer + Oil at 25.00°C	41.4752 g.
Pycnometer + Crystals	32.8664 g.
Pycnometer + Crystals + Oil at 25.00°C	42.1310 g.
The density of the crystal is 1.570 g./cm. ³	

5. X-RAY PHOTOGRAPHY

The X-ray powder pattern of this complex compound is so complicated that I did not bother to index it. Use has been made of the powder photograph to identify different preparations. Figure 3 is a print of the powder pattern. The photograph was taken on No-Screen film in a camera of radius five centimeters with well-filtered Copper $K\alpha$ radiation.

A single crystal was mounted on a glass fiber by means of Aquanite clear lacquer in a rather usual manner. The crystals selected for X-ray work were mostly good enough to be oriented optically. Occasionally small adjustment by Laue photography was also made, when the orientation by optical goniometer turned out not to be completely satisfactory.

Laue photographs were taken on No-Screen film with a crystal-to-film distance of five centimeters and with white radiation whose minimum wave length was 0.24 \AA . Two crystals mounted along two different axes were used.

Rotation photographs were taken on No-Screen film in the camera of radius five centimeters with well-filtered Copper $K\alpha$ radiation. Orientations along three axes in turn were used. This set of photographs permitted accurate measurement of the layer line distances.

Weissenberg photographs for the zero and first levels along three axes were taken with filtered Copper $K\alpha$ radiation in a



Figure 3. Powder photograph of hexamethylenetetramine complex with manganous chloride, $\text{MnCl}_2 \cdot 2(\text{CH}_2)_6\text{N}_4 \cdot 2\text{H}_2\text{O}$, taken with $\text{Cu K}\alpha$ radiation.

camera which has a diameter of 57.30 mm. and moves 2 mm. per degree of rotation of the crystal. This set of Weissenberg photographs served to give information only regarding the systematic extinctions and the possible space group. Another set of Weissenberg photographs on quadruple No-Screen films was taken with the same radiation and in the same camera. Crystals were carefully selected so that due to their spherical shape and small size the absorption correction to the intensities could be omitted. Due to the fact that the a_2 axis was 22 \AA . long, it was necessary to use a Weissenberg camera which has a very narrow slit to avoid the occurrence of reflections belonging to more than one level.

6. THE SYMMETRY, UNIT CELL, AND SPACE GROUP OF THE CRYSTAL

Morphological evidence and goniometric measurements indicated that the crystal is orthorhombic. I also found two mirror planes normal to each other in all three Laue photographs. The Laue symmetry was established to be D_{2h} -mmm. The point group must be either C_{2v} or D_2 due to the lack of a center of symmetry shown by the piezo-electric test.

The preliminary values for the lattice constants were calculated from the measurements of positions of layer lines in rotation photographs along three axes. The calculation data are given in Table II. The wave lengths I used in translating film distances to lattice spacings were:

$$\text{Copper } K\alpha_1 = 1.5405 \text{ \AA}.$$

$$\text{Copper } K\alpha_2 = 1.5443 \text{ \AA}.$$

$$\text{Copper } K\alpha \text{ (weighted average)} = 1.5418 \text{ \AA}.$$

The radius of the camera in which the rotation and oscillation photographs were taken was calibrated to be 5.015 cm. The preliminary values for the three axes were:

$$a_1 = 11.79 \text{ \AA}.$$

$$a_2 = 21.95 \text{ \AA}.$$

$$a_3 = 7.195 \text{ \AA}.$$

In indexing the Weissenberg photographs for the zero and first levels along a_2 and a_3 I found that the a_1 axis of length 11.80 \AA . is only a pseudo-axis, and the true identity distance in this direction is $A_1 = 2a_1 = 23.60 \text{ \AA}$. Reflections which corroborate this doubling of a_1 were then found to be present but extremely weak on the rotation photograph about a_1 . Indices hkl throughout this paper refer to the pseudo unit, and not to the true unit.

The precise determination of the lattice constants was based upon measurements of positions of the equatorial reflections which occurred in my rotation and F. D. Ordway's oscillation photographs. In taking averages for the values for b_1 from measurements of reflections containing h_1 in their indices a weighting factor h_1 was always used. Reflections $h00$ and $0k0$ were used to determine the preliminary values for b_1 and b_2

respectively. Then reflections $hk0$ with $h \geq 3k$, and with the knowledge of the preliminary value for b_2 , were included to give the final average value for b_1 . In a similar manner I used reflections $hk0$ with $k \geq 5h$, and the preliminary value for b_1 . The calculation of b_3 was based on the final values of b_1 , b_2 and measurements of some equatorial reflections on the rotation photographs along a_3 . The results are presented in Table III.

Table II.

Determination of Lattice Constants from Layer-Line Measurements

(a) Determination of a_1

h	$\tan \alpha$	α	$\sin \alpha$	a_1
1	0.1316	0.1309	0.1305	11.810
2	0.2712	0.2648	0.2617	11.779
3	0.4258	0.4026	0.3918	11.800
4	0.6132	0.5501	0.5228	11.791
Average				11.795 Å.

(b) Determination of a_2

k	$\tan \alpha$	α	$\sin \alpha$	a_2
1	0.0699	0.0698	0.0697	22.109
2	0.1426	0.1416	0.1411	21.844
3	0.2154	0.2122	0.2106	21.953
4	0.2921	0.2842	0.2804	21.984
5	0.3748	0.3934	0.3833	20.107 (omitted)
6	0.4655	0.4357	0.4220	21.911
7	0.5652	0.5145	0.4921	21.912
8	0.6800	0.5972	0.5623	21.926
Average				21.954 Å.

(c) Determination of a_3

l	$\tan \alpha$	α	$\sin \alpha$	a_3
1	0.2194	0.2160	0.2143	7.191
2	0.4726	0.4415	0.4273	7.200
Average				7.195 Å.

Table III.

Determination of Lattice Constants from
Measurements of Equatorial Reflections

(a) Determination of b_1

Reflection	$\sin \theta$	b_1	Weight
600	0.3920	0.08480	6
800	0.5229	0.08330	8
10.0.0	0.6518	0.08460	10
12.0.0	0.7829	0.08467	12

Weighted average of above determinations 0.08471 Å.⁻¹

720	0.4631	0.08487	7	With $b_2 = 0.04545$ Å. ⁻¹
820	0.5280	0.08490	8	
920	0.5925	0.08484	9	
11.2.0	0.7212	0.08468	11	
12.4.0	0.7952	0.08466	12	

Weighted average of all determinations 0.08474 Å.⁻¹

Mean weighted deviation 0.00009 Å.⁻¹

(b) Determination of b_2

Reflection	$\sin \theta$	b_2	Weight
020	0.0697	0.04521	2
040	0.1401	0.04544	4
060	0.2098	0.04538	6
080	0.2804	0.04549	8
0.10.0	0.3512	0.04558	10
0.12.0	0.4202	0.04544	12
0.14.0	0.4904	0.04546	14
0.16.0	0.5590	0.04534	16
0.20.0	0.7002	0.04544	20
0.22.0	0.7710	0.04548	22

Weighted average of above determinations 0.04545 Å.⁻¹

160	0.2206	0.04558	6	With $b_1 = 0.08474$ Å. ⁻¹
180	0.2880	0.04550	8	
1.10.0	0.3559	0.04540	10	
2.10.0	0.3736	0.04542	10	
2.12.0	0.4409	0.04554	12	
1.12.0	0.4248	0.04539	12	
2.14.0	0.5067	0.04538	14	
1.16.0	0.5640	0.04542	16	

Table III. (Continued)

(b) Determination of b_2 (Continued)

Reflection	$\sin \theta$	b_2	Weight
2.16.0	0.5755	0.04547	16
3.20.0	0.7275	0.04547	20
1.22.0	0.7735	0.04547	22
2.22.0	0.7816	0.04547	22
3.22.0	0.7958	0.04551	22
Weighted average of all determinations		0.04545	\AA^{-1}
Mean weighted deviation		0.00005	\AA^{-1}

(c) Determination of b_3

Reflection	$\sin \theta$	b_3	Weight
011	0.1125	0.13868	1 With $b_1 = 0$
002	0.2137	0.13862	2 0.08474\AA^{-1}
004	0.4275	0.13865	4 $b_2 = 0$
303	0.3760	0.13876	3 0.04545\AA^{-1}
Weighted average of all determinations		0.13868	\AA^{-1}
Mean weighted deviation		0.00008	\AA^{-1}

(d) Calculation of a_1, a_2, a_3

$$a_1 = 11.80 \pm 0.01 \text{\AA}$$

$$a_2 = 22.00 \pm 0.02 \text{\AA}$$

$$a_3 = 7.21 \pm 0.01 \text{\AA}$$

The volume of the pseudo unit cell is $1874 \pm 6 \text{ \AA}^3$. The number of molecules in the pseudo unit cell is $Z = 4$.

The axial ratio calculated from the values given above is

$$a_1 : a_2 : a_3 = 0.536 : 1.000 : 0.328,$$

in reasonably good agreement with that obtained from goniometric measurements; namely,

$$a_1 : a_2 : a_3 = 0.530 : 1.000 : 0.325.$$

The information I obtained from the Weissenberg photographs by neglecting those weak reflections mentioned above, and which led to the assignment of the pseudo space group, is listed below.

1. Reflections $hk\ell$ occur for all values of h , k , ℓ .
2. Reflections $Ok\ell$ occur for all values of k , ℓ and $k + \ell$.
3. Reflections $hk0$ occur only for k even.
4. Reflections $h0\ell$ occur only for $h+\ell$ even.

The extinctions listed above were observed on Weissenberg photographs which contain reflections of high order, and the missing reflections were numerous. Aside from the complications due to the weak reflections mentioned previously the assignment of the pseudo space group was rather straightforward.

The interpretation of each of the four observations listed above follows in order.

1. The unit cell is primitive.
2. There can be no glide plane normal to a_1 .
3. There is an a_2 glide plane normal to a_3 .
4. There is an n glide plane normal to a_2 .

The appropriate space group is $C_{2v}^9-P2_1nb$. If there were a center of symmetry in the structure, the appropriate space group would be $D_{2h}^{16}-Pmnb$. In this case the four manganese atoms should take one of the three sets of special positions. If they took the special positions at centers of symmetry, one should have been able to observe a heavy peak at $(1/2, 0, 0)$ corresponding to manganese-manganese interactions in the Patterson distribution function. This is found to be incorrect. On the other hand if the manganese atoms took the special positions on the mirror planes, each complex molecule should have a mirror plane normal to a_1 . This is incorrect also. Therefore the assignment of $C_{2v}^9-P2_1nb$ instead of D_{2h}^9-Pmnb as the pseudo space group of the crystal is not completely dependent upon the positive test for the piezo-electricity. On the other hand I can, to a certain extent, distinguish whether the microscopic symmetry element along a_1 is a mirror plane or a two-fold axis by a close statistical study of the morphology of a great number of well-grown crystals from a single batch. In this particular case, if one observes that on most of those crystals the pair of faces $\bar{1}20, 120$ as well as the pair $\bar{1}20, \bar{1}\bar{2}0$ has equal size, and that the two pairs are not equivalent, one will say that the a_1 axis is a two-fold axis. This was the case.

Weissenberg and rotation photographs which contain spots due to the A_1 axis of length $23.60 \overset{\circ}{\text{Å}}$ are shown in Figure 4, 5, 6 and 7. That the identity distance in this direction is not less

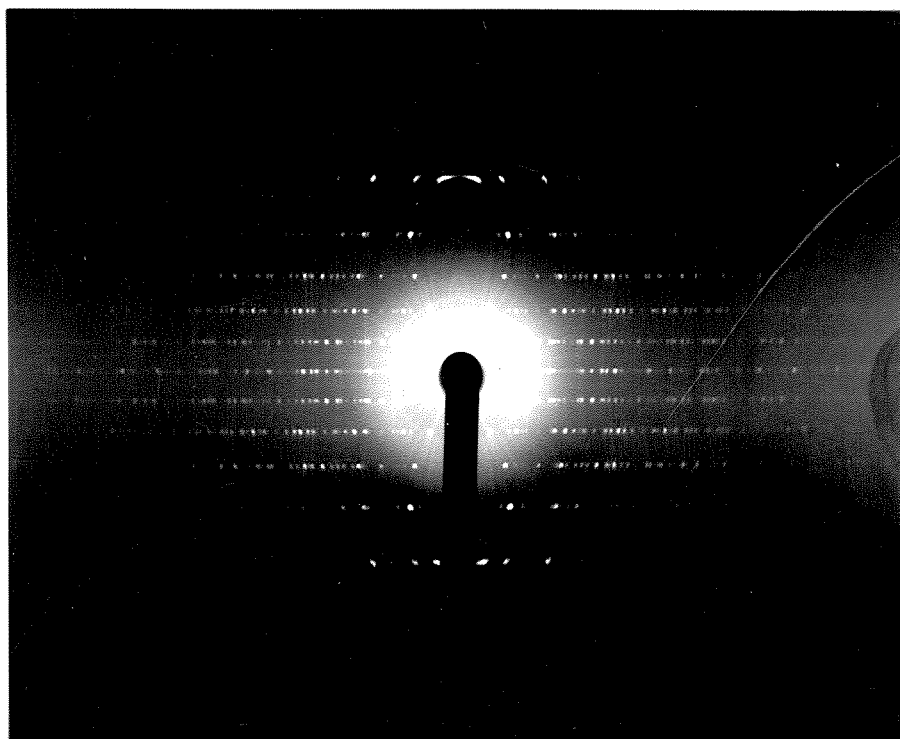


Figure 4. Photograph taken with crystal rotating along a_1 . Layer lines correspond to $h = 0, 1, 2, 3, 4, 5$. Note weak spots corresponding to H odd.

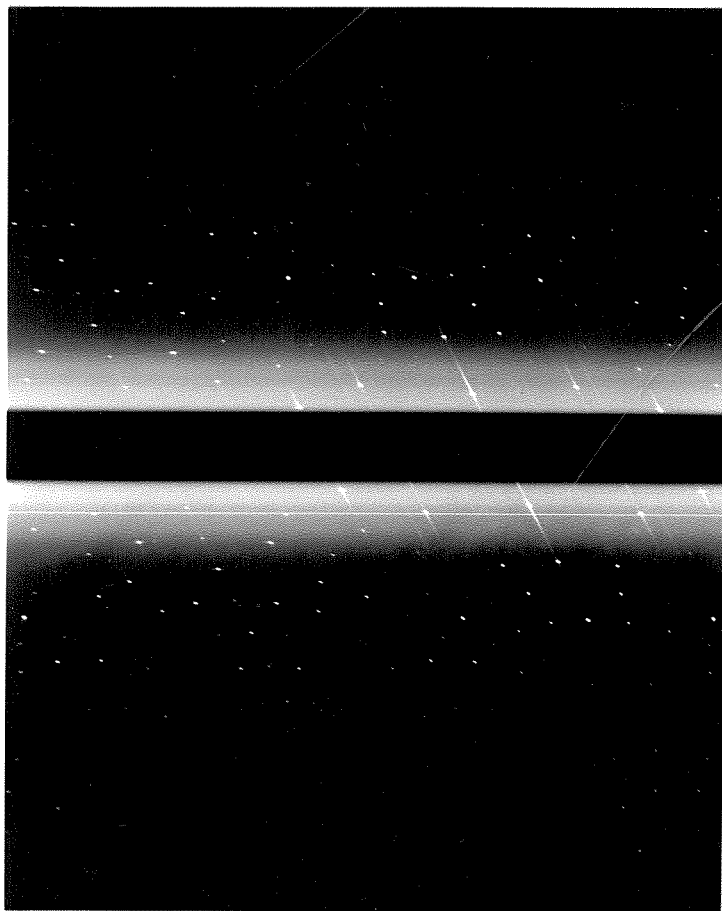


Figure 5. Weissenberg photograph for the zero level taken with crystal rotating along a_3 . No spot corresponding to H odd can be found on this photograph.

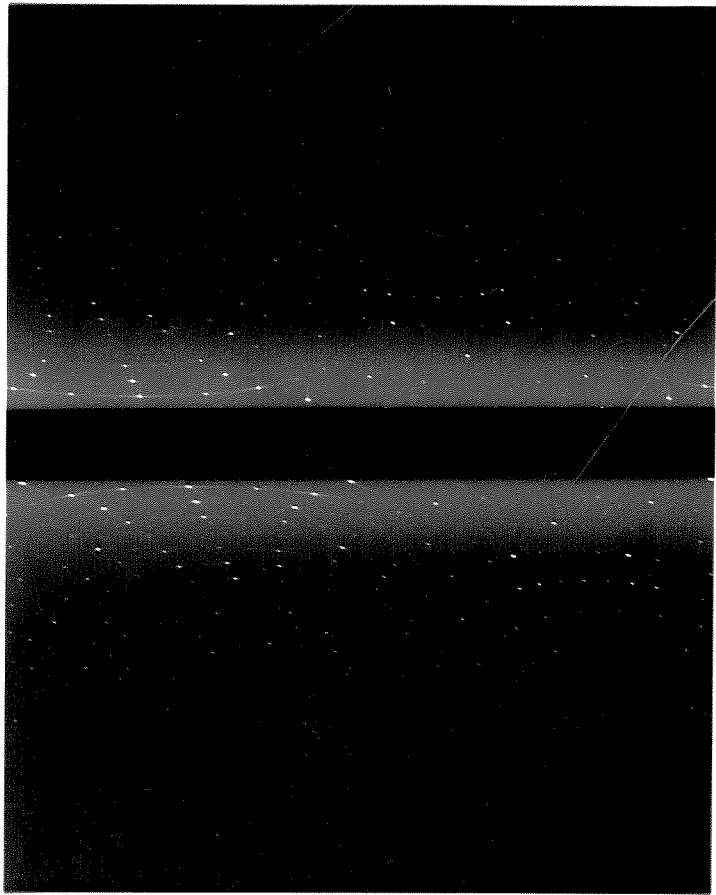


Figure 6. Weissenberg photograph for the first level taken with crystal rotating along a_3 . Note spots correspond to H odd.

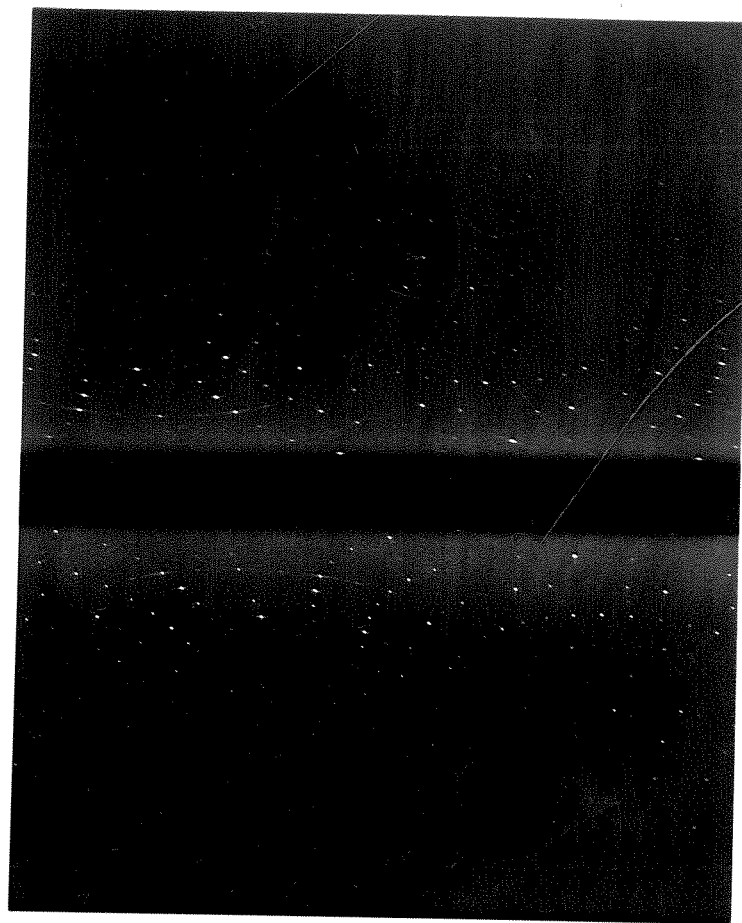


Figure 7. Weissenberg photograph for the second level taken with crystal rotating along a_3 . Note weak spots with H odd.

than 23.60 \AA . has been proved beyond reasonable doubt. I also found that the reflection which is indexed as 131 on the true unit cell, and which is one of the strongest with H odd, occurs on an oscillation photograph prepared by F. D. Ordway and dated April 6, 1948. Due to the fact that I did not observe any spot which corresponds to an identity distance longer than 23.60 \AA . on the heavily exposed rotation and Weissenberg photographs which contain the spots corresponding to the identity distance of 23.60 \AA ., the true structure probably has an identity distance not longer than 23.60 \AA . along A_1 .

Now I shall discuss what the symmetry and space group of the true structure would be by taking account of the weak but measurable reflections due to the true unit cell. On the basis of the true unit cell I observe:

1. Reflections $Hk\ell$ for all values of H, k and ℓ .
2. Reflections $Ok\ell$ for all values of k, ℓ and $k + \ell$.
3. Reflections $Hk0$ only for k even.
4. Reflections $H0\ell$ only for H even.
5. Reflections 00ℓ only for ℓ even.

These observations may be interpreted as follows:

1. The unit cell is primitive.
2. There can be no glide plane normal to A_1 .
3. There may be an a_2 glide plane normal to a_3 .
4. There may be an A_1 glide plane normal to a_2 and a two-fold screw axis along A_1 .
5. There may be a two-fold screw axis along a_3 .

The fact that no appropriate space group can account for all of these glide planes and the screw axes strongly suggests that some of these observed extinctions must be only accidental. As we know well, while a glide plane or a screw axis gives rise to systematic extinctions, a few observed extinctions do not necessarily mean the presence of a corresponding glide plane or screw axis. In the light of the approximate structure I found one will see that only the a_2 glide plane normal to a_3 really needs to exist in the true unit cell. Extinctions 4 and 5 are inherited from the n glide plane normal to a_2 of the pseudo space group. Thus the true symmetry is only monoclinic domatic. The true space group is C_s^2 -Pb.

The approximation based on the pseudo unit cell can be justified due to many reasons. As far as the equatorial Weissenberg photographs are concerned, the reflections with H odd are too weak to be measured or even detected at least within the angular range I can observe on the photographs. In other words none of the three two-dimensional projections based upon reflections occurring on the equatorial Weissenberg photographs will show any minor features which repeat according to A_1 . In view of the weak but measurable reflections with H odd on Weissenberg photographs for higher levels, the exact structure is undoubtedly based on the larger unit cell, and the apparent absence of the reflections with H odd on all equatorial Weissenberg photographs is due to the limits of experimental technique. All of the reflections with H odd together contribute

only about one percent to the sum of the corrected intensities, and the strongest one among them has a value of 20 for the structure factor. For the purpose of this investigation the difference between the exact and approximate structures is not significant.

7. THE COLLECTION OF INTENSITY DATA

Weissenberg photographs for collecting intensity data were taken with quadruple films. Small selected crystals were mounted on glass fibers and oriented optically. Laue photography was used to check the orientation and the perfection of the crystal. Crystals for different orientations were so selected that they would suit the particular orientation in their shape and size. They had dimensions of the order of 0.1 to 0.15 mm. The maximum difference in paths was about 0.03 mm. The absorption coefficient of Cu $K\alpha$ calculated for this crystal is about 9 mm.⁻¹ No attempt was made to correct for the absorption nor for the extinction error.

Equi-inclination Weissenberg photographs were taken of the following layer lines with Cu $K\alpha$ radiation:

$$a_1 : h = 0, 1, 2, 3, 4, 5, 6$$

$$a_2 : k = 0, 1, 2, 3, 4, 5, 6, 7, 8, 9, 10, 11, 12, 13$$

$$a_3 : l = 0, 1, 2, 3, 4$$

These are about all the layer lines that can be photographed with a maximum inclination angle of less than 30° in the Weissenberg goniometer used. On each layer line reflections may be

observed out to 1.21 \AA^{-1} from the origin in reciprocal space ($\sin \theta_{\max} = 0.930$). By using three crystals I made 1286 reflections in an octant of a sphere of radius 1.2 \AA^{-1} in the reciprocal lattice available for estimation of intensity. Among these 1286 reflections 68 are not on the pseudo reciprocal lattice.

In estimating the intensities of the reflections the procedure of the visual method improved by Dr. D. P. Shoemaker⁽⁵⁾ was followed. The Eastman No-Screen Duplitized Safety X-Ray Film was used throughout. Adequate care was taken to develop the intensity films. A film factor of 3.7 was used.

The intensities of reflections on the three equatorial Weissenberg photographs were estimated first. The estimation of the intensities of the reflections on the four equi-inclination Weissenberg photographs along a_3 followed. By using the ratios of estimated intensities of reflections $0k0$ to those of $0kl$ on the equatorial Weissenberg photograph along a_1 or ratios of those of $h00$'s to those of $h0l$'s on the equatorial Weissenberg along a_2 I brought the estimated intensities of reflections on the zero and first layer lines to a common scale. In a very similar manner all of the five Weissenberg photographs along a_3 were linked together. Reflections $hk5$, $hk6$, $hk7$ and $hk8$ are all weak. These last reflections were extracted from Weissenberg photographs along a_1 and a_2 , and their estimated intensities were tied together by a similar method. In determining the scale factors by comparing the estimated intensities

of reflections on different layer lines the part of Lorentz factor which depends on the equi-inclination angle ν was always taken into consideration. In view of the crystal form and the quality of spots on the photographs I relied much more on the set of Weissenberg photographs along a_3 than those along a_1 or a_2 . Due to the fact that a_3 is the shortest axis, each Weissenberg photograph along this axis contains more spots than those along a_1 or a_2 . This point has a two-fold advantage. The occurrence of a great number of spots on a single Weissenberg photograph facilitates the estimation work on the one hand and reduces the number of the scale factors one has to determine on the other.

The estimated intensity i from equi-inclination Weissenberg photographs taken with unpolarized monochromatic X-rays for a small, rotating, ideally imperfect (mosaic) crystal was corrected by polarization and Lorentz factors according to the equation⁽⁶⁾ given below.

$$i = k F_{hkl}^2 \frac{1 + \cos^2 2\theta}{\sin 2\theta} \frac{1}{\sqrt{1 - \frac{\sin^2 \nu}{\sin^2 \theta}}},$$

where $k F_{hkl}^2$ is the corrected intensity, F_{hkl}^2 is the square of the absolute value of the structure factor for the reflection hkl , and the angles θ and ν are the Bragg angle and the equi-inclination angle respectively. The factor k here is the absolute scale factor.

In order to extend the usefulness of the intensity data I tried to determine the factor k by the method suggested by

A. J. C. Wilson⁽⁷⁾. In case the following relationship exists to a close approximation,

$$\overline{F_{hkl}^2} = \sum_i \bar{f}_i^2,$$

where $\overline{F_{hkl}^2}$ is the average square of the structure factors for all reflections either hypothetically occurring or actually observed on photographs within a given range of $\sin^2 \theta / \lambda^2$, and \bar{f}_i is the atomic f value for the center of range of $\sin^2 \theta / \lambda^2$, then it will follow that

$$(k \overline{F_{hkl}^2} / \sum_i \bar{f}_i^2) = k e^{-2B \frac{\sin^2 \theta}{\lambda^2}},$$

and by taking logarithms on both sides we obtain

$$\ln (k \overline{F_{hkl}^2} / \sum_i \bar{f}_i^2) = \ln k - 2B \left(\frac{\sin^2 \theta}{\lambda^2} \right).$$

This equation provides the possibility of determining k and the temperature factor B simultaneously by making a plot of $\ln (k \overline{F_{hk}^2} / \sum_i \bar{f}_i^2)$ against $\sin^2 \theta / \lambda^2$.

I used all of the 1218 reflections observed on the pseudo reciprocal lattice, and included all of the rest which only exist hypothetically on the lattice by assigning zero intensity to each of them. The ranges I chose were $\sin = 0.3-0.4, 0.4-0.5, 0.5-0.6, 0.6-0.7, 0.7-0.8$ and $0.8-0.9$. The values of $\sum_i \bar{f}_i^2$ were calculated for centers of ranges on the basis that the pseudo unit cell contains four molecules of $\text{MnCl}_2 \cdot 2(\text{CH}_2)_6\text{N}_4$. The data used in the plot are given in Table V.

Table V.

$\sin^2 \theta / \lambda^2$	$\ln (k \overline{F_{hk\ell}^2} / \sum_i \overline{f_i^2})$
0.053	-4.2
0.086	-5.0
0.128	-5.2
0.178	-5.3
0.239	-5.6
0.321	-6.2

By extrapolation a value of -4.5 was obtained for $\ln k$. Then k is 1/100. The temperature factor B is 2.64×10^{-16} .

As I had assigned zero intensity to quite a number of reflections and used the anhydrous formula, I believed that the scale factor k could be too high, but never much too low. The absolute value of the structure factor calculated from the structure is about 15% higher than the observed ones which were calculated from the intensities reduced to an absolute scale. This is about what I expected.

8. THE SEARCH FOR A TRIAL STRUCTURE

In this section I shall derive trial structures from the chemical composition of the compound, the knowledge of the space group, the intensities of a few remarkably strong reflections, the known structure of the hexamethylenetetramine molecule, steric considerations, and a few reasonable assumptions. One of the trial structures thus derived leads to a satisfactory interpretation of the projections and the sections of the Patterson distribution function, thus to the determination of

the parameters for the heavy atoms and the hexamethylenetetramine molecules, and finally to the confirmation of the structure by a Fourier projection and by calculation of structure factors.

1) The number of complex molecules in the unit cell.---

A crop of carefully grown small crystals was dried first by centrifuging, then over silica gel, until constant weight was reached. About 100 mg. of hand-picked crystals were sent to Dr. A. Elek for microchemical analysis for manganese, chlorine, carbon, nitrogen, and hydrogen. The result is given in Table VI.

Table VI.

Element	Found	% Calculated*	Number of atoms in the pseudo	
			A Found	B Assumed*
Mn	12.25	12.40	4.04	4
Cl	16.07	16.03	8.10	8
C	32.84	32.60	48.40	48
N	25.06	25.35	31.80	32
H	3.58	6.40	63.60	112
O	<u>10.20</u>	<u>7.22</u>		8
	100.00	100.00		

* For the formula $\text{MnCl}_2 \cdot 2(\text{CH}_2)_6\text{N}_4 \cdot 2\text{H}_2\text{O}$.

The numbers in the fourth column in Table VI are the numbers of atoms of the respective elements calculated from the percentages

found in the microchemical analysis on the basis that the density of the crystal is 1.570 g./cm.³ and that the volume of the pseudo unit cell is 1874 Å.³ The numbers in the fifth column give the numbers of atoms in a pseudo unit cell which contains four molecules of the complex compound $\text{MnCl}_2 \cdot 2(\text{CH}_2)_6\text{N}_4 \cdot 2\text{H}_2\text{O}$. The general agreement is about as good as one would expect from any microchemical analysis of this kind; in particular, a large error in the result for hydrogen is not unexpected. While the formula of the anhydrous part of the complex compound is beyond reasonable doubt to be $\text{MnCl}_2 \cdot 2(\text{CH}_2)_6\text{N}_4$, it sounds rather strange that crystals prepared from organic solvents as I described in Section 3 should contain water. However the recrystallization took place in a volume of solvent very large compared to the crystals, and over a period of a few days to a few weeks; thus it is not surprising at all that the compound may have water of hydration, if water can form fairly strong bonds with manganese atoms. Further evidence regarding this point was gathered. The crystals become opaque in a desiccator over calcium chloride and remain transparent over silica gel. An opaque but not deformed crystal gave essentially the same Laue photograph as a transparent one.

2) The Orientation of the hexamethylenetetramine molecules in the crystal.---For 600, the strongest reflection, F^2 on an absolute scale is about 75000. The value can be only too small, because in reducing the intensities to an absolute scale I

assumed four molecules of the anhydrous complex compound in the unit cell, and I assigned zero intensity to each of those apparently absent reflections. In other words the absolute value of the structure factor F_{600} is equal to or greater than 275. The sum of the atomic f values for 600 from all atoms in the unit cell is 375. The sum of the f values of all manganese and chlorine atoms is only 146. This strongly suggests that even if all manganese and chlorine atoms are in phase, there still must be a large contribution from the carbon and nitrogen atoms in the hexamethylenetetramine molecules. It has been assumed throughout this work that the hexamethylenetetramine molecule has essentially the same structure* as found in its crystal. Calculation of F_{600} for all possible orientations of the molecule in the crystal indicated that the carbon and nitrogen atoms will contribute enough to make up the F_{600} with manganese and chlorine atoms in phase, when and only when one of the four three-fold axes of each hexamethylenetetramine molecule is approximately lines up along a_1 . In this case the hexamethylenetetramine molecules will contribute about 150 to the F_{600} . Figure 8 shows a comparison of the dimensions of the hexamethylenetetramine molecule with the (600) spacing.

* The molecule has symmetry T_d-43m .⁽¹⁾ The shortest C-N and N-N distances are 1.45 Å. and 2.42 Å., respectively.⁽⁸⁾

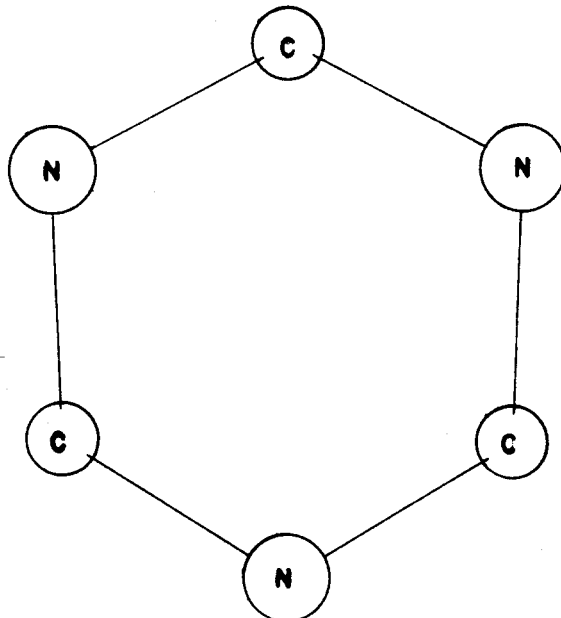
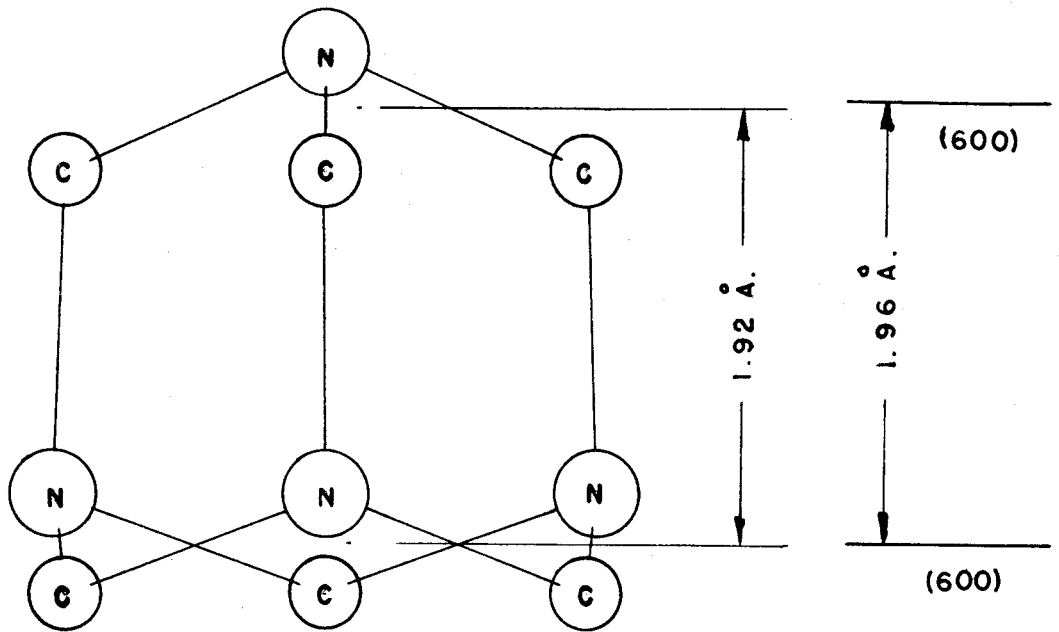
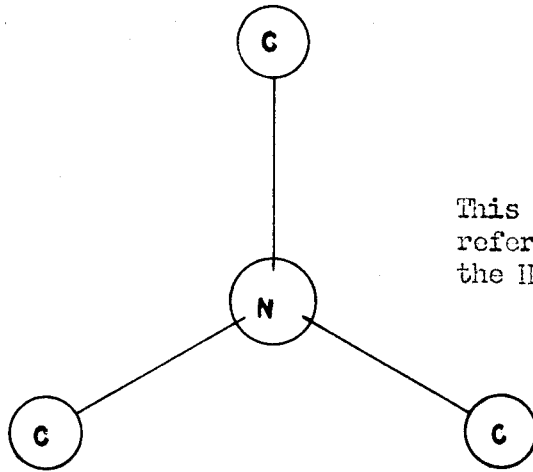
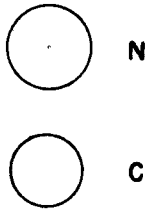


Figure 8. A comparison of the dimensions of the HMT molecule with the (600) spacing.

The carbon and nitrogen atoms as well as the manganese and chlorine atoms must distribute themselves in the neighborhood of a set of (600) planes.* It is remarkable that the apex and the base of a hexamethylenetetramine molecule are separated by a distance of about $2 \overset{\circ}{\text{A}}$., which is $d_{100}/6$.

3) The symmetry of the complex molecule.---The space group $C_{2v}^9-P2_1nb$ provides four general positions but no special ones. Each complex forms a crystallographically equivalent set. The space group does not require any symmetry for the complex molecule. However the formula $MnCl_2 \cdot 2(CH_2)_6N_4 \cdot 2H_2O$ of the complex compound suggests that there can be some sort of two-fold symmetry element passing through the central manganese atom. Each complex molecule or each equivalent set contains 25 atoms whose positions are determinable by ordinary X-ray diffraction methods. The knowledge of the hexamethylenetetramine structure reduces this problem to a 27-parameter one.

The assumption of a two-fold axis or mirror plane in the complex molecule will prevent the interpretation of the heavy peaks in the Patterson distribution function, and results in prohibitively short chlorine-chlorine distance. A center of symmetry turns out to be the right symmetry element of order two for the complex molecule.

* I define (600) planes as a set of (100) planes among which the distance between two successive ones is equal to $d_{100}/6$. Without loss of generality I specialize them to a set of (600) planes one of which passes through the origin.

With a center of symmetry in the complex molecule the approximate structure contains 15 parameters. However the calculation of structure factors still involves 25 atoms.

4) The coordination of the two hexamethylenetetramine molecules in a single complex molecule along a_1 .---Figure 9 shows the space group diagram for (100). In Figure 10 the configuration of the four equivalent points related by the symmetry operations of the space group is illustrated. Points 1 and 2 are related through an a_2 glide plane normal to a_3 : so are points 3 and 4. Either pair of points can be derived from the other either by means of a two-fold screw axis parallel to a_1 or by an n glide plane normal to a_2 .

Figure 11 shows the five possible arrangements of the two unequivalent hexamethylenetetramine molecules in an asymmetric quadrant of the unit cell, with reference to the x coordinates and direction only. In Figure 11 HMT I and HMT II are any pair of unequivalent hexamethylenetetramine molecules taken from the eight hexamethylenetetramine molecules in the unit cell.

With the assumption of a center of symmetry in the complex molecule one can exclude the arrangements 11-2 and 11-3. Due to the fact that the manganese atom at the center of a complex molecule must be on one of the same set of (600) planes and that F_{400} is equal to or greater than 180, the arrangement in Figure 11-1 is the only appropriate one, and HMT I and HMT II in Figure 11-1 belong to one complex molecule.

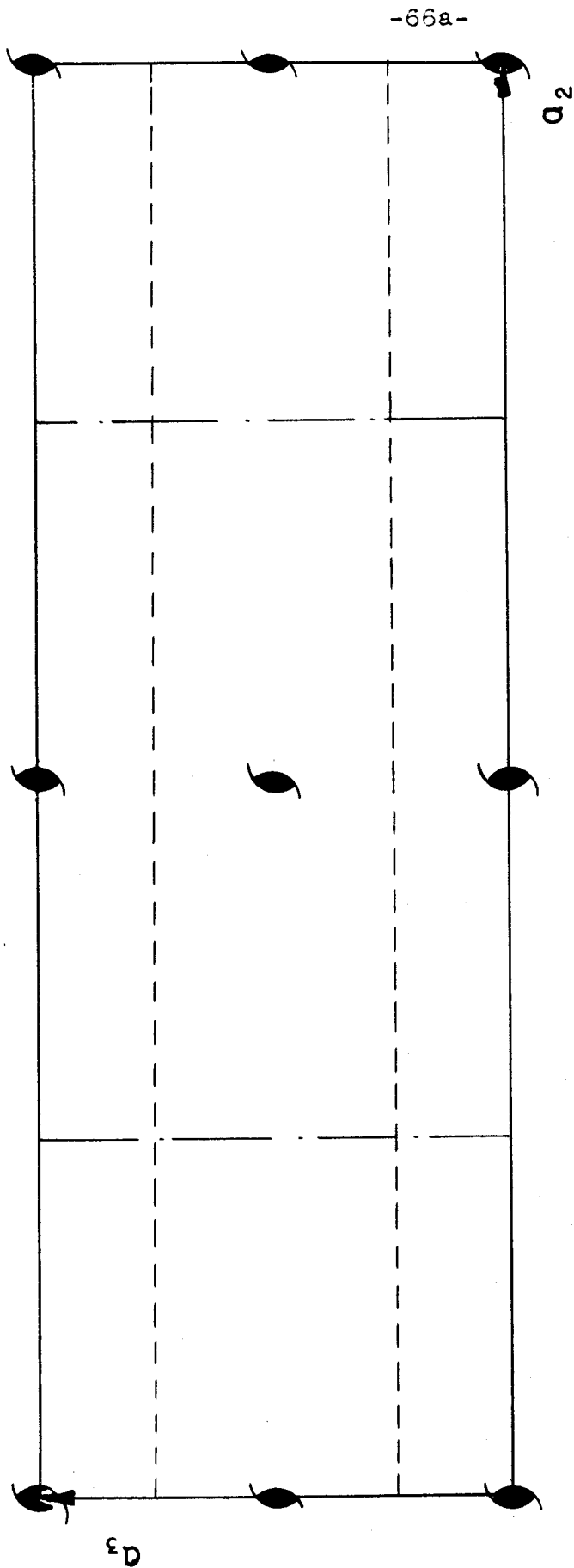


Figure 9. Symmetry elements of the space group $C_{2v}^9-P2_1nb$.
The a_1 axis is perpendicular to the plane of the paper.

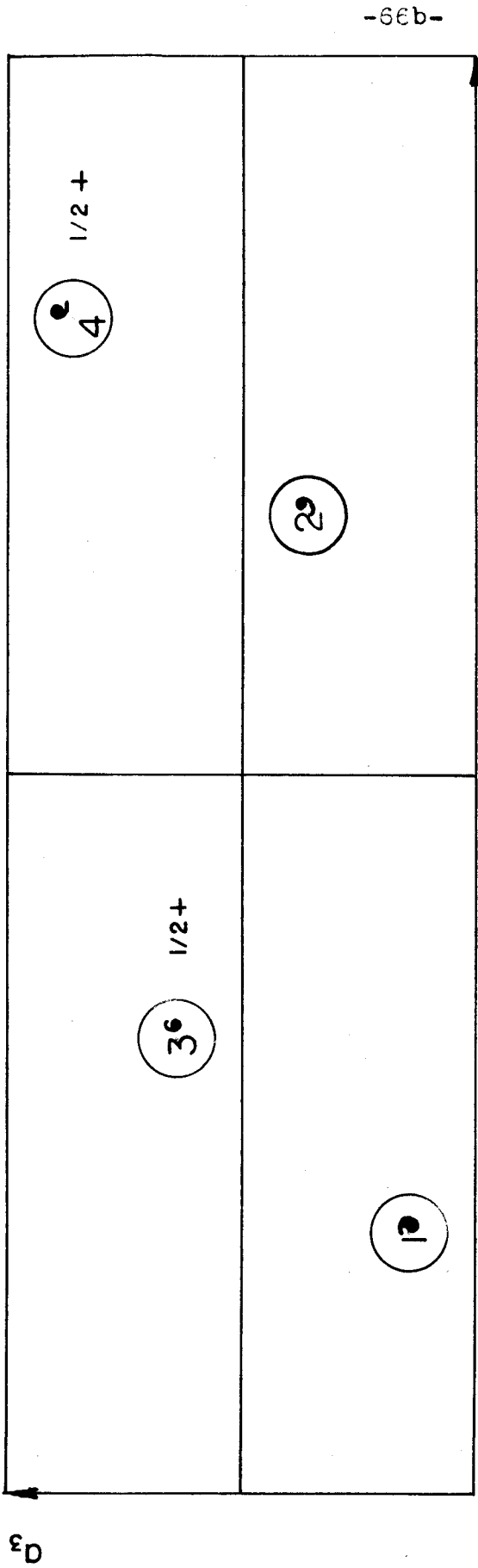


Figure 10. The configuration of four crystallographically equivalent points in the space group $C_{2v}-P2_1nb$.

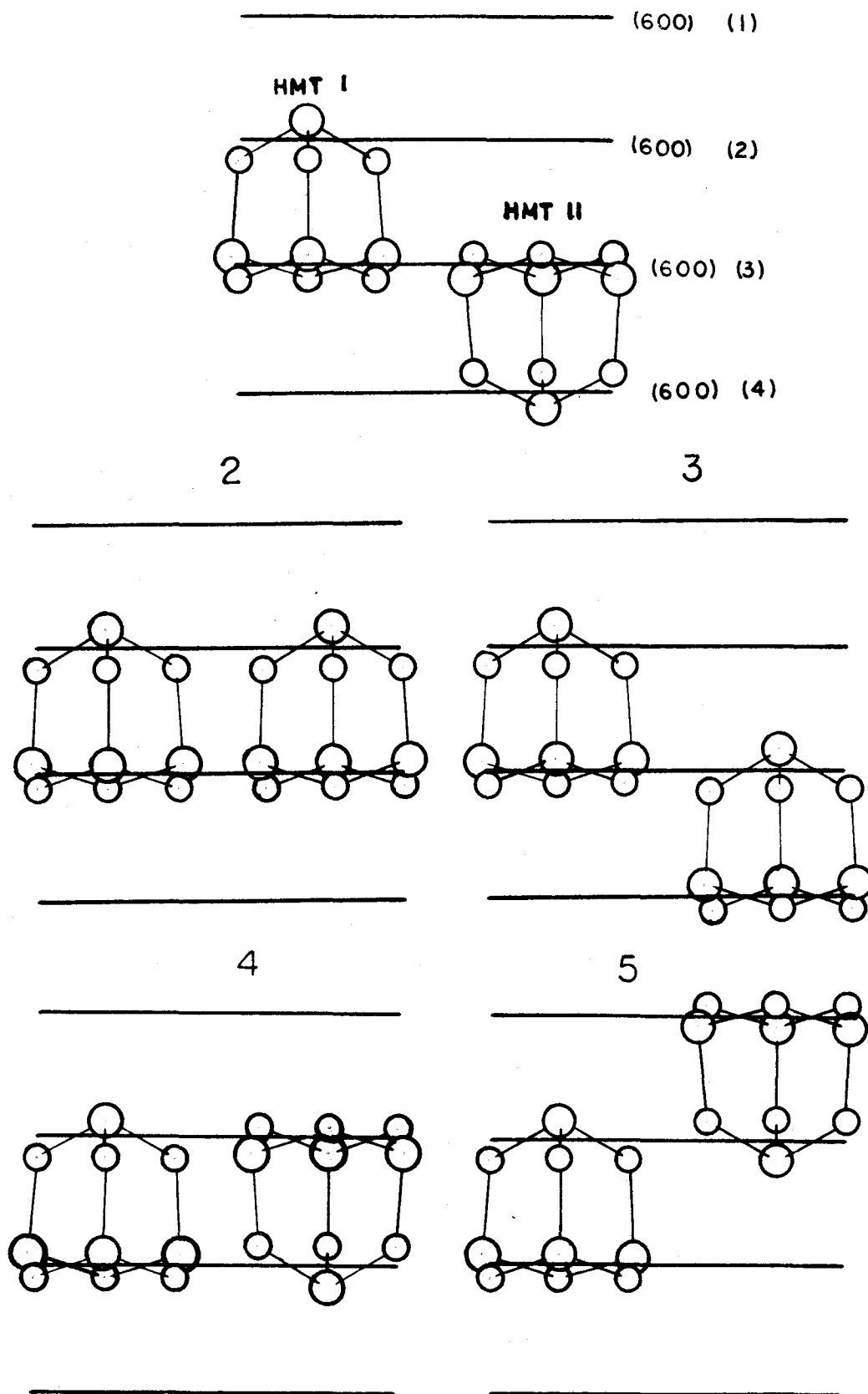


Figure 11. The five possible arrangements of the two unequivalent HMT molecules in an asymmetric quadrant of the unit cell, with reference to the x coordinates and direction only.

5) The location of the manganese atom and the center of the hexamethylenetetramine molecules, with reference to the y, z coordinates only.---With arrangement 11-1 the carbon and nitrogen atoms of the bases of the two hexamethylenetetramine molecules are distributed in the neighborhood of the plane (600) (3). On (100) atoms will be duplicated by the operation of an a_2 glide normal to a_3 . In Figure 12 one will see that the carbon and nitrogen atoms of the base of the hexamethylenetetramine molecule are distributed approximately on the circumference of a circle of radius $1.4 \overset{\circ}{\text{Å}}$. As we know well, the atoms must be kept apart from the others of the neighboring hexamethylenetetramine molecules by a van der Waals distance. The van der Waals radii for the nitrogen atom and the methyl group are 1.5 and $2.0 \overset{\circ}{\text{Å}}$. respectively⁽⁹⁾. The base of the hexamethylenetetramine molecule then has an effective radius of $3.3 \overset{\circ}{\text{Å}}$. in the plane (600) (3) in Figure 11-1. This value will be further supported by considering the presence of manganese atoms in the plane. The effective radius $3.0 \overset{\circ}{\text{Å}}$. found in the hexamethylenetetramine crystal structure along a body diagonal is obviously too small for the present application due to the different coordination of the hexamethylenetetramine molecules here. The effective radius along the cube edge is $3.5 \overset{\circ}{\text{Å}}$.

By accepting the value $3.3 \overset{\circ}{\text{Å}}$. for the effective radius and using the operation of the a_2 glide plane I can by steric considerations confine the bases of the hexamethylenetetramine

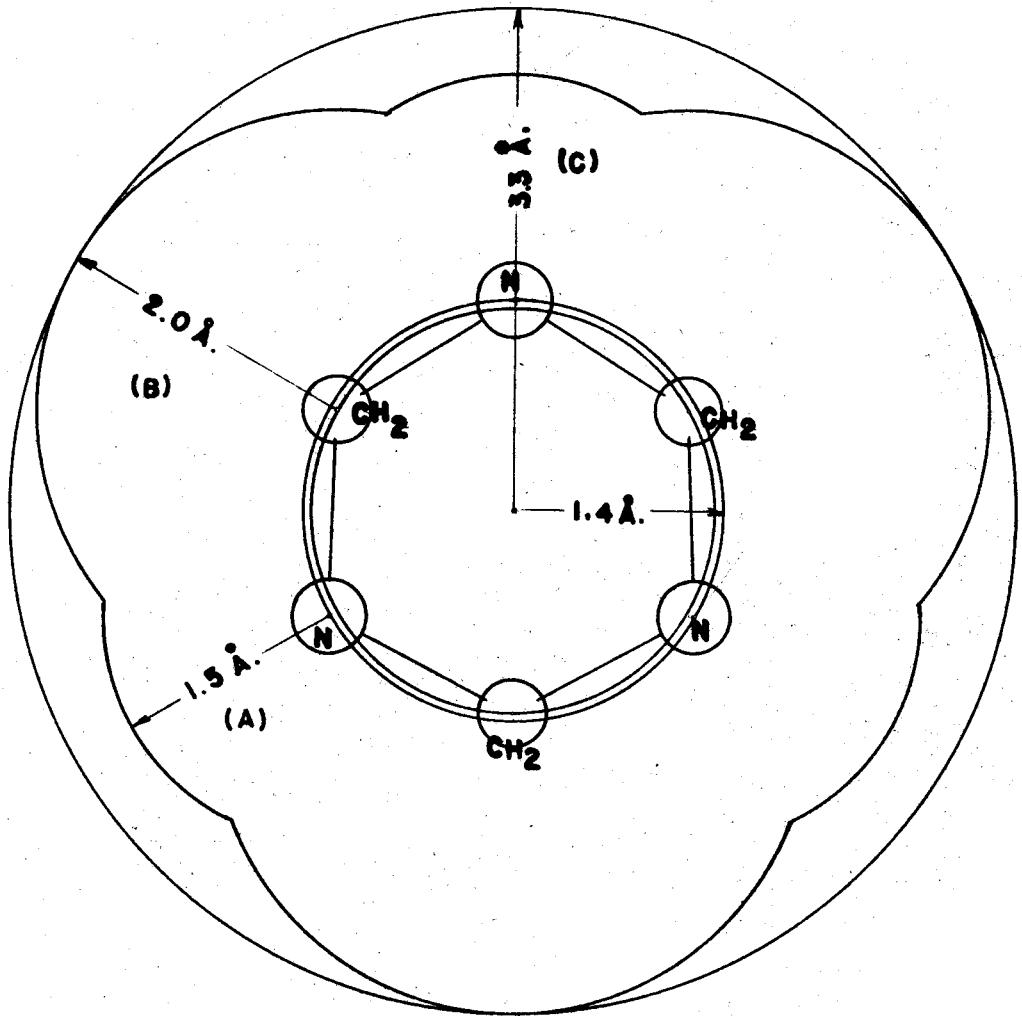


Figure 12. The effective radius of the base of a HMT molecule. (A) The van der Waals radius of a nitrogen atom. (B) The van der Waals radius of a methyl group. (C) The effective radius of the base of a HMT molecule.

molecules with respect to the y, z coordinates as shown in Figure 13. By means of the center of symmetry of the complex molecule I can confine the manganese atoms as well. However the values of the y coordinates relative to the symmetry elements remain unfixed. The approximate coordinates of the four manganese atoms in the unit cell can be given as below.

$$\begin{aligned} \text{Mn}_1 & \quad (1/2, y_0 + 1/8, 0) \\ \text{Mn}_2 & \quad (1/2, y_0 + 5/8, 1/2) \\ \text{Mn}_3 & \quad (0, 3/8 - y_0, 1/2) \\ \text{Mn}_4 & \quad (0, 7/8 - y_0, 0) \end{aligned}$$

The x coordinates are exact as far as the space group is exact. However the z coordinates inherited their uncertainties from the above derivation.

6) The x coordinates of the two chlorine atoms in the complex molecules.--- The chlorine atoms must be distributed on the planes of the same set of (600) planes as I concluded in paragraph (2) of this section. With the arrangement in Figure 11-1 one chlorine atom will be on the plane (600) (2), and the other on (600) (4), inasmuch as there is no room on (600) (3). The approximate x coordinates of the eight chlorine atoms which are consistent with the previous assignment of the x coordinates of the manganese atoms are the following:

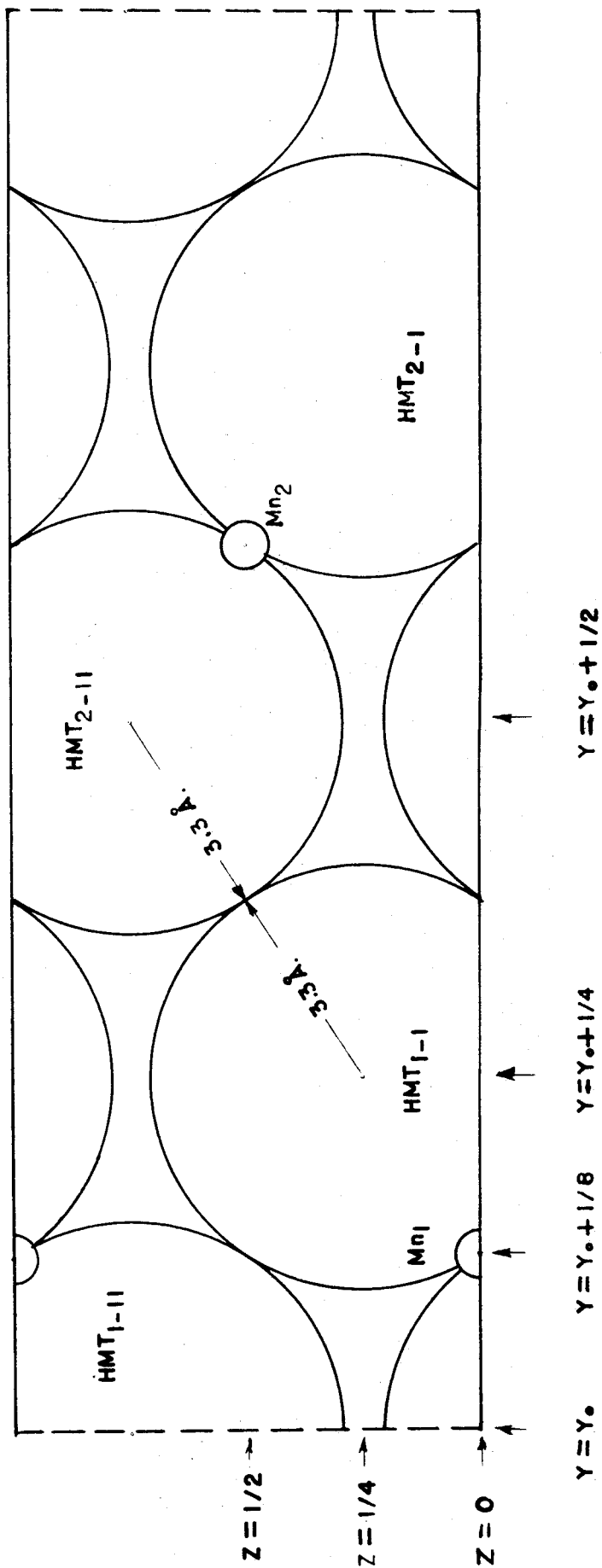


Figure 13. The confinement by steric considerations of the manganese atoms and the centers of the bases of the HMT molecules, with respect to their y, z coordinates.

Cl ₁ -I	2/3
Cl ₁ -II	1/3
Cl ₂ -I	2/3
Cl ₂ -II	1/3
Cl ₃ -I	1/6
Cl ₃ -II	-1/6
Cl ₄ -I	1/6
Cl ₄ -II	-1/6

9. THE DETERMINATION OF THE APPROXIMATE STRUCTURE

Summary.---Several Patterson sections and projections were calculated. Guided by the trial structure I could correlate most of the important peaks with vectors which fix the positions of manganese, chlorine, and the hexamethylenetrarnine molecules. A few important features in the Patterson function indicate that the assumption about the symmetry of the complex molecule used in deriving the trial structure is sound. However a better confirmation of the general features of the approximate structure was achieved by making a two-dimensional Fourier projection on (100), a projection which shows a center of symmetry. The agreement between the calculated and observed structure factors for reflections $Ok\ell$ is satisfactory, if one considers the fact that the structure factors for most reflections of this type are only a small fraction of F_{000} . The reflections $h00$ are on the other hand mostly outstandingly strong. A one-dimensional

Fourier projection onto the a_1 axis reproduces the succession of layers along this axis in the unit cell. The agreement between the calculated and observed $|F|$'s for maxima $h00$ is good. Information regarding the probable positions of oxygen atoms belonging to water molecules, whose presence was indicated by the microchemical analysis and determination of density, will be presented in a latter part of this section. In the last part the whole approximate structure will be described both graphically and analytically.

1) The application of the Patterson synthesis.---Due to the symmetry of the space group $C_{2v}^9-P2_1nb$ of the crystal the Patterson distribution has a symmetry D_{2h}^1-Pmmm . In other words one has to calculate the Patterson function only for one octant; namely $u = 0$ to $1/2$, $v = 0$ to $1/2$, and $w = 0$ to $1/2$. For the Patterson projection on (001) one has to calculate only for $u = 0$ to $1/2$, and $v = 0$ to $1/4$, because the projected structure in the plane in question has an identity distance in the direction $[010]$ only half of the a_2 axis due to the presence of the a_2 glide plane normal to a_3 .

By assuming four complex molecules of the formula $MnCl_2 \cdot 2(CH_2)_6N_4 \cdot 2H_2O$ in the unit cell, classifying manganese and chlorine atoms as heavy atoms, and carbon, nitrogen, and oxygen as light atoms, and ignoring the hydrogen atoms, one will have 12 heavy atoms and 88 light atoms to consider, and will expect theoretically distinct peaks as listed below.

Class	Kind of Interaction responsible for the Peak	Number of theoretically distinct Peaks
1	Harker, heavy atom-heavy atom	9
	Non-Harker, heavy atom-heavy atom	12
2	Harker, heavy atom-light atom	0
	Non-Harker, heavy atom-light atom	264
3	Harker, light atom-light atom	66
	Non-Harker, light atom-light atom	924
	Peak at origin	<u>1</u>
	Total	1276

It was fully realized at the beginning that at best the Patterson projection can resolve only the peaks of Class 1, while suitable Patterson sections can show some recognizable peaks of Class 2. Actually this prediction works fairly well. This consideration provides an excuse for omitting most of the elaborate technique in preparing the Patterson summation. The application of the sharpening technique and a modification function to the reflections I observed for this crystal would have been very time consuming, although its merit is quite doubtful, inasmuch as the useful heavy peaks will stand out anyway, and the sharpening and use of modification function may give rise to some undesirable complications. However, in one or two projections I made, the heavy doublet peaks could have been resolved, if I had used those techniques.

The Patterson summations were carried out by means of the L cards on the International Business Machines. (10)

In the following two parts I shall present the results from the Patterson synthesis and the theoretical analysis which led to the determination of the coordinates of the heavy atoms, and to that of the positions of the hexamethylenetetramine molecules, respectively.

a) Determination of the coordinates of the heavy atoms in the crystal by the Patterson synthesis.---A Patterson projection on (100) was made by carrying out the summation

$$P(v, w) = \sum_{k=-\infty}^{+\infty} \sum_{l=-\infty}^{+\infty} F_{0kl}^2 \cos 2\pi kv \cos 2\pi lw.$$

The projection is plotted in Figure 14.

The Patterson projection on (001) was prepared by carrying out the following summation:

$$P(u, v) = \sum_{h=-\infty}^{+\infty} \sum_{k=-\infty}^{+\infty} F_{hk0}^2 \cos 2\pi hu \cos 2\pi kv.$$

It is presented in Figure 15.

The identification and interpretation of the heavy peaks of Class 1 on both projections were carried out in the following manner. From the approximate coordinates for the manganese atoms derived for the trial structure one expects outstanding Harker peaks due to manganese-manganese interactions as given below.

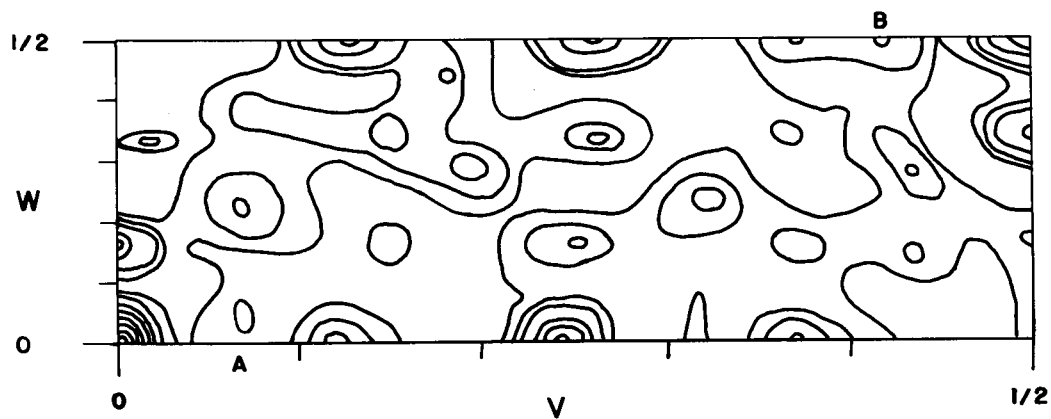
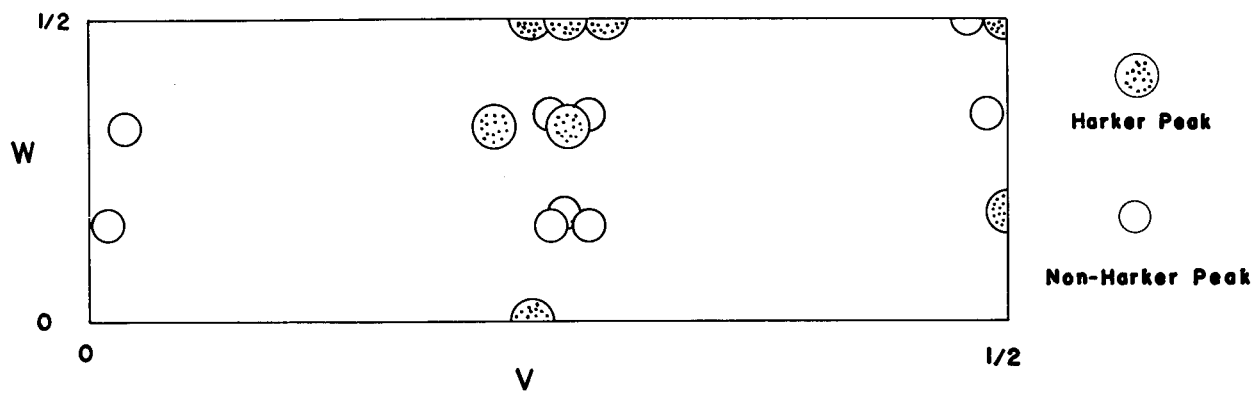
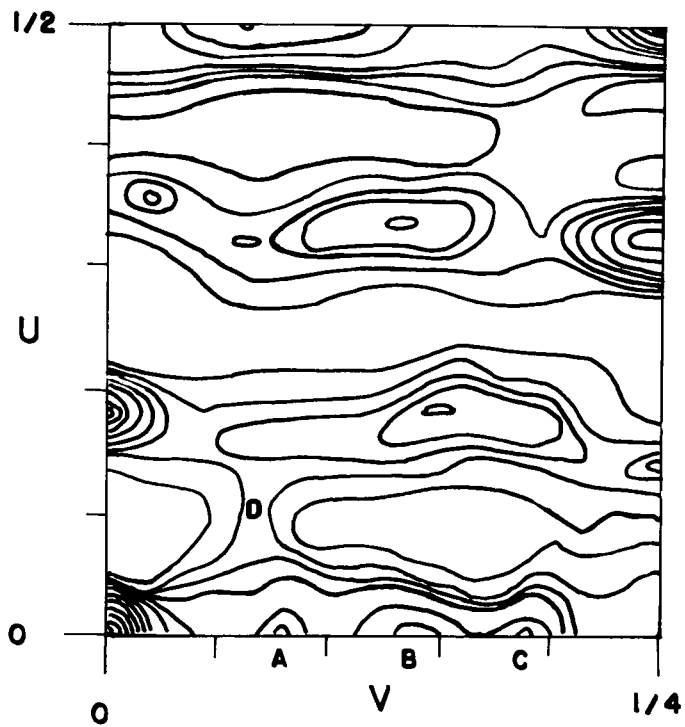
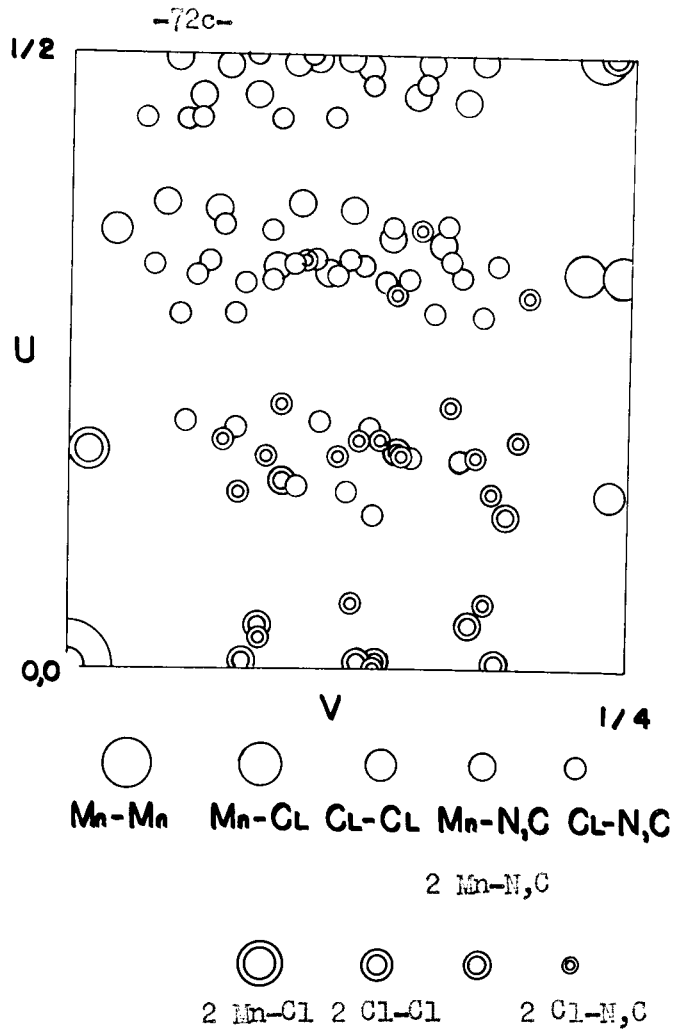


Figure 14. The Patterson projection $P(v, w)$ with the theoretical map for the interatomic vectors between the heavy atoms. The contour line intervals on an arbitrary scale are 900, 1250, 1500, 2000, 2500, 3000, 3500, and 4000.

Figure-15. The patterson projection $P(u,v)$ with the theoretical map for the interatomic vectors between heavy atoms and between heavy and light atoms. The contour line intervals on an arbitrary scale are -100, 0, 50, 100, 200, 300, 400, 500, 600, 700, 800, 900, 1000, 1200, and 1300.



Peak	Interactions	Positions
1	Mn_1-Mn_3, Mn_2-Mn_4	$(1/2, 2y_0 + 1/4, 0)$
2	Mn_1-Mn_2, Mn_3-Mn_4	$(0, 1/2, 1/2)$
3	Mn_1-Mn_4, Mn_2-Mn_3	$(1/2, 2y_0 - 1/4, 1/2)$

In the Patterson projection $P(v, w)$ one will find peak 1 in the neighborhood of the line $w = 0$. However three peaks were found in that neighborhood. If the peak at $(1/8, 0)$ in Figure 14 were the peak 1, then there would be a Mn-Mn peak corresponding to peak 3 in the neighborhood of $(3/8, 1/2)$ on the projection $P(v, w)$, and a Mn-Mn peak corresponding to peak 1 in the neighborhood of $(1/2, 1/8)$ on the projection $P(u, v)$ in Figure 15. The peak at $(3/8, 0)$ in $P(v, w)$ cannot be the peak 1 either due to the fact that no peak corresponding to peak 1 can be found in the neighborhood of $(1/2, 1/8)$ on the projection $P(u, v)$. Thus I identified unambiguously the peak at $(0.240, 0)$ or approximately at $(1/4, 0)$ on the projection $P(v, w)$ with peak 1. Then y_0 is -0.005 .

Furthermore after adjusting the minimum value in $P(v, w)$ I found that the peak at $(1/4, 0)$ has a strength of $1/4$ to $1/2$ of that of the peak at origin. In other words two manganese-manganese interactions alone as assigned to peak 1 will not adequately account for the observed height of the peak. The pairs Mn_1, Mn_4 , and Mn_2, Mn_3 whose interactions give rise to this peak are related by the two-fold screw axis parallel to a_1 .

It can be shown that if there is in the complex molecule a center of symmetry or a two-fold axis parallel to a_1 , then the projections of the complex molecules in the plane (100) will form two parallel pairs, 1 and 4, and 2 and 3, respectively, and therefore will give the observed strength to the peak 1. I have already mentioned that the two-fold axis is not the right symmetry element of order two for the complex molecule. This analysis supports the assumption of a center of symmetry in the complex molecule.

In Section 8-5, 8-6 I assigned exact x coordinates for the manganese atoms and approximate ones for the chlorine atoms. With knowledge of their values one will identify easily the heavy peak in the neighborhood of $(1/6, 0)$ on the projection $P(u, v)$ in Figure 15, as the peak due to the interactions Mn-Cl within each complex molecule. I identified the peak in the neighborhood of $(0, 1/6)$ on the projection $P(v, w)$ in Figure 14 as due to the same Mn-Cl interactions. In view of the elongated shape of both peaks one will expect that the manganese atom and the two chlorine atoms in each complex molecule will not have same y coordinates. This peak could have been resolved into two peaks related by a mirror plane by using those techniques I mentioned previously. However I was still able to determine the y coordinates sufficiently accurately for the chlorine atoms from these unresolved peaks. In order to confirm this interpretation of Mn-Cl peaks I made a Patterson section by carrying out the summation,

$$P(u, 0, w) = \sum_{h=-\infty}^{+\infty} \sum_{l=-\infty}^{+\infty} \left[\sum_{k=-\infty}^{+\infty} F_{hkl}^2 \right] \cos 2\pi hu \cos 2\pi lw$$

The summation is plotted in Figure 16.

Inasmuch as I can find only one intra molecular manganese-chlorine vector from the Patterson distribution function, the two chlorine atoms must distribute themselves around the manganese atom to give a center of symmetry. This is further supported by the chlorine-chlorine peak in the section $P(u, 0, w)$.

The identifications described above, if they are correct, are sufficient to give complete information regarding the positions of all heavy atoms in the complex molecule and in the unit cell. The coordinates of the heavy atoms in the complex molecule 1 are given below.

Mn ₁	(0.500, 0.120, 0)
Cl _{1-I}	(0.683, 0.130, -0.170)
Cl _{1-II}	(0.317, 0.110, 0.170)

On the basis of these values I calculated the height of the 21 peaks of Class 1, and also their positions. The results I present in Table VII and in the theoretical maps for the interatomic vectors between heavy atoms included in Figure 14 and Figure 15. Due to the presence of a center of symmetry in the complex molecule there are only 19 theoretically distinct peaks of Class 1 instead of 21. In the projections the number of

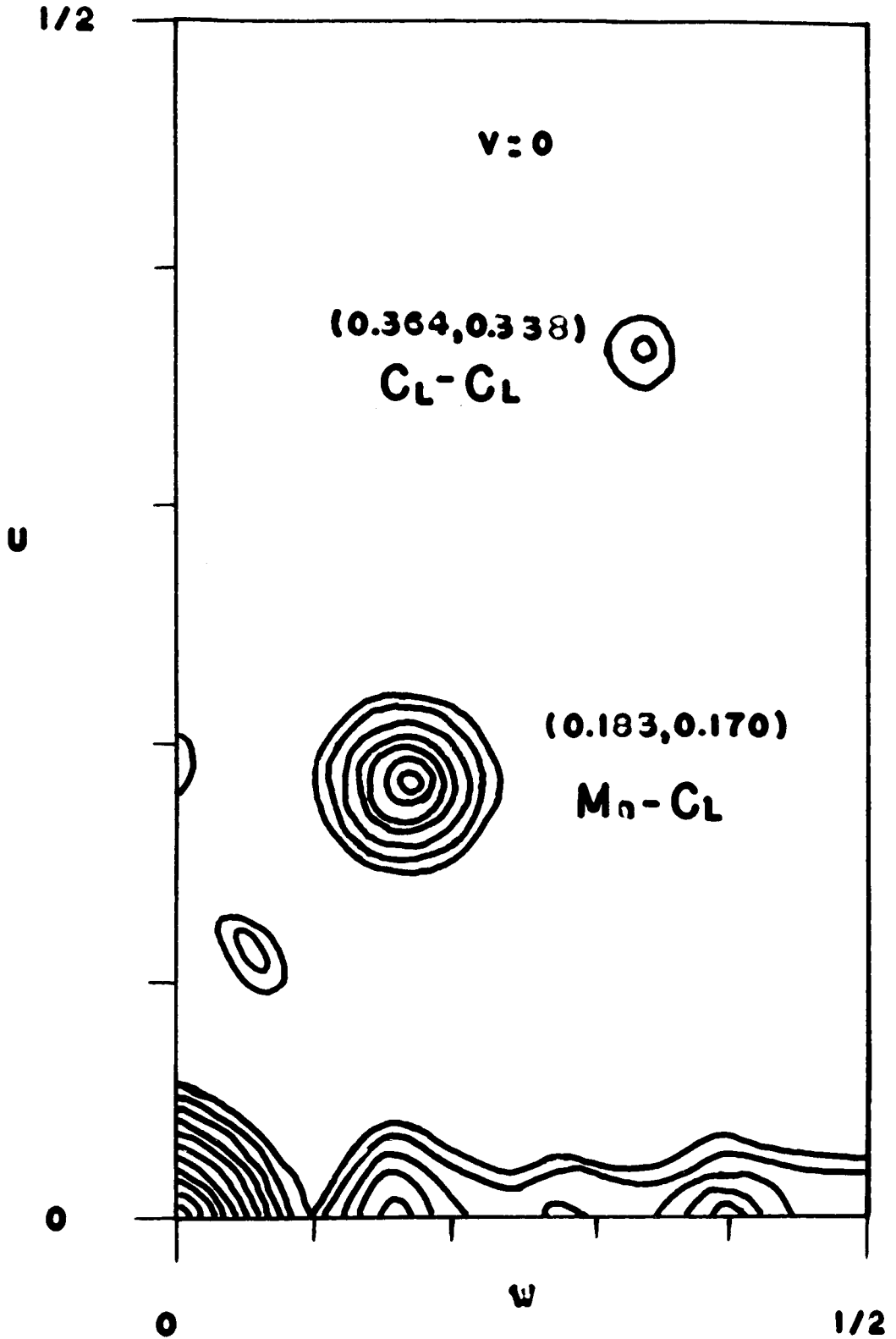


Figure 16. The Patterson section $P(u, 0, w)$. The contour line intervals on an arbitrary scale are 100, 150, 200, 250, 300, 350, 400, 500, 1000, 1500, and 2000.

theoretically distinct peaks is further reduced. The last column in Table VII refers to the particular Patterson summations among those I have presented in which one can find the respective peak and identify it easily.

Table VII.

Coordinates of Peak in P (u, v, w)			Interaction	Order of* Symmetry at uvw	Occurrence
u	v	w			
0	1/2	0.500	Harker 2 Mn-Mn	<u>8</u>	P(v, w)
1/2	0.240	0.000	Harker 2 Mn-Mn	4	P(v, w) & P(u, v)
1/2	0.260	1/2	Harker 2 Mn-Mn	4	P(v, w) & P(u, v)
0	1/2	0.160	Harker 2 Cl-Cl	4	P(v, w) & P(0,v,w)
1/2	0.260	0.340	Harker 2 Cl-Cl	2	P(v, w) & P(u, v)
1/2	0.240	1/2	Harker 2 Cl-Cl	4	P(v, w) & P(u, v)
0	1/2	0.160	Harker 2 Cl-Cl	4	P(v, w) & P(0,v,w)
1/2	0.220	0.340	Harker 2 Cl-Cl	2	P(v, w) & P(u, v)
1/2	0.280	1/2	Harker 2 Cl-Cl	4	P(v, w) & P(u, v)
0.183	0.010	0.170	Non-Harker 8 Mn-Cl	<u>2</u>	P(v,w),P(u,v) & P(u,0,w)
0.183	0.490	0.330	Non-Harker 8 Mn-Cl	<u>2</u>	P(v, w) & P(u, v)
0.317	0.250	0.330	Non-Harker 4 Mn-Cl	1	P(v, w) & P(u, v)
0.317	0.270	0.330	Non-Harker 4 Mn-Cl	1	P(v, w) & P(u, v)
0.317	0.250	0.170	Non-Harker 4 Mn-Cl	1	P(v, w) & P(u, v)
0.317	0.230	0.170	Non-Harker 4 Mn-Cl	1	P(v, w) & P(u, v)
0.366	0.020	0.340	Non-Harker 4 Cl-Cl	<u>2</u>	P(v,w),P(u,v) & P(u,0,w)
0.366	0.480	0.500	Non-Harker 4 Cl-Cl	<u>4</u>	P(v, w) & P(u, v)
0.134	0.260	0.160	Non-Harker 4 Cl-Cl	1	P(v, w) & P(u, v)
0.134	0.240	0.000	Non-Harker 4 Cl-Cl	<u>2</u>	P(v, w) & P(u, v)

* This column gives the order of the symmetry group at uvw in P(u, v, w). The height of a peak at uvw is increased by a factor equal to this order.

b) Determination of the positions of hexamethylenetetramine molecules in the crystal by the Patterson synthesis.---In Sections 8-4 and 8-5 I was already able to confine the centers of the bases of the hexamethylenetetramine molecules in a small region in the plane (600) (3) in Figure 11 (Figures 12 and 13). If we now consider that a manganese atom will be placed between the two centers of the two hexamethylenetetramine molecules in that plane, it is quite obvious that the manganese atom will be immediately surrounded by two nitrogen atoms rather than two methylene groups. In the first place there is not enough room between two such methylene groups to accommodate a manganese atom. However the manganese atom will find ample room between two nitrogen atoms, if the two hexamethylenetetramine molecules are so arranged that each of them has a nitrogen atom lying on the line connecting their centers. Figures 12 and 13 are illuminating for this point. With this picture of the situation in mind one will be able to see the hexamethylenetetramine molecule even on the projection $P(v, w)$ in Figure 14. If one remembers the shape of the hexamethylenetetramine molecule when it is projected onto its base, then he will recognize that the peaks other than A, B, and those of Class 1 are due to the interactions between the manganese atom and the light atoms of a whole hexamethylenetetramine molecule. A closer analysis reveals that the interactions between the chlorine atoms and the light atoms are not important in this projection, though they may give rise to some perturbations of the manganese-light atom peaks.

In the projection $P(u, v)$ in Figure 15 one may at first be discouraged by the shape of the peaks of Class 2. However a closer study shows that the peaks A, B, and C in the neighborhood of the line $u=0$ can be due only to the intra molecular interactions of Class 2, and they are in a fairly resolved form. The peaks A, B, and C together with the rough arrangement of hexamethylenetetramine molecules deduced from Figure 13 or 14 or earlier fix the two hexamethylenetetramine molecules around one manganese atom; namely, the carbon and nitrogen atoms must lie at such levels along a_1 that they interact with the manganese atom to give A, B, and C.

The three peaks will be resolved in the sections $P(0, v, w)$, and $P(1/60, v, w)$. Furthermore the peaks thus resolved will be immediately identifiable as due to manganese-carbon or manganese-nitrogen vectors, respectively, because the interatomic distances in the hexamethylenetetramine molecule are known. I prepared the two Patterson sections by carrying out the following two summations:

$$P(0, v, w) = \sum_{k=-\infty}^{+\infty} \sum_{l=-\infty}^{+\infty} \sum_{h=-\infty}^{+\infty} F_{hkl}^2 \cos 2\pi kv \cos 2\pi lw$$

$$P(1/60, v, w) = \sum_{k=-\infty}^{+\infty} \sum_{l=-\infty}^{+\infty} \left[\sum_{h=-\infty}^{+\infty} F_{hkl}^2 \cos 2\pi h \cdot \frac{1}{60} \right] \cos 2\pi kv \cos 2\pi lw$$

The sections are plotted in Figure 17. The pair of peaks 1 and 2 were identified as due to the Mn-C interactions, the pair 3 and 4 to Mn-N. The distance between the first pair of peaks is essentially the C-C distance found in the hexamethylenetetramine molecule. The N-N distance was reproduced by the pair 3 and 4. This strongly suggests that the respective pairs of atoms are coplanar normal to a_1 . The distance between the pairs of peaks 1, 3, and 2, 4 is the C-N distance projected in this plane. Furthermore the peaks 1, 2, 3, and 4 have essentially the same prominence in both sections. On the basis of this evidence I assumed that the pairs of carbon and nitrogen atoms in question are distributed approximately on the levels $x = x_{Mn} \pm \frac{1}{120}$. With the information given out by the three peaks A, B, and C in the projection $P(u, v)$ one can exclude all alternative assignments for the signs of the last part in the expression for x to respective pairs of carbon and nitrogen atoms except one; namely $-\frac{1}{120}$, $\frac{1}{120}$ for the pairs of carbon and nitrogen atoms in the hexamethylenetetramine molecule I, and $\frac{1}{120}$, $-\frac{1}{120}$ for the respective pairs in the molecule II. (See Figure 18).

Figure 18 illustrates the complex molecule 1. The pairs of carbon and nitrogen atoms (shaded) on the levels mentioned above. Their respective distances from the atom Mn_1 and the angle β are determined by means of the Patterson sections in Figure 17. These parameters suffice to describe the positions

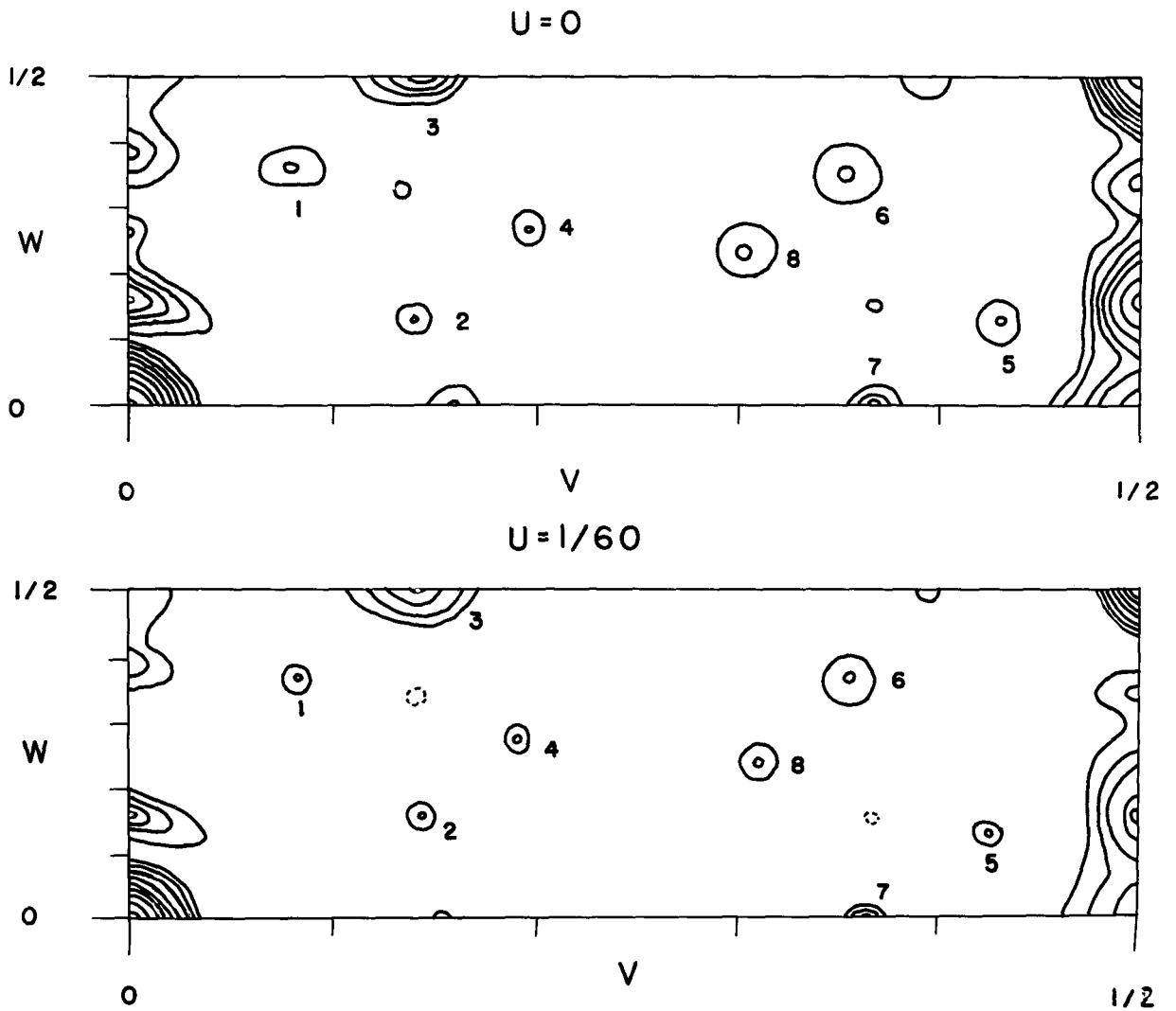


Figure 17. The Patterson sections $P(0, v, w)$ and $P(1/60, v, w)$. The contour line intervals on an arbitrary scale are 100, 150, 200, 250, 300, 400, 500, 1000, 1500, and 2000.

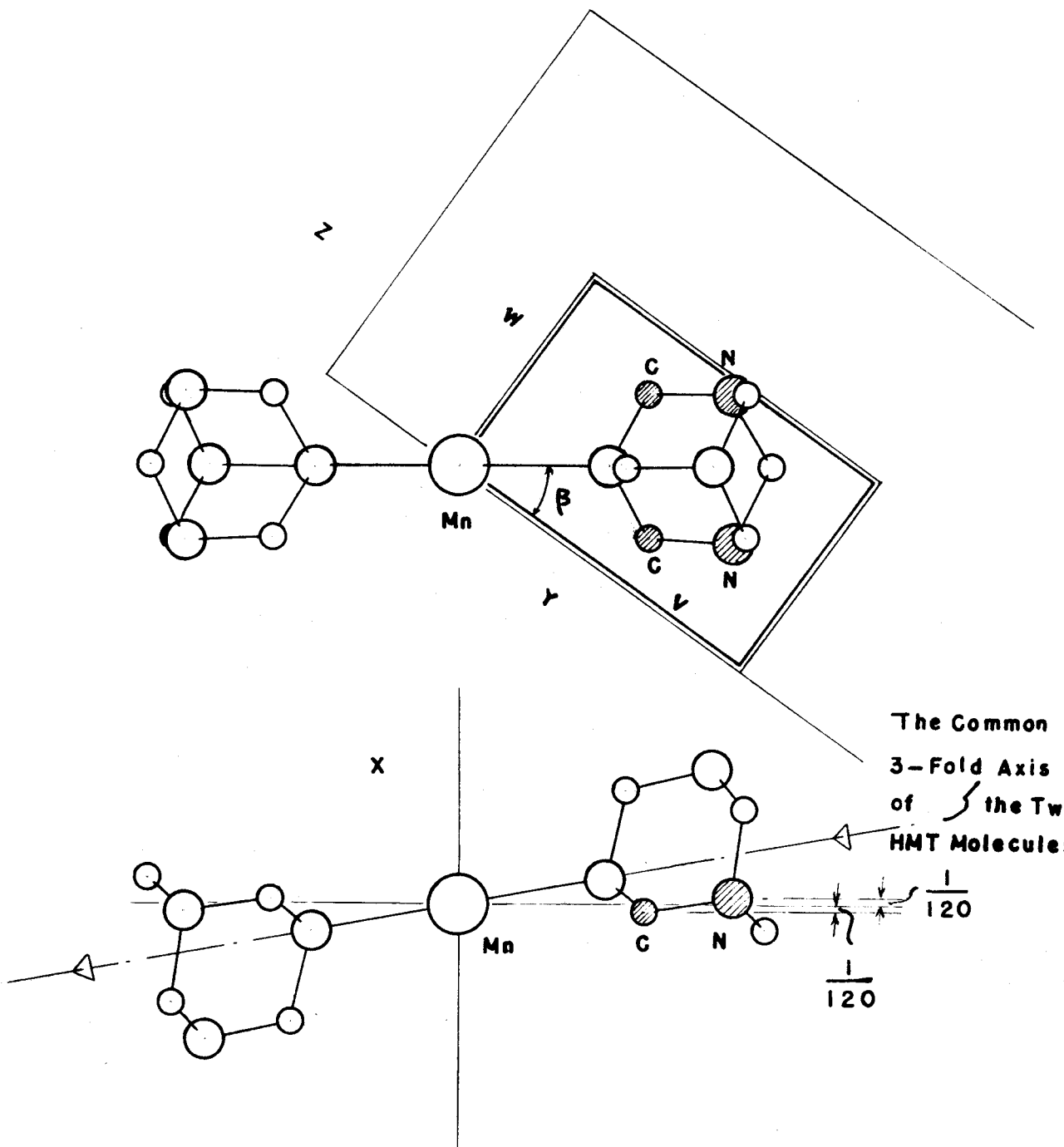


Figure 18. The coordination of the two hexamethylenetetramine molecules as determined by the Patterson projections and sections. The double line refers to an octant of the Patterson unit cell. The single line refers to the structural unit cell.

of the hexamethylenetetramine molecules in the crystal in terms of the coordinates of the manganese atoms. It turns out that the manganese atom lies on the common three-fold axis of two hexamethylenetetramine molecules.

The Patterson sections indicated that the two hexamethylenetetramine molecules also are distributed around the manganese atom centro-symmetrically. The assumption of a center in the complex molecule is now completely justified.

A theoretical map for the interatomic vectors of both Class 1 and 2 for the projection $P(u, v)$ is presented with the corresponding projection in Figure 15. The preparation of this theoretical map consisted mainly in describing in the plane in question the whole complex molecule I from the centers of the atoms Mn_1 , Cl_{1-I} , Cl_{1-II} , and Mn_3 , Cl_{3-I} , Cl_{3-II} graphically.

2) Projections of the distribution function for electron density; the calculation of structure factors.---In Section 9-(1) I determined an approximate structure for the crystal by a method, namely Patterson synthesis, which avoided the need for definite knowledge as to whether or not the unit cell contained other components than $MnCl_2 \cdot 2(CH_2)_6N_4$. Sufficient information was obtained to permit next the preparation of projections of the distribution function for electron density. Two projections, $\rho(x)$ and $\rho(y, z)$, were made. Both are centrally symmetric, the first because of the center in the complex

molecule, the second by the space group. While both projections confirmed the approximate structure, they did not refine the parameters much. For the latter purpose additional Fourier projections or sections with more X-ray data would be necessary, but they might well give too little new information to justify the effort involved.

a) The Fourier projection $\rho(x)$ and the calculation of structure factors for reflections $h00$.---The real part A of the structure factor for $h00$ is given by the formula,

$$A = 4 \sum f \cos 2\pi hx,$$

where the summation is over all atoms in the complex molecule 1. Due to the center of symmetry present in each complex molecule the imaginary part vanishes. With the x coordinates taken from the Patterson synthesis I obtained the values for F_{h00} which are listed in Table VIII Column A. The observed value for F_{600} , readjusted by a new scale factor, are included for comparison.

Table VIII.

h00	F observed	A	F calculated B
000		748	748
200	212	207	212
400	169	143	122
600	320	292	283
800	47	57	67
10.0.0	120	94	102
12.0.0	80	88	85

The agreement is good. For the reflections (h00),

$$\frac{\sum ||F|_{\text{obs.}} - |F|_{\text{calc.}}|}{\sum |F|_{\text{obs.}}} = 11.2\%$$

The Fourier projection onto the a_1 axis was prepared from the data listed above, and is plotted in Figure 19.

b) The Fourier projection $\rho(y, z)$ and the calculation of structure factors for reflections $Ok\ell$.---In the space group $C_{2v}^9-P2_1$ nb the projection onto (100) has a center of symmetry. The structure factor for $F_{Ok\ell}$ is given by the two formulas,

$$F_{Ok\ell} = 4 \sum_j f_j \cos 2\pi ky_j \cos 2\pi \ell z_j, \text{ for } k + \ell = 2n;$$

$$F_{Ok\ell} = 4 \sum_j f_j \sin 2\pi ky_j \sin 2\pi \ell z_j, \text{ for } k + \ell = 2n + 1.$$

The summation is over all atoms in the complex molecule 1.

Using the parameters obtained in the previous section I calculated the signs of the structure factors for about 75 reflections $Ok\ell$ which occur at lower Bragg angles and are not too weak. I carried out the summation

$$A \rho(y, z) = \sum_{\substack{k=-\infty \\ k+\ell=2n}}^{+\infty} \sum_{\substack{\ell=-\infty \\ \ell=2n-k}}^{+\infty} F_{Ok\ell} \cos 2\pi ky \cos 2\pi \ell z - \sum_{\substack{k=-\infty \\ k+\ell=2n+1}}^{+\infty} \sum_{\substack{\ell=-\infty \\ \ell=2n+1-k}}^{+\infty} F_{Ok\ell}$$

$$\sin 2\pi ky \sin 2\pi \ell z$$

for $y = 0$ to $1/4$ and $z = 0$ to 1 by means of the L cards on the

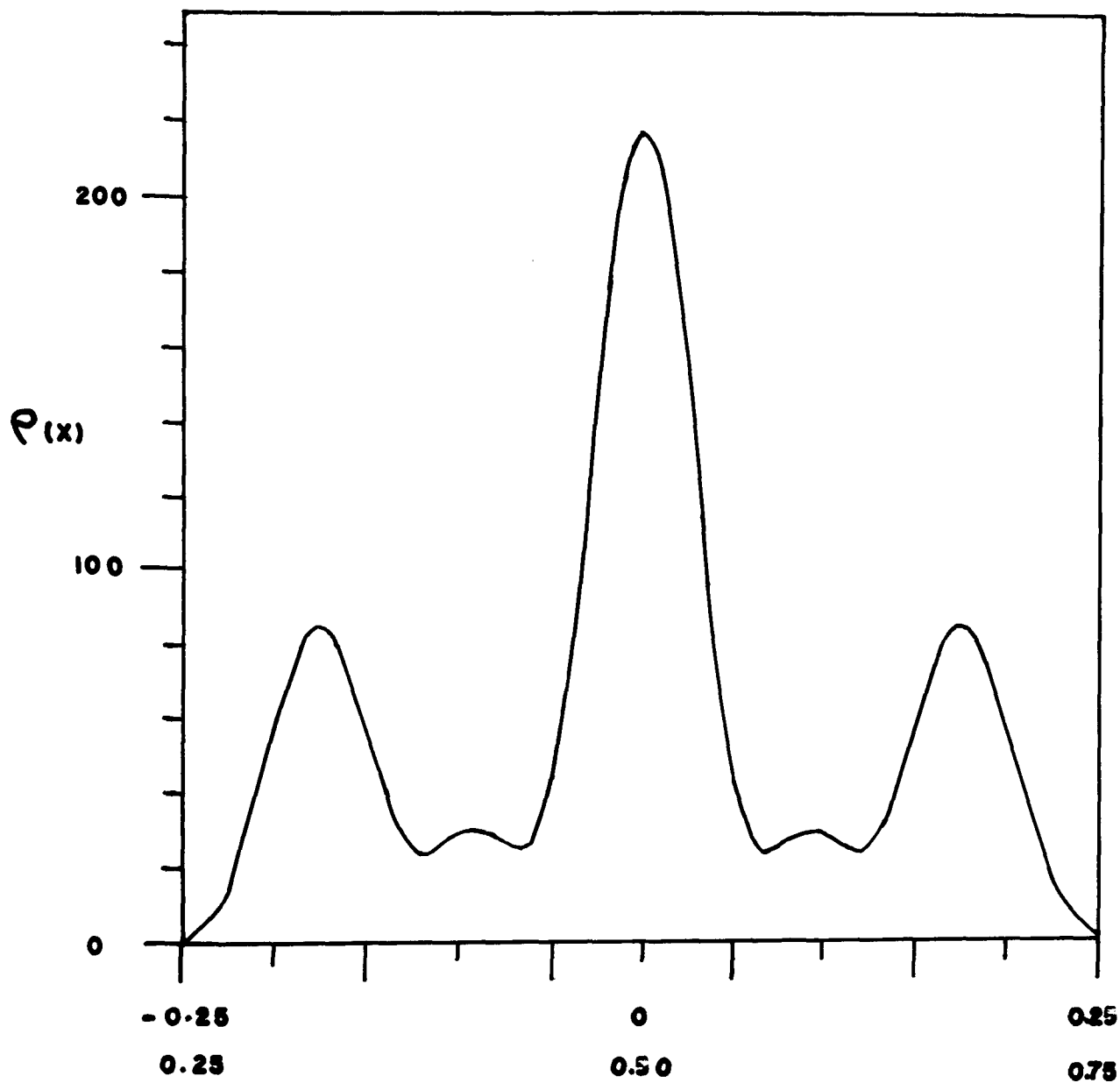


Figure 19. Projected density function $\rho(x)$ in units of electrons per Å.

International Business Machines. Peaks were got back for all atoms approximately at the positions I assumed for them in the calculation of structure factors. While the projection does not help at all to refine the parameters of the light atoms, a new set of values for the y, z parameters of the manganese and chlorine atoms were determined from their respective peaks. The new values are given below.

	y	z
Mn ₁	0.119	0.008
Cl ₁ -I	0.128	- 0.155
Cl ₁ -II	0.110	0.172

With these new values for the heavy atoms and with light atom parameters revised on the basis of the new manganese parameters I calculated structure factors for all observed reflections $Ok\ell$, 109 in number, and carried out another Fourier summation which is plotted as $\rho(y, z)$ in Figure 20. Comparison of the projection with Figure 21 confirms the approximate structure in a convincing fashion.

The crowding of the atoms in this projection and the disparity in their atomic numbers create a pattern which at many points is beyond the resolving power of the 109 reflections $Ok\ell$ which could be observed with copper $K\alpha$ radiation out to $\sin \theta = 0.93$. Specifically, carbon and nitrogen atoms separated

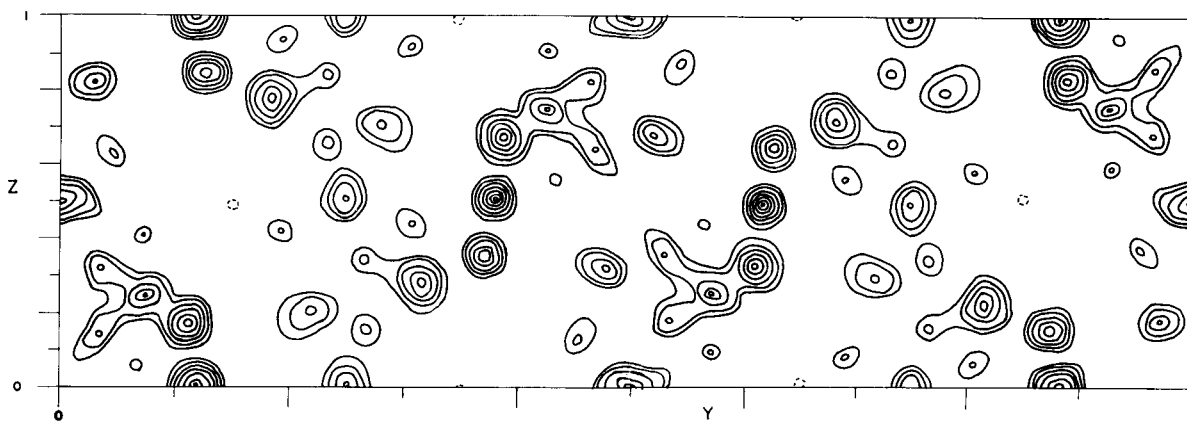


Figure 20. The Fourier projection $P(y, z)$. Contour intervals in number of electrons per \AA^2 are 7.5, 10, 15, 20, 25, 35, and 45.

by less than about $0.2 \overset{\circ}{\text{Å}}$. were not resolved. A Fourier projection on (001) may be expected to give better resolution. For the purpose of this work we are, however, satisfied with the projection in Figure 20, inasmuch as it shows all isolated atoms and groups of superimposed atoms, and they can be recognized readily.

The calculated structure factors for the reflections $0k\ell$ are given as entry A in Table IX along with the observed $|F|$'s, which have been adjusted by a new and slightly different scale factor such that $\sum |F|_{\text{calc.}} = \sum |F|_{\text{obs.}}$. The value for the expression
$$\frac{\sum ||F|_{\text{obs.}} - |F|_{\text{calc.}}|}{\sum |F|_{\text{obs.}}} \text{ is } 33\%.$$

3) The probable positions of the oxygen atoms in the crystal.---As I mentioned at an earlier stage of this work the density determination and the microchemical analysis indicated that each complex molecule probably contains two molecules of water. However the crystals were prepared from mixture of relatively dry organic solvents such as absolute alcohol and c.p. acetone, and did not change composition when kept over silica gel. Surely then if water molecules are present in the structure, they must be held very strongly, most likely by bonds with manganese atoms. One is struck by two features of the approximate structure. First, the manganese atom has a coordination number 4 instead of 6, although 6 occurs more frequently.*

* Private communication from Professor Linus Pauling.

Second, there is enough room for two water molecules around each manganese atom. In determining the anhydrous part of the structure I took advantage of the high atomic numbers of the heavy atoms and of the known structure of the huge hexamethylenetetramine molecules. A search for eight oxygen atoms in the unit cell has no such guideposts. Most Patterson projections I made have however been almost completely interpreted, and the Fourier projection converged to an extent such that one might expect to find some information regarding the oxygen atoms. In fact I did probably find X-ray evidence concerning them.

In the projection $P(v, w)$ in Figure 14 the peaks A and B were not explained, nor were the positive values near D in Figure 15. These features do not correspond to any possible vector between atoms belonging to the anhydrous part of the complex molecules. However, they may be accounted for by putting two oxygen atoms into the complex molecule 1 at the positions given below.

	x	y	z
O_{1-I}	0.610	0.052	0.064
O_{1-II}	0.390	0.186	0.048

If one refers to the Fourier projection $\rho(y, z)$, one will find a resolved peak in the neighborhood of (0.052, 0.064), and an unresolved one which covers the atom O_{1-II} and the closely situated carbon atom in the projected structure.

Table IX.

Calculated and Observed Structure Factors (Okℓ)
(F₀₀₀ = 748)

Okℓ	F _{obs.}	F _{calc.} (A)	(B)	Okℓ	F _{obs.}	F _{calc.} (A)	(B)
Ok0							
020	13	11	16	0.17.2	58	52	61
040	26	5	12	0.20.2	34	14	19
060	34	-73	-63	0.21.2	47	-40	-45
080	84	160	117	0.22.2	48	-47	-38
0.10.0	52	66	59	Ok3			
0.12.0	110	-105	-115	013	75	-55	-42
0.14.0	89	-81	-94	023	10	4	4
0.16.0	108	84	102	033	8	-14	-22
0.18.0	43	-24	-21	043	55	10	-24
0.20.0	72	-77	-70	053	52	-14	-5
0.22.0	51	-87	-75	073	12	-9	-17
0.24.0	37	22	16	083	52	-46	-53
0.26.0	49	37	36	093	30	-39	-49
Ok1				0.10.3	8	4	-3
011	58	76	112	0.11.3	10	-8	-5
021	18	-28	-28	0.12.3	43	-39	-21
031	103	-138	-148	0.13.3	17	-28	-37
041	120	-75	-93	Ok4			
051	62	-124	-102	004	67	54	60
071	34	63	42	014	15	30	39
081	72	80	76	044	6	-9	-9
091	85	106	78	074	23	-24	-22
0.11.1	32	-47	-46	084	20	26	21
0.13.1	90	-81	-98	094	60	-87	-100
0.17.1	52	65	78	0.10.4	24	28	31
0.18.1	53	45	49	0.12.4	37	20	22
0.20.1	52	-31	-34	0.13.4	40	19	34
0.21.1	77	-58	-44	0.16.4	50	27	30
0.24.1	35	33	31	0.17.4	53	-21	-8
0.25.1	38	49	42	0.21.4	68	58	49
Ok2				Ok5			
002	54	-42	-2	015	63	70	66
012	9	9	13	025	37	-22	-20
042	18	-5	-2	035	82	-63	-67
052	50	-7	-28	045	24	-20	-43
072	65	52	50	055	29	-77	-75
082	130	113	85	075	21	-18	-15
0.11.2	11	2	14	095	48	68	72
0.12.2	14	-1	-7	0.10.5	23	-50	-56
0.13.2	18	-40	-28	0.11.5	23	-40	-36
0.16.2	53	53	66	0.12.5	54	49	65
				0.13.5	72	-44	-43
				0.17.5	62	56	54
				0.18.5	24	-38	-28
				0.21.5	36	-52	-54

Table IX. (Cont.)

Ok ℓ	F _{obs.}	F _{calc.} (A)	(B)	Ok ℓ	F _{obs.}	F _{calc.} (A)	(B)
Ok6				Ok7			
006	132	125	115	017	26	17	8
016	23	-46	-39	037	40	-68	-68
046	45	-57	-58	057	74	-76	-75
076	70	51	46	067	24	22	24
086	122	142	149	077	40	57	63
0.10.6	18	5	11	097	42	47	56
0.12.6	70	73	77	0.11.7	35	-26	-29
0.13.6	29	56	65	0.13.7	48	-55	-48
0.14.6	41	-63	-61	0.14.7	28	14	13
0.17.6	37	-13	-4	0.16.7	47	34	35
0.19.6	35	-34	-35	Ok8			
				008	35	50	37
				048	31	-12	-14
				088	36	28	40
				098	40	17	13

The Mn-O distance based on this tentative parameter assignment is 2.00 Å.

Structure factors were calculated with inclusion of the eight oxygen atoms. They are appended as entry B in Tables VIII and IX. The values of the expression

$$\frac{\sum ||F|_{\text{obs.}} - |F|_{\text{calc.}}|}{\sum |F|_{\text{obs.}}}$$

are 13.5 percent and 34 percent, respectively.

4) The description of the approximate structure.---The approximate structure based on the final values of the parameters is shown in Figures 21 and 22. Each atom is labeled by an Arabic numeral referring to the complex molecule, a Roman numeral (in the third position) referring to one or the other enantiomorphous half of the complex molecule, and a second Arabic numeral specifying the atom.

The approximate parameters of the 25 atoms in the complex molecule 1 are given in Table X.

Figure 23 shows the anhydrous part of a complex molecule. The bond angle between the Mn-Cl and Mn-N bonds is calculated to be 93°50'. The deviation from 90° is within the limits of experimental error. There are six mirror planes in each hexamethylenetetramine molecule. The orientation of the two hexamethylenetetramine molecules in the complex molecule is almost such that one of the mirror planes of each hexamethylenetetramine molecule

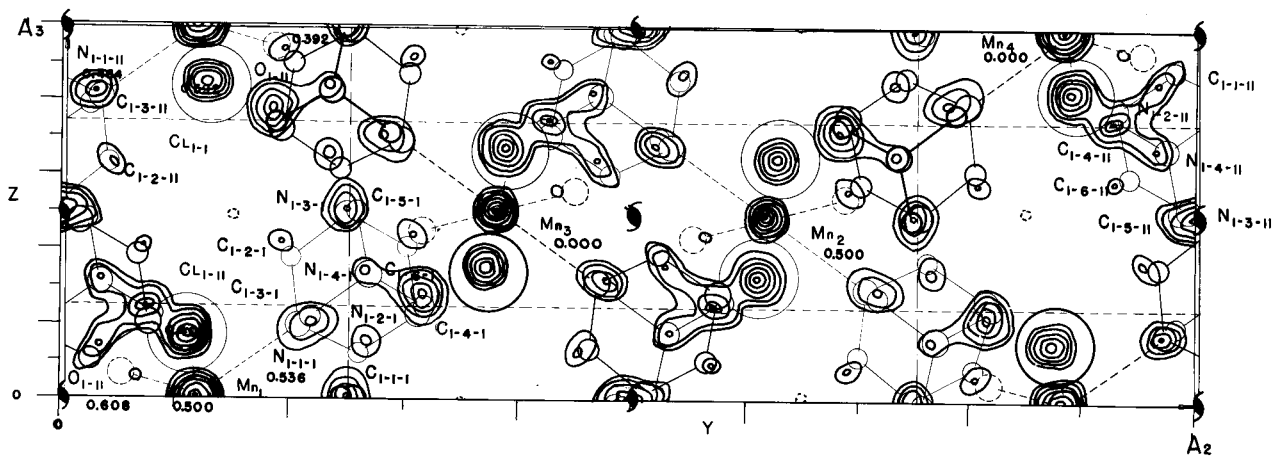


Figure 21. The approximate structure of the hexamethylenetetramine complex with manganous chloride. One unit cell is shown; the a_1 axis is normal to the plane of the paper and points away from the reader. In decreasing order of their sizes, the circles represent chlorine, manganese, oxygen, nitrogen, and carbon atoms. Hydrogen atoms are not shown.

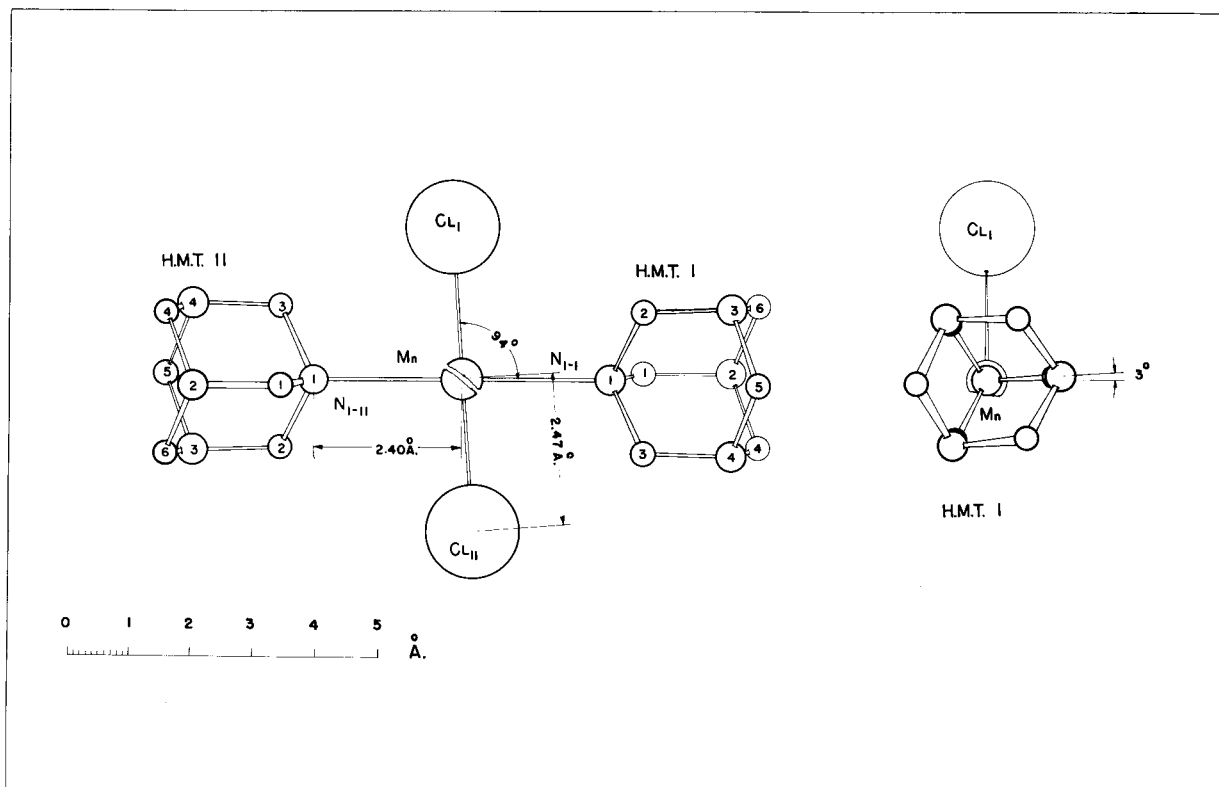


Figure 23. The anhydrous part of a complex molecule.

is perpendicular to the plane of the Mn-N and Mn-Cl bonds. The manganese atom lies exactly on the common three-fold axis of the two hexamethylenetetramine molecules at the center of symmetry of the complex molecule. Bond distances are also shown in Figure 23.

Table X.

	x	y	z		x	y	z
Mn ₁	0.500	0.119	0.008				
Cl _{1-1-I}	0.684	0.128	-0.155	Cl _{1-1-II}	0.316	0.110	0.172
O _{1-I}	0.610	0.052	0.064	O _{1-II}	0.390	0.186	0.048
N _{1-1-I}	0.536	0.206	0.198	N _{1-1-II}	0.464	0.032	-0.183
N _{1-2-I}	0.683	0.313	0.227	N _{1-2-II}	0.317	-0.076	-0.212
N _{1-3-I}	0.507	0.249	0.496	N _{1-3-II}	0.493	-0.012	-0.480
N _{1-4-I}	0.507	0.268	0.334	N _{1-4-II}	0.493	-0.030	-0.319
Cl _{1-1-I}	0.492	0.259	0.122	Cl _{1-1-II}	0.508	-0.022	-0.106
Cl _{1-2-I}	0.492	0.021	-0.205	Cl _{1-2-II}	0.508	0.038	-0.363
Cl _{1-3-I}	0.657	0.217	0.222	Cl _{1-3-II}	0.343	0.021	-0.205
Cl _{1-4-I}	0.630	0.318	0.249	Cl _{1-4-II}	0.370	-0.080	-0.231
Cl _{1-5-I}	0.630	0.258	0.502	Cl _{1-5-II}	0.370	-0.019	-0.487
Cl _{1-6-I}	0.465	0.303	0.409	Cl _{1-6-II}	0.535	-0.065	-0.392

10. CONCLUSIONS

In view of the evidence provided by the Patterson functions, structure factors, and Fourier syntheses the approximate structure described in Figures 21 and 22, and analytically in Table X is a highly probable one. While the evidence regarding the anhydrous part of the complex molecules is sufficiently conclusive, the identification of the oxygen atoms of the water molecules in the crystal and the determination of their positions need further evidence in addition to that presented in 9(3).

The structure found in this work for the hexamethylenetetramine complex with manganous chloride explains its stability. The structure also proves the analogy between the hexamethylenetetramine and ammonia complexes in that the hexamethylenetetramine molecule interacts with the manganese atom through the unshared pair of electrons of one of its four nitrogen atoms. This type of bonding may have considerable generality in the hexamethylenetetramine complexes.

The structure is compatible with the result for the magnetic susceptibility. The value of five unpaired electrons predicted for the manganese atom forming ionic bonds by using Pauling's magnetic criterion was found experimentally. The bond distances are essentially ionic.

The relation between the approximate structure based on the pseudo unit cell and the exact structure based on the true

unit cell is not all clear. Very likely the difference between the two structures lies only in the shift among the complex molecules rather than in the configuration within each complex molecule.

11. REFERENCES

- (1) Roscoe G. Dickinson and Albert L. Raymond, (1923),
J.A.C.S., 45.
- (2) F. D. Ordway, Doctoral Thesis, California Institute of
Technology, (1948).
- (3) L. Vanino and A. Schinner, Arch. Pharm., (1914), 252,
449-459.
- (4) G. Scagliarini and G. Tartarini, Atti. Accad. Lincei (6),
(1926), 4, 387-389.
- (5) D. P. Shoemaker, Doctoral Thesis, California Institute
of Technology, (1947).
- (6) G. Tunell, Am. Mineralogist, (1939), 24, 448.
- (7) A. J. C. Wilson, Nature, (1942), 150, 152.
- (8) P. A. Shaffer, Jr., J.A.C.S., (1947), 69, 1557.
- (9) L. Pauling, 'The Nature of the Chemical Bond', Second
Edition, 189 pp., Cornell University Press, Ithaca,
New York, (1942).
- (10) P. A. Shaffer, Jr., Verner Schomaker, and Linus Pauling,
J. Chem. Phys., (1946), 14, 11, 648-658.

PROPOSITIONS

1. An alternative trial structure is proposed for the complex of hexamethylenetetramine with stannic chloride. It is compatible with the experimental evidence presented by F. D. Ordway⁽¹⁾ in his Thesis. Besides, it has the advantage that the tin atom lies on the common three-fold axis of two hexamethylenetetramine molecules and interacts with two nitrogen atoms through their unshared pairs of electrons.

(1) F. D. Ordway, Doctoral Thesis, C.I.T., 1948.

2. The discrepancy between the two sets of conductivity data of the β -thallium phase in the system lead-thallium at 18°C as reported by Kurnakow and Schemtschushny⁽²⁾ and by Guertler and Schulze⁽³⁾ can be interpreted as an indication for the occurrence of a superstructure, such as (Pb,Tl)Tl, in the β -thallium phase.

(2) N. S. Kurnakow and S. F. Schemtschushny, Z. anorg. Chem., (1909), 64, 149.

(3) W. Guertler and A. Schulze, Z. physikal, Chem., (1923), 104, 269.

3. In each complex molecule of hexamethylenetetramine with manganous chloride $2(\text{CH}_2)_6\text{N}_4 \cdot \text{MnCl}_2 \cdot 2\text{H}_2\text{O}$ ⁽⁴⁾ the bonds from the manganese atom to the surrounding chlorine, nitrogen, and oxygen atoms need not be of the extreme ionic type; resonance with covalent bonds of the $4s4p^34d^2$ type, which have the same magnetic properties, could occur.⁽⁵⁾

PROPOSITIONS (Continued)

- (4) This Thesis.
- (5) Linus Pauling, 'The Nature of the Chemical Bond', Second Edition, p. 187, Cornell University Press, Ithaca, New York, (1942).

4. (1) If the transition of a binary alloy in the system P-Q from random replacement to the regular arrangement of a superlattice is a simple segregation of atoms to particular atom sites with no change of configuration in terms of coordinates of all sites, the structure amplitudes of the superlattice reflections have the form,

$$F(hk\ell) = (f_P - f_Q) \sum_m \left[\frac{q_m}{p_m + q_m} \sum_{i=1}^{p_m} \exp 2\pi i (hx_i + ky_i + \ell z_i) - \frac{p_m}{p_m + q_m} \sum_{j=1}^{q_m} \exp 2\pi i (hx_j + ky_j + \ell z_j) \right],$$

where m refers to a particular set of equivalent sites occupied by a statistical atom $\frac{p_m}{p_m + q_m} P, \frac{q_m}{p_m + q_m} Q$ as in the random structure and the same set resolves on segregation into two subsets with p_m sites for P and q_m for Q respectively.

(2) From the structural point of view the superstructures Cu_3Au ,⁽⁶⁾ $CuAu$ ⁽⁷⁾ and Cr_2Al ⁽⁸⁾ represent the three classes of superstructures. The first two conform to the condition of a simple segregation and therefore give superlattice reflections with a structure amplitude always containing the factor $(f_P - f_Q)$. They differ, however, in the fact that the segregation in the

PROPOSITIONS (Continued)

case of CuAu results in lower symmetry, and gives rise to the splitting of cubic lines in the powder pattern. The superstructure Cr_2Al , which does not satisfy the condition for a simple segregation, forms the third class.

- (6) C. H. Johansson and J. O. Linde, Ann. Physik, (1925), 78, 439.
- (7) C. H. Johansson and J. O. Linde, Ann. Physik, (1927), 82, 449.
- (8) A. J. Bradley and S. S. Lu, Z. Krist., (1937), 96, 20.

5. From a study of the relation between the hydrogen overvoltage and different kinds of atomic spacing for sixteen metals H. Leidheiser, Jr.⁽⁹⁾ found out the following two things. First, instead of the length of cube edge or face diagonal the distance of closest approach of atoms is an important factor in the catalysis under consideration. Second, the crystal structure is also of importance; the face-centered and body-centered cubic metals form two distinct classes.

However, if one uses $2(R(\text{CNS}) + 0.053)$ ⁽¹⁰⁾ instead of the distance of closest approach of atoms for the body-centered cubic metals mentioned in his work, the two classes are satisfactorily unified.

- (9) H. Leidheiser, Jr., J.A.C.S., (1949), 71, 3634.
- (10) Linus Pauling, J.A.C.S., (1947), 69, 542.

PROPOSITIONS (Continued)

6. It would be interesting to investigate by the method of absorption spectrum in the infrared a few alcohol-aldehyde systems⁽¹¹⁾ whose freezing point-composition curves have a broad rounded hump with a maximum at approximately 50 mole percent. Structure determination of a crystalline compound of alcohol and aldehyde with constant composition 1:1 is also suggested.

(11) F. E. McKenna, H. V. Tartar and E. C. Lingafelter, J.A.C.S., (1949), 71, 729.

7. (1) The experience from the structure determination for the complex of hexamethylenetetramine with manganous chloride⁽¹²⁾ could be very useful in the determination of the structure of the compound dipyridinomanganous chloride.⁽¹³⁾, (14)

(2) Accurate determination of interatomic distances in these two manganese complexes would probably add to the understanding of the nature of the anomaly of manganese radius.⁽¹⁵⁾

(12) This Thesis.

(13) E. G. Cox, A. J. Shorter, W. Wardlaw, and W. J. R. Way, J. Chem. Soc., (1937), 1556.

(14) David P. Mellor and Charles D. Coryell, J.A.C.S., (1938), 60, 1786.

(15) Linus Pauling, 'The Nature of the Chemical Bond', Second Edition, p. 186, Cornell University Press, Ithaca, New York, (1942).

8. An empirical method is proposed to predict roughly the tetragonality c/a for a binary alloy after its transition from the cubic random structure to the tetragonal superstructure.

PROPOSITIONS (Continued)

9. The precipitate from the Maun and Swift iodometric determination of zinc⁽¹⁶⁾ has been compared with the precipitate $K_2Zn_3[Fe(CN)_6]_2$ by their powder patterns. On the basis of the fact that no impurity lines have been found the Maun and Swift precipitate is probably a homogeneous phase. The empirical factor 1.019 can be eliminated by adopting the formula $K_{32}Zn_{52}[Fe(CN)_6]_{34}$ for the precipitate.

(16) Eugene K. Maun and Ernest H. Swift, Analytical Chem., (1949), 21, 798.